UNIVERSITÉ DU LUXEMBOURG

PhD-FSTM-2022-080
The Faculty of Sciences, Technology and Medicine

DISSERTATION

Presented on 04/07/2022 in Luxembourg

to obtain the degree of

DOCTEUR DE L'UNIVERSITÉ DU LUXEMBOURG

EN INFORMATIQUE

by

Anyue WANG
Born on 20 February 1993 in Anhui (CHINA)

NON-ORTHOGONAL MULTIPLE ACCESS FOR NEXT-GENERATION SATELLITE SYSTEMS: FLEXIBILITY EXPLOITATION AND RESOURCE OPTIMIZATION

Dissertation defence committee:

Dr Lei LEI, dissertation supervisor
Associate Professor, Xi'an Jiaotong University

Dr Symeon CHATZINOTAS, vice chairman
Professor, Université du Luxembourg

Dr Ana Isabel PÉREZ-NEIRA
Professor, Centre Tecnològic de Telecomunicacions de Catalunya

Dr Bhavani SHANKAR, chair
Assistant Professor, Université du Luxembourg

Dr John THOMPSON
Professor, University of Edinburgh

“Don’t let anyone rob you of your imagination,
your creativity, or your curiosity.”

Mae Jemison
Astronaut

To my family and friends

Abstract

In conventional satellite communication systems, onboard resource management follows pre-design approaches with limited flexibility. On the one hand, this can simplify the satellite payload design. On the other hand, such limited flexibility hardly fits the scenario of irregular traffic and dynamic demands in practice. As a consequence, the efficiency of resource utilization could be deteriorated, evidenced by mismatches between offered capacity and requested traffic in practical operations. To overcome this common issue, exploiting multi-dimension flexibilities and developing advanced resource management approaches are of importance for next-generation high-throughput satellites (HTS).

Non-orthogonal multiple access (NOMA), as one of the promising new radio techniques for future mobile communication systems, has proved its advantages in terrestrial communication systems. Towards future satellite systems, NOMA has received considerable attention because it can enhance power-domain flexibility in resource management and achieve higher spectral efficiency than orthogonal multiple access (OMA). From ground to space, terrestrial-based NOMA schemes may not be directly applied due to distinctive features of satellite systems, e.g., channel characteristics and limited onboard capabilities, etc. To investigate the potential synergies of NOMA in satellite systems, we are motivated to enrich this line of studies in this dissertation. We aim at resolving the following questions: 1) How to optimize resource management in NOMA-enabled satellite systems and how much performance gain can NOMA bring compared to conventional schemes? 2) For complicated resource management, how to accelerate the decision-making procedure and achieve a good tradeoff between complexity reduction and performance improvement? 3) What are the mutual impacts among multiple domains of resource optimization, and how to boost the underlying synergies of NOMA and exploit flexibilities in other domains?

The main contributions of the dissertation are organized in the following four chapters:

First, we design an optimization framework to enable efficient resource allocation in general NOMA-enabled multi-beam satellite systems. We investigate joint optimization of power allocation, decoding orders, and terminal-timeslot assignment to improve the max-min fairness of the offered-capacity-to-requested-traffic ratio (OCTR). To solve the mixed-integer non-convex programming (MINCP) problem, we develop an optimal fast-convergence algorithmic framework and a heuristic scheme, which outperform conventional OMA in matching capacity to demand.

Second, to accelerate the decision-making procedure in resource optimization, we attempt to solve optimization problems for satellite-NOMA from a machine-learning perspective and reveal the pros and cons of learning and optimization techniques. For complicated resource optimization problems in satellite-NOMA, we introduce deep neural networks (DNN) to accelerate decision making and design learning-assisted optimization schemes to jointly optimize power allocation and terminal-timeslot assignment. The proposed learning-optimization schemes achieve a good trade-off between complexity

and performance.

Third, from a time-domain perspective, beam hopping (BH) is promising to mitigate the capacity-demand mismatches and inter-beam interference by selectively and sequentially illuminating suited beams over timeslots. Motivated by this, we investigate the synergy and mutual influence of NOMA and BH for satellite systems to jointly exploit power- and time-domain flexibilities. We jointly optimize power allocation, beam scheduling, and terminal-timeslot assignment to minimize the capacity-demand gap. The global optimal solution may not be achieved due to the NP-hardness of the problem. We develop a bounding scheme to tightly gauge the global optimum and propose a suboptimal algorithm to enable efficient resource assignment. Numerical results demonstrate the synthetic synergy of combining NOMA and BH, and their individual performance gains compared to the benchmarks.

Fourth, from the spatial domain, adaptive beam patterns can adjust the beam coverage to serve irregular traffic demand and alleviate co-channel interference, motivating us to investigate joint resource optimization for satellite systems with flexibilities in power and spatial domains. We formulate a joint optimization problem of power allocation, beam pattern selection, and terminal association, which is in the format of MINCP. To tackle the integer variables and non-convexity, we design an algorithmic framework and a low-complexity scheme based on the framework. Numerical results show the advantages of jointly optimizing NOMA and beam pattern selection compared to conventional schemes.

In the end, the dissertation is concluded with the main findings and insights on future works.

Acknowledgements

First and foremost, I would like to express my sincere gratitude to my thesis supervisor, Prof. Lei Lei, for his continuous support, instruction, trust, and patience. During my Ph.D. study, he has shared his invaluable experience in academics and life. The thesis would not have been accomplished without his generous assistance and encouragement. I would like to extend my special gratitude to Prof. Symeon Chatzinotas and Dr. Eva Lagunas for their constant advice on my research topics and assistance in improving my research skills and critical thinking. My swift progress requires their selfless help. Besides, I must also thank the external member of my CET committee member, Prof. Ana Isabel Pérez-Neira, for her gentle and invaluable suggestions on my research works, which significantly help to enhance the quality of the thesis.

I am deeply grateful to my research collaborators, Prof. Lei Lei, Dr. Eva Lagunas, Prof. Symeon Chatzinotas, Prof. Ana Isabel Pérez-Neira, Prof. Björn Ottersten, and Prof. Xin Hu, for their invaluable assistance and critical comments, which refine the models and improve the quality of my research papers.

The pursuit of a Ph.D. degree is always deemed as tough and dull work. But I would never forget the meaningful experience in the Interdisciplinary Centre for Security, Reliability and Trust (SnT) at the University of Luxembourg. I would like to offer my special thanks to my colleagues in SnT, Yaxiong, Lin Chen, Puneeth, Liz, Hieu, Himani, Shahida, Long, Kexin, Ehsan, Robin, Arsham, Gabriel, Ahmed, Ruizhi, Linlong, Tong, Deyi, Farbod, Tedros, Lin Xiang, Bhavani, and Yuan, for extensive discussions and for providing a comfortable work environment. I would like to thank my friends, Yaxiong, Jiale, Bowen, Puneeth, Lin, Yu, Jing, Clément, Yuwei, Jingjing, Shange, Yan, Qibo, Hongru, Pan, Yanyao, and Jiaqi, for bringing endless happiness to my life and accompanying me during this difficult time.

Last but not least, I would like to thank my parents for their unwavering support and belief in me. Many thanks to my lovely Apollo, and Étoile. Thanks to the University of Luxembourg community for providing an inspiring environment and lots of opportunities to grow. The generous financial help from the Fonds National de la Recherche (FNR-Luxembourg National Research Fund) via University of Luxembourg is gratefully acknowledged.

List of Abbreviations

SatCom	satellite communications
NTN	non-terrestrial networks
HTS	high-throughput satellite
MPA	multi-port amplifier
DTP	digital transparent processor
TDMA	time-division multiple access
BH	beam hopping
RF	radio-frequency
BFN	beamforming network
NOMA	non-orthogonal multiple access
PDMA	pattern division multiple access
SCMA	sparse code multiple access
OMA	orthogonal multiple access
SIC	successive interference cancellation (SIC)
OCTR	offered-capacity-to-requested-traffic ratio
NP	nondeterministic polynomial-time
KKT	Karush-Kuhn-Tucker
MINCP	mixed-integer nonconvex programming
SCA	successive convex approximation
BCD	block coordinate descent

PF	Perron-Frobenius
DNN	deep neural networks
DVB-S2	digital video broadcasting-satellite-second generation
DVB-S2X	digital video broadcasting-satellite-second generation extensions
SINR	signal-to-interference-plus-noise ratio
EIRP	effective isotropic radiated power
QoS	quality of service
IoT	internet of things
CSI	channel state information
MIMO	multiple input multiple output
MISO	multiple input single output
JOPD	joint optimization of power allocation and decoding orders
MaxCC	maximum channel correlation
JOPDT	joint optimization of power allocation, decoding orders, and terminal-timeslot scheduling
LEO	low earth orbit
GEO	geostationary earth orbit
MMSE	minimum mean square error
MCMU	monotonic constrained max-min utility
CUF	competitive utility function
MC	monotonic constraint
ESA	European space agency
MICP	mixed-integer convex/conic programming
DL	deep learning
MINLP	mixed-integer non-linear programming
DDCO	dual DNNs and convex optimization
CP	conic programming
SM	swap matching
BW	best-worst
FTPC	fractional transmit power control

SD	single DNN
TT&C	telemetry, tracking, and command
MIECP	mixed-integer exponential conic programming
UBA	upper-bound approach
LBA	lower-bound approach
E-JPBT	efficient algorithm for joint power allocation, beam scheduling, and terminal-timeslot assignment
MILP	mixed-integer linear programming
mMTC	massive machine type communications
RL	reinforcement learning
DRL	deep reinforcement learning
FLOP	floating-point operation
MinCCI	minimal co-channel interference
MaxSINR	maximal SINR
FFR	full frequency reuse
B5G	beyond fifth-generation
6G	sixth-generation
SVM	support vector machine
JPST	joint optimization for power allocation, beam pattern selection, and terminal scheduling
LC-PST	low-complexity scheme for power allocation, beam pattern selection, and terminal scheduling

Notations

$\log(x)$	natural logarithm function of x
e^x	exponential function of x
$[\cdot]^T$	transpose operator
$[\cdot]^H$	conjugate transpose operator
$\lvert \cdot \rvert$	cardinality of a set or absolute value
$\lVert \cdot \rVert$	Euclidean norm of a vector
$[\cdot]_{i,j}$	the element in the i-th row and the j-th column of the matrix
$f(x;y)$	function $f(x,y)$ with fixed y
$\max$	maximum operation
$\min$	minimum operation
argmax	finding the argument that gives the maximum value
argmin	finding the argument that gives the minimum value
$[x]^+$	equivalent the calculation of $\max\{x, 0\}$
$\mathcal{X} \times \mathcal{Y}$	Cartesian product of two sets

Preface

This Ph.D. Thesis has been carried out from October, 2018 to June, 2022 at Interdisciplinary Centre for Security, Reliability and Trust (SnT), University of Luxembourg, Luxembourg, under the supervision of Prof. Lei Lei, firstly as a Research Scientist at SnT, University of Luxembourg, Luxembourg, and later as an Associate Professor at Xi'an Jiaotong University, China. Additionally, the Ph.D. Thesis was co-supervised by Prof. Symeon Chatzinotas and Dr. Eva Lagunas at SnT, University of Luxembourg, Luxembourg. The time-to-time evaluation of the Ph.D. Thesis was duly performed by the CET members constituting the supervisor, co-supervisors, and Prof. Ana Isabel Pérez-Neira from Centre Tecnològic de Telecomunicacions de Catalunya, Spain.

Contents

This Ph.D. Thesis entitled *Non-Orthogonal Multiple Access for Next-Generation Satellite Systems: Flexibility Exploitation and Resource Optimization* is divided into seven chapters. In Chapter 1, the background, motivations, research questions, and contributions of the thesis are described. Chapter 2 provides a survey of state-of-the-art works on NOMA-based resource allocation in satellite systems and summarizes the limitations. In Chapter 3, a resource optimization framework for general NOMA-enabled multi-beam satellite systems is designed to investigate the applicability and benefits of NOMA in SatCom. Learning-assisted approaches are proposed to accelerate the decision-making procedure in NOMA-based resource optimization for satellite systems in Chapter 4. Chapter 5 studies the potential synergy of NOMA and beam hopping and designs a bounding approach to jointly exploit power- and time-domain flexibilities. To investigate underlying mutual influence of flexibilities in power and spatial domains, Chapter 6 provides a joint scheme to optimize NOMA and adaptive beam patterns. Finally, the conclusions and future works are summarized in Chapter 7.

Support of the Thesis

This Ph.D. Thesis has been fully supported by the Luxembourg National Research Fund under project ROSETTA (C17/IS/11632107). The effort of collaborators and dissemination costs were supported by other projects, namely, the FNR CORE FlexSAT (C19/IS/13696663) and ASWELL (C19/IS/13718904)), the European Research Council under Project AGNOSTIC (742648), and the ministry of Science, Innovation and Universities, Spain, under project TERESA (TEC2017-90093-C3-1-R). Additionally, the time-to-time support from SIGCOM is also gratefully acknowledged.

Contents

List of Figures

List of Tables

Chapter 1

Introduction

Satellite communications (SatCom) can provide broadband data transmission to a wide-range area [1, 2]. In the SatCom systems, satellites in the space function as relays to transceive signals from/to targeted remote areas [1], which greatly extends the coverage compared to terrestrial cellular systems. This allows SatCom to provide ubiquitous service, even for some sparsely populated regions that are hard-to-reach for incumbent terrestrial systems, e.g., oceans, mountains, and deserts [1, 2, 3]. To embrace the trend of the explosive growth of wireless traffic and requirements of ubiquitous connectivity [4], SatCom has been drawing tremendous attention from the wireless communication society and is envisioned as one of the key components for future communication systems, e.g., non-terrestrial networks (NTN) [3] and space-air-ground integrated networks [5, 6].

Resource allocation is of great significance in wireless systems. By leveraging the flexibilities in different domains, e.g., power/frequency/time/code/spatial, the allocation of wireless resources can be optimized to achieve performance improvement and satisfy various requirements. In SatCom, satellite payloads at the space segment play an important role in resource allocation for data transmission [1]. The allocation of on-board resources, e.g., transmit power and bandwidth, is decided at the gateways on the ground. Then the decision is communicated to the satellite in the space so that the resource management can be realized at the payload. Conventionally, the design of satellite payloads is with limited flexibility. On-board resources are fixed and uniformly allocated to each beam [7]. Besides, all the beams keep illuminated and beam radiation patterns stay constant irrespective of traffic demand during service time [1]. This conventional design may lead to the following typical issues:

- *Mismatch between requested traffic and offered capacity.* In practice, requested traffic in satellite systems is irregularly distributed across regions and dynamically changed over time [8, 9]. The conventional pre-designed resource allocation scheme could fail to adapt to the non-uniform traffic distribution, which would cause unmet and unused capacity [10]. Both cases are undesired since the former results in undelivered user demands and the latter wastes on-board resources.

- *Low spectral efficiency.* In conventional satellite systems, the management of on-board resources cannot be adaptively adjusted, which may cause large co-channel interference, especially when aggressive frequency-reuse patterns are applied [11, 12], e.g., full-frequency reuse scheme. In this case, the spectral efficiency is low and thus the performance deteriorates severely.

- *Obstacles of integration or coexistence with other systems.* In satellite-terrestrial integrated networks or multi-layer satellite networks, one may concern about the issues of co-channel interference caused by fierce competition among various systems for the same frequency band [13, 14].

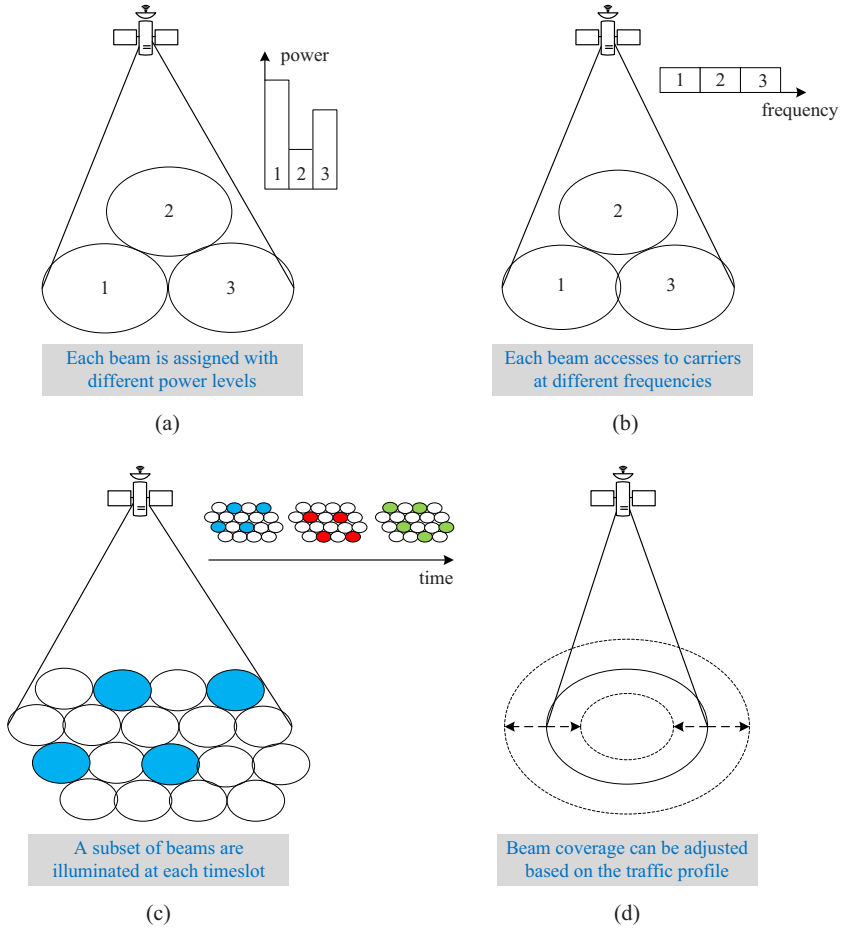

Figure 1.1: Illustrative examples of flexibilities in (a) power domain; (b) frequency domain; (c) time domain; (d) spatial domain.

Fixed resource allocation schemes discourage the seamless integration of SatCom to terrestrial systems [15].

- *High operational cost.* For instance, high transmit power can affect the lifetime of satellites, which could be worse if transmit power cannot be adjusted [16]. Another typical issue is that the payload weight and the corresponding manufacturing cost are large if all the spot beams are permanently illuminated [17].

To address the emerging challenges, more flexibilities are introduced to next-generation high-throughput satellite (HTS) systems.

1.1 Flexibilities in Satellite Payloads

In the past few decades, the SatCom society has witnessed a technical breakthrough in satellite payloads. The digitalization of payloads makes it possible to introduce more flexibilities in resource management and adaptively assign on-board resources to cater to the dynamics in satellite systems [2]. The upgraded satellite payloads can offer the following flexibilities.

- *Power-domain flexibility* (referring to Fig. 1.1(a)): In conventional payload, transmit power is equally assigned to different carriers or beams since they share the same amplifier. By adopting multi-port amplifiers (MPA) and digital transparent processors (DTP), the sharing of transmit power among beams or carriers is enabled, and the transmit power can be tuned adaptively [18, 19, 20]. Flexible power allocation can be designed to meet terminals' or beams' demands to reduce unmet and unused capacity [21]. Additionally, flexible power allocation is able to save on-board energy, which is advantageous to satellites' lifetime [16].

- *Frequency-domain flexibility* (referring to Fig. 1.1(b)): With a group of band-pass filters, frequency conversion and bandwidth assignment can be realized [1, 22, 23]. The assignment of bandwidth can be facilitated discretely or continuously [1]. In this way, bandwidth allocation can be optimized based on the demands of different beams or terminals. Besides, co-channel interference can be mitigated by allocating different frequency bands to adjacent beams or terminals.

- *Time-domain flexibility* (referring to Fig. 1.1(c)): The satellite payload is equipped with a transparent bent-pipe architecture with a switching matrix to activate/deactivate the selected beams within several hundred nanoseconds [2]. Ferrite switch is a mature technology for the implementation of beam hopping (BH) [24, 25]. BH can support time-division multiple access (TDMA) among different beams and leverage time-domain flexibility. The decision of beam illumination at each timeslot is made according to traffic distribution and/or co-channel interference level. Besides, as fewer beams are activated, the number of radio-frequency (RF) chains can be reduced, and thus the mass of the payload can be smaller [2].

- *Spatial-domain flexibility* (referring to Fig. 1.1(d)): Thanks to the application of active antennas and beamforming networks (BFN), beam radiation patterns can be adjusted to alter the resulted beam coverage (or footprint) [26]. In this case, beam patterns can be adaptively changed to cater for irregular traffic profile [26], mitigate co-channel interference [27], and improve integration to terrestrial systems [28].

With the introduction of these flexibilities, the resource allocation in SatCom can be more adaptive to the dynamic wireless environment and the co-channel interference can be reduced so that the resource utilization could be enhanced.

Flexible payloads offer a platform for the sophisticated design of resource allocation schemes to achieve performance gain. In this context, the emerging resource management problems and algorithmic solutions need further investigation. On the one hand, flexibility in each domain has not been fully exploited yet. For example, in conventional satellite systems, each orthogonal resource (e.g., time-frequency resource unit) can be accessed by only one terminal, which limits its spectral efficiency and applicability in the scenarios with the requirements of massive connectivity, e.g., in the case of delivering massive machine type communications (mMTC) services. On the other hand, the study on resource optimization for multi-dimension flexibilities is necessary for further performance improvement. Therefore, flexibility exploitation of one or more domains and the development of advanced resource management approaches are of importance for next-generation HTS systems.

1.2 Non-Orthogonal Multiple Access: Enhancement of Power-Domain Flexibility

Non-orthogonal multiple access (NOMA) is one of the promising new radio techniques for future mobile communication systems [29]. The term NOMA usually includes power-domain NOMA, pattern division

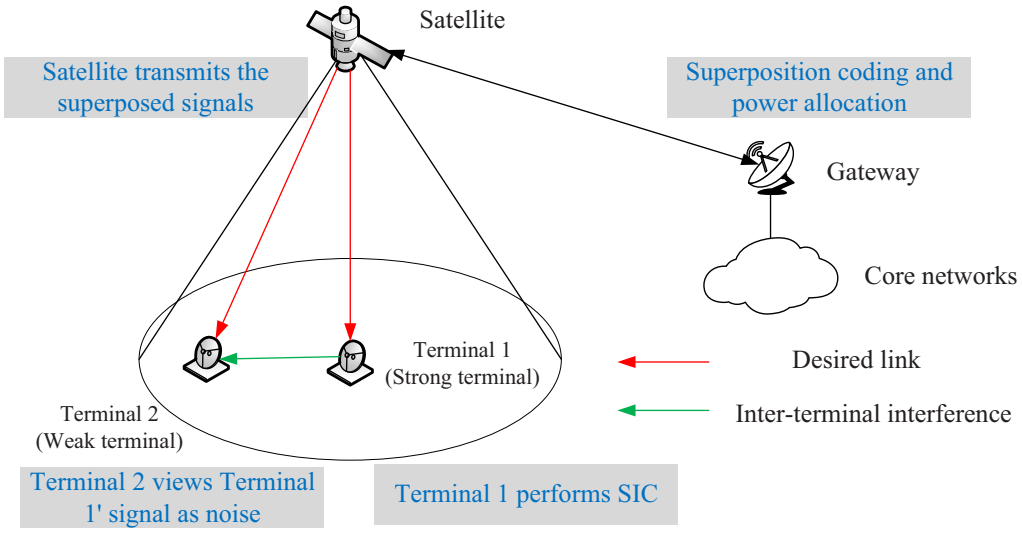

Figure 1.2: An illustrative satellite-NOMA scenario of downlink transmission. Terminal 1 is at the beam center with better channel gain while terminal 2 is at the beam edge with worse channel gain. The gateway is in charge of superposition coding and power allocation. The satellite relays the superposed signals to ground terminals. Terminal 1 performs SIC to decode and remove terminal 2's signal whereas terminal 2 directly decodes its own signal by viewing terminal 1's signal as noise.

multiple access (PDMA), sparse code multiple access (SCMA), etc [30]. In the dissertation, NOMA refers to power-domain NOMA. In conventional orthogonal multiple access (OMA), each orthogonal time-frequency resource unit can be accessed by only one terminal. This can avoid co-channel interference but meanwhile limit further performance improvement. In NOMA, superposition coding and successive interference cancellation (SIC) are adopted at the transmitter side and receiver side, respectively [31]. The non-orthogonality of time-frequency resource can be introduced and the power-domain flexibility can be enhanced [31].

We illustrate the basis of NOMA by an example in Fig. 1.2, where the satellite provides downlink transmission to two ground terminals with asymmetric channel gains. Terminal 1 is located at the beam center with better channel gain (called "strong terminal") whereas terminal 2 stands at the beam edge with worse channel gain (called "weak terminal"). At the gateway side, terminals' signals are superposed with different power levels. Then the superposed signal is transmitted to the satellite and then delivered to the two terminals. Terminal 1 firstly performs SIC to decode and remove the signal of terminal 2 such that the co-channel interference from terminal 2 can be canceled. Terminal 2 decodes the received signal directly by viewing terminal 1's signal as noise. In this way, more than one terminal can be multiplexed at the same time-frequency resource unit and the spectral efficiency can be improved compared to conventional OMA [32]. The performance gain of NOMA in terrestrial systems has been demonstrated, e.g., capacity improvement, power reduction, energy efficiency enhancement, etc.

We note that the applications of NOMA may result in some practical issues and challenges. For example, additional computational complexity will be introduced to the receivers when processing SIC. Besides, security issues might arise among receivers since some terminals can decode other terminals' signals.

By introducing NOMA to SatCom, the flexibility in power domain can be enhanced and the performance can be potentially improved [33]. But due to the exclusive properties of satellite scenarios, terrestrial-NOMA resource optimization strategies may not be simply applied in SatCom. The main differences between terrestrial-NOMA and satellite-NOMA resource optimization are summarized as

follows:

- First, the channel propagation models in SatCom are distinctive. In a multi-beam satellite system, terminals located closely to each other have highly correlated channels, but meanwhile, these terminals with homogeneous receive antennas may have similar channel gains [34]. The strategy of pairing terminals with highly correlated channels and large channel gain difference is widely adopted in terrestrial multiple-input multiple/single-output (MIMO/MISO) systems [35, 36, 37, 38, 39, 40], but may not be suitable in satellite systems [41]. When the number of terminals exceeds two and terminals are with heterogeneous traffic demand, the grouping strategies could be more sophisticated. Another concern is weak receive signals and large propagation delay caused by long-distance transmission [2].

- Second, the characteristics of SatCom are different from terrestrial networks, which leads to new constraints [2], e.g., on-board power constraints, signal distortion, non-linearities of amplifiers, etc. Besides, the complexity issues might occur if we directly apply terrestrial-NOMA schemes in multi-beam satellite systems due to the existence of a large number of beams [34].

- Third, in SatCom, the targeted goals of resource management are different from those in terrestrial systems. For example, sum-rate/weighted-sum-rate maximization is widely discussed in terrestrial-NOMA systems, which aims at improving total throughput or proportional fairness [42, 43]. But this objective may not be practical in satellite systems. This is because sum-rate/weighted-sum-rate maximization ignores the influence of heterogeneous traffic distribution, which would cause severe capacity-traffic mismatch issues [44]. Thus, more practical goals specific to SatCom should be considered.

As new challenges arise when NOMA is applied, it is of great significance to investigate the design of resource allocation schemes for NOMA-based satellite systems.

1.3 Motivations and Research Questions

In SatCom, NOMA has proven its advantages in enhancing capcaity [41, 45] and outage rate [46], improving capability of supporting massive connectivity [47], guaranteeing fairness [48] and security [49], etc., which attracts studies on resource allocation for NOMA-based satellite systems. A detailed literature review will be provided in Chapter 2. However, resource allocation for satellite-NOMA systems is still not fully studied. To investigate the potential synergies of NOMA in satellite systems, we are motivated to enrich this line of studies in this dissertation. We aim at resolving the following three research questions.

Question 1: How to optimize resource allocation when NOMA is applied and how much performance gain can be obtained by enhancing power-domain flexibility compared to conventional schemes?

Early-attempt works mainly focused on studying resource optimization in NOMA-enabled satellite systems, where the applied performance metrics are targeted for general communication systems, e.g., capacity, outage rate, fairness, etc. But whether and how NOMA can help to enhance the performance metrics related to practical SatCom scenarios are unknown yet. As mentioned above, resource allocation with limited flexibility may not adapt to heterogeneous traffic distribution, leading to unnecessary unmet and unused capacity. To enhance the utilization of onboard resources, it is necessary to improve the match

between offered capacity and requested traffic. Thus, metrics that capture capacity-demand mismatch effects should be considered, e.g., offered-capacity-to-requested-traffic rate (OCTR) and capacity-demand gap. By augmenting power-domain flexibility, NOMA may have potentials to alleviate the capacity-demand mismatch. In this dissertation, we are going to investigate algorithmic design for resource allocation to reduce capacity-demand mismatch effects and fathom how much performance gain NOMA can bring to satellite systems.

Question 2: For complicated resource management, how to accelerate the decision-making procedure and achieve a good tradeoff between complexity reduction and performance improvement?

Regarding satellite-NOMA resource allocation, the typical optimization problems can be combinatorial with discrete decision variables, which are generally difficult to solve, even for small- or medium-scale instances. Approaches that can attain optimum or near-optimum would consume a large amount of computational efforts and time, which may not be desired for practical implementation. It is challenging to design efficient schemes that can speed up the decision-making process and achieve a good tradeoff between performance and complexity. The conventional way is to design model-based approaches under the analysis of convex optimization theory. As an alternative, we apply machine learning to assist the procedure of decision making. Compared to model-based approaches, data-driven learning techniques can exploit useful information from empirical data first, and approximate optimal decisions with less computational complexity. However, applying learning techniques to solve optimization problems may encounter some challenges, e.g., how to utilize the exploited information and guarantee the feasibility of the predicted solutions. In this dissertation, we attempt to address this open issue to enable an efficient resource allocation scheme for NOMA-satellite systems.

Question 3: What are the mutual impacts among multiple dimensions of resource optimization, and how to boost the underlying synergies of NOMA and exploit flexibilities in other domains?

As we discuss in Section 1.1, besides power domain, advanced satellite payloads offer flexibilities in other domains, e.g., time and spatial domains. Potential performance gain may be obtained by optimizing resource allocation with multi-dimension flexibilities. But it is unknown how NOMA can be coordinated with these techniques, e.g., BH with time-domain flexibility and adaptive beam patterns with spatial-domain flexibility, which requires investigation of the mutual impacts and underlying synergies of different domains. In the scenarios with the coexistence of NOMA and BH, for instance, the decision of beam illumination patterns is coupled with terminal-timeslot assignment and power allocation in the NOMA process, which may not be captured by mathematical expressions and is challenging to study.

1.4 Methodologies

Resource allocation can be modeled by mathematical languages and the corresponding optimization problems can be formulated. An optimization problem includes objective, parameters, variables, and constraints [50]. Before solving the resource optimization problems, the first step is to identify which category the formulated problem falls into (e.g., linear programming, convex programming, etc.) and reveal the implicit properties of the problem (e.g., non-deterministic polynomial-time (NP) hardness, monotonicity). Then we design approaches to find a feasible solution to the problem based on the convex optimization theory or from the perspective of machine learning.

1.4.1 Optimization-Based Approaches

Conventionally, we analyze the problem via convex optimization theory and employ optimization-based approaches to design algorithmic solutions. Compared to learning-assisted approaches, optimization-based approaches are with solid mathematical analysis, e.g., the guarantee of convergence, optimality or local optimality, Karush-Kuhn-Tucker (KKT) conditions, etc. [50]. The approaches can be designed with the assistance of mature optimization solvers, e.g., MOSEK [51], and widely-applied methods.

Due to the nonconvex expression of rate functions w.r.t. transmit power and the existence of integer variables, optimization problems for NOMA-based satellite systems can be in the format of mixed-integer nonconvex programming (MINCP) [42, 43, 52]. Solving MINCP is non-trivial in general, where the difficulty lies in tackling the nonconvexity and binary variables [53].

Nonconvex programming is more complicated than convex programming or linear programming due to the presence of several local optimums. Here we introduce some methods to tackle the nonconvexity in satellite-NOMA problems:

- In single-cell/beam NOMA scenarios, the nonconvex power allocation problem can be transformed into an equivalent convex rate assignment problem by a widely-used substitution approach [42]. In multi-beam satellite systems, we can apply this approach to reveal the implicit convexity of the problem and obtain the optimum via mature approaches for convex programming, e.g., interior-point method [54].

- Considering the properties of the rate function, the problem can be tackled by the fixed-point iteration method. For example, the max-min problem satisfying a set of certain conditions can be solved by Parron-Frobenius (PF) Theory based fixed-point iteration approach [55]. By tuning power iteratively, the fast convergence to the optimum can be guaranteed. Another instance is to apply the fixed-point iteration method to tackle fractional programming. In the rate function, the expression of signal-to-interference-plus-noise (SINR) is in a fractional format, which can be converted to a convex quadratic formulation. A stationary point can be obtained by iteratively solving a series of convex quadratic programming problems [56].

- The nonconvex problems can be tackled by convex approximation approaches, e.g., successive convex approximation (SCA) [57]. In SCA, we can at each iteration construct a convex problem that can tightly approximate the nonconvex problem at a local point. The problem can be solved by iteratively tackling a sequence of convex problems. SCA is widely applied to deal with complex nonconvex problems due to its simplicity of implementation.

- For more complicated problems with the presence of a large number of variables, we can apply the idea of the block coordinate descent (BCD) method [58]. In BCD, the variable set can be divided into several mutually exclusive blocks. The original problem can be decomposed into multiple subproblems, where each subproblem is only with a subset of variables and thus is simpler compared to the original problem. Compared to directly tackling the difficult problem, BCD is much easier to implement by iteratively solving smaller-scale subproblems. Moreover, BCD can be executed in a distributed way.

In the decision-making procedure, the optimal integer solution can be found via exhaustive search but with exponential-time complexity [59], which cannot be realized in practical scenarios. Some alternative methods can be considered to accelerate the decision-making procedure and reduce the computational complexity and time:

- Branch-and-bound approach is a popular method, which can find the optimal integer solutions to mixed-integer linear programming (MILP). The typical branch-and-bound approach performs in

a tree structure [60]. In the branching stage, an integer variable is branched into several possible nodes, where each node refers to a potential solution. At each node, the unexplored integer variables are relaxed and a continuous subproblem is solved. Based on the optimums to these subproblems, the upper and lower bounds to the original problem can be obtained. In the bounding stage, the nodes beyond the bounding range, which do not contain the optimal solution, will be pruned. The operation of pruning reduces the search space of solutions and thus leads to smaller complexity compared to the exhaustive search method. Together with the outer-approximation approach, the branch-and-bound approach can be extended to solving mixed-integer convex programming (MICP) with the performance guarantee [53]. Furthermore, since the branch-and-bound approach is powerful in achieving the optimum/near-optimum of MILP/MICP, it is widely adopted in optimization solvers, e.g., Gurobi [61] and MOSEK [51]. However, the branch-and-bound approach may exhaustively search all the potential integer solutions in the worst case, which could lead to cumbersome computation in solving medium-/large-scale problems.

- The integer part of the problem can be reformulated as a typical game problem, e.g., matching problem [62]. In the past few years, matching theory becomes a hot topic to tackle the optimization problems in wireless networks, e.g., user association and subcarrier scheduling [63]. In one-to-one/many matching problems, each player formulates a preference list. Players from one side propose a matching request to the players from the other side based on the list. Then players from the other side decide to accept/reject the requests according to the priority in the preference list. In the end, the two-sided exchange stability can be achieved. In many-to-many matching problems, the operation of swapping matching pairs is adopted to iteratively improve the utility of the problem.

- Relaxation of integer variables can simplify the decision-making process by transforming mixed-integer problems into continuous problems. The complexity can be reduced by solving a continuous problem instead of directly tackling a mixed-integer problem. Several heuristic approaches can be applied to obtain integer solutions. For instance, rounding is one of the widely-used methods [64]. The obtained continuous solutions can be rounded to the nearest integer values. Besides, we can penalize the objective if the relaxed variables are not integer [65].

1.4.2 Learning-Assisted Approaches

Optimization-based approaches are based on theoretical analysis to reveal the internal properties of the targeted problems, which, however, may not be a trivial task in general, especially for the problems involving decision making. Methods like the branch-and-bound approach may consume a large amount of computational efforts and time in attaining the optimum or near-optimum. Alternatively, we can tackle the difficult part of the mixed-integer problem from the angle of learning. Different from optimization-based approaches, data-driven machine learning techniques can first exploit useful information from empirical data and then approximate the optimal decisions with much smaller computational complexity [66].

Supervised learning, as one of the main subcategories of machine learning, can excavate the implicit information of labeled data sets to train a learning model to classify or predict data within a short period [67]. Thereinto, deep learning (DL) techniques, which imitate the structure of human brains to acquire knowledge, have received tremendous attention due to their advantages in handling a huge amount of data [68]. DL has proven its advantages in several learning tasks, e.g., classification, regression, complex function approximation, etc. [68, 69]. By treating part of the algorithmic framework as a black box, deep neural networks (DNN) can be employed to learn the underlying relationships between input and output

instead of performing the algorithmic operations [69, 70]. With a well-trained DNN, a good trade-off between complexity reduction and performance guarantee can be achieved.

However, DL may not be directly applicable to sophisticated mixed-integer optimization problems. End-to-end learning, for example, predicts the optimal integer solution in a straightforward way [66], which can be applied to problems with simple constraints or unconstrained problems. But for problems with more complex structures, end-to-end learning may not perform well since imperfect prediction will lead to dissatisfaction of some constraints and thus causes the infeasibility issue. It is essential to identify whether the predicted solution is feasible or not and to obtain a near-optimal feasible solution efficiency. How to design a learning-assisted approach to appropriately address the feasibility issues and achieve a good trade-off between complexity and performance is non-trivial, and requires careful design in a tailored way.

1.5 Contributions and Related Publications

In this dissertation, we aim at providing answers to the three research questions as summarized in Section 1.3 and investigate the exploitation of single- and multi-dimension flexibilities and resource optimization for NONA-based satellite systems. The contributions are summarized as follows:

Chapter 2

We first provide a literature review of state-of-the-art flexible resource allocation schemes in SatCom. Then we review related works on resource management in terrestrial-NOMA and satellite-NOMA systems. At last, we discuss the limitations of related works.

Chapter 3

We address **Question 1** in this chapter and design an optimization framework to enable efficient resource allocation in general NOMA-enabled multi-beam satellite systems. Concerning practical metrics of capacity-demand mismatch in satellite systems, we investigate joint optimization of power allocation, decoding orders, and terminal-timeslot assignment to improve the max-min fairness of the offered-capacity-to-requested-traffic ratio (OCTR). The problem is identified as a MINCP problem, which is challenging in general. We provide an optimal fast-convergence algorithmic framework of power allocation and decoding-order decision under fixed terminal-timeslot assignment. Based on the framework, we design a heuristic scheme for the considered joint optimization problem, which iteratively updates terminal-timeslot assignment and recoding vectors, and improves the overall OCTR performance. Numerical results demonstrate that the performance gain of the proposed NOMA scheme in matching capacity to demand compared to the conventional OMA scheme.

Related publications:

[J1] **A. Wang**, L. Lei, E. Lagunas, A. I. Pérez-Neira, S. Chatzinotas, and B. Ottersten, "NOMA-enabled multi-beam satellite systems: Joint optimization to overcome offered-requested data mismatches," *IEEE Transactions on Vehicular Technology (TVT)*, vol. 70, no. 1, pp. 900-913, Jan. 2021, doi: 10.1109/TVT.2020.3047453.

[C1] **A. Wang**, L. Lei, E. Lagunas, A. I. Pérez-Neira, S. Chatzinotas, and B. Ottersten, "On fairness optimization for NOMA-enabled multi-beam satellite systems," in *Proc. IEEE 30th Annual Inter-*

national Symposium on Personal, Indoor and Mobile Radio Communications (PIMRC), 2019, pp. 1–6, doi: 10.1109/PIMRC.2019.8904429.

Chapter 4

In Chapter 4, we aim to answer **Question 2** with an attempt to tackle the resource allocation problem in satellite-NOMA systems from the perspective of learning. To accelerate the decision-making procedure in mixed-integer programming problems, we introduce DNN to predict integer variables and design learning-assisted optimization schemes to jointly optimize power allocation and terminal-timeslot assignment. To address the feasibility issues of end-to-end learning, we provide a post-processing approach and a dual-DNN approach to improve the feasibility ratio. The proposed learning-optimization schemes achieve a good trade-off between complexity and performance compared to the optimal/near-optimal solution and other benchmarks. Besides, we discuss the pros and cons of learning-based and optimization-based approaches in tackling mixed-integer problems.

Related publications:

[J2] **A. Wang**, L. Lei, E. Lagunas, S. Chatzinotas, and B. Ottersten. "Completion time minimization in NOMA systems: Learning for combinatorial optimization," *IEEE Networking Letters*, vol. 3, no. 1, pp. 15-18, Mar. 2021, doi: 10.1109/LNET.2021.3052891.

[C2] **A. Wang**, L. Lei, E. Lagunas, S. Chatzinotas, and B. Ottersten, "Dual-DNN assisted optimization for efficient resource scheduling in NOMA-enabled satellite systems," in *Proc. 2021 IEEE Global Communications Conference (GLOBECOM)*, 2021, pp. 1-6, doi: 10.1109/GLOBECOM46510. 2021.9685660.

Chapter 5

Both Chapter 5 and Chapter 6 focus on resolving **Question 3** by exploiting multi-dimension flexibilities. From the time-domain perspective, BH is promising to mitigate the capacity-demand mismatch effects and inter-beam interference by selectively and sequentially illuminating different subsets of beams over timeslots. Motivated by this, in Chapter 5, we investigate the potential synergies and mutual influence between NOMA and BH in multi-beam satellite systems and study flexible resource allocation in power and time domains. We jointly optimize power allocation, beam scheduling, and terminal-timeslot assignment to minimize the gap between offered capacity and requested demand. The global optimum may not be achieved due to the NP-hardness of the problem. We develop a bounding scheme to tightly gauge the global optimum and propose a suboptimal algorithm to enable efficient resource assignment. Numerical results demonstrate the benefits of combining NOMA and BH and validate the superiority of the proposed BH-NOMA schemes over conventional BH and OMA schemes.

Related publications:

[J3] **A. Wang**, L. Lei, E. Lagunas, A. I. Pérez-Neira, S. Chatzinotas, and B. Ottersten, "Joint optimization of beam-hopping design and NOMA-assisted transmission for flexible satellite systems." Accepted by *IEEE Transaction on Wireless Communications (TWC)*.

[C3] **A. Wang**, L. Lei, E. Lagunas, S. Chatzinotas, A. I. Pérez-Neira, and B. Ottersten, "Joint beam-hopping scheduling and power allocation in NOMA-assisted satellite systems," in *Proc. 2021 IEEE Wireless Communications and Networking Conference (WCNC)*, 2021, pp. 1-6, doi: 10. 1109/WCNC49053. 2021.9417306.

Chapter 6

In this chapter, we provide an analytical response to **Question 3** by exploiting spatial- and time-domain flexibilities. In the spatial domain, adaptive beam patterns can adjust the beam coverage to serve irregular traffic demand and alleviate co-channel interference. For performance improvement, adaptive beam patterns are introduced in NOMA-based low earth orbit (LEO) satellite systems. We investigate resource allocation with the coordination of power- and spatial-domain flexibilities. We formulate a joint optimization problem of power allocation, beam pattern selection, and terminal association. Due to the coupling between NOMA and adaptive beam patterns, the corresponding algorithmic design is challenging. To ease the discrete and nonconvex properties, we design an algorithmic framework for joint optimization. To reduce the complexity of the joint approach, we analyze the implicit characteristics via a special case and put forward a low-complexity scheme based on the analysis. Numerical results show the advantages of jointly optimizing NOMA and beam pattern selection compared to conventional schemes.

Related publications:

[J4] **A. Wang**, L. Lei, X. Hu, E. Lagunas, A. I. Pérez-Neira, and S. Chatzinotas, "Joint optimization of adaptive beam patterns and NOMA for LEO satellite systems: Exploitation of power- and spatial-domain flexibilities." To be submitted to *IEEE Transaction on Wireless Communications (TWC)*.

[C4] **A. Wang**, L. Lei, X. Hu, E. Lagunas, A. I. Pérez-Neira, and S. Chatzinotas, "Joint optimization of NOMA and adaptive beam patterns in LEO satellite systems," submitted to *2022 IEEE Global Communications Conference (GLOBECOM)*.

Chapter 7

In the final chapter, we conclude the dissertation by summarizing the contributions and discussing potential future directions.

Chapter 2

Literature Review

In this chapter, we first provide a literature survey for general flexible resource allocation schemes in satellite systems. Next, we review the works of state-of-the-art resource allocation schemes for terrestrial-NOMA and satellite-NOMA systems. Finally, we summarize the limitations of related works beyond the state-of-the-art.

2.1 Flexible Resource Allocation in Satellite Systems

Thanks to the development of satellite payloads, flexibilities in resource allocation are introduced to satellite systems for performance improvement. How to manage flexibilities in single or multiple domains becomes a challenging task. Related works of flexible resource optimization in SatCom are summarized in Table 2.1.

Flexible power allocation provides an opportunity to adjust transmit power to adapt to dynamic variation of channel conditions and traffic demands, instead of being uniformly distributed to beams/carriers. To improve the adaptation to channel variation caused by unstable weather conditions, the authors in [71] and [72] investigated the design of dynamic power allocation schemes to minimize the number of non-served terminals. But the change of channel conditions is not the only factor influencing the transmission quality in SatCom. Concerning the impacts of traffic demands and channel conditions, the authors in [44] optimized power allocation to minimize the gap between capacity and demand to enhance the utilization of on-board resources in multi-beam satellite systems. However, the coupling among beams raised by co-channel interference, which can generally complicate the resource optimization problems, was not included in those early-attempt works. To tackle the difficulty in optimization brought by co-channel interference, the authors in [21] and [16] designed flexible power allocation schemes to minimize unmet capacity and power consumption. From the perspective of dynamic games, the authors in [73] proposed a novel market-based power allocation scheme to ease the impacts of co-channel interference. Besides, a deep reinforcement learning (DRL) framework was designed in [74] for continuous power optimization. Further, in [75], the authors discussed the implementation and evaluated the performance of several popular artificial algorithms in solving power optimization problems.

As frequency-domain flexibility was introduced, flexible bandwidth/carrier allocation became an open issue. To reduce the capacity-demand gap, the authors in [76] moved from power to frequency domain and proposed a flexible bandwidth allocation scheme based on channel conditions and traffic demands. The work in [77] provided a comprehensive discussion of bandwidth allocation strategies when different fairness metrics are considered. In [78], the authors optimized bandwidth allocation to reduce

Table 2.1: Related works of flexible resource allocation in SatCom (Power, frequency, time, and spatial are simplified as P., F., T., and S.)

Ref.	Objective	Flexibility			
		P.	F.	T.	S.
[71, 72]	Min the number of non-served terminals	√			
[44]	Min capacity-demand gap	√			
[21, 16, 74, 75]	Min unmet capacity and power consumption	√			
[73]	Max payoff function	√			
[76]	Min capacity-demand gap		√		
[77]	Max fairness (different metrics)		√		
[78]	Min packet loss and power consumption		√		
[79]	Max throughput		√		
[80, 81]	Min capacity-demand gap	√	√		
[82]	Max throughput	√	√		
[10]	Max satisfaction-gap objective	√	√		
[83]	Min the number of occupied carriers and power consumption	√	√		
[24]	Max throughput and min power consumption			√	
[84]	Max throughput			√	
[85]	Max-min OCTR			√	
[86]	Min delay, max throughput, min delay fairness			√	
[87]	Min capacity-demand gap, coverage error, and cost				√
[26]	Max fair distribution of demand				√
[27]	Max SNR and min interference to terrestrial networks				√
[88]	Max OCTR, min capacity-demand gap		√	√	
[89]	Max traffic accommodation rate	√			√
[90]	Max throughput and delay fairness	√	√	√	
[91]	Min capacity-demand gap, EIRP, and used bandwidth	√	√		√

packet loss and transmit power consumption. In [79], frequency-domain flexibility was further exploited, where the underlying interplay of bandwidth adjustment between adjacent beams was investigated.

In addition, growing attention has been drawn to the exploitation of power- and frequency-domain flexibilities for more performance gain. Power and bandwidth allocation was optimized to improve the rate matching to demand in [80], but without the discussion of the influence of inter-beam interference. In [81], inter-beam interference was introduced, where a more complicated joint optimization problem was studied. Regarding the transmission of real-time and non-real-time services, the authors in [82] proposed a scheme of power and bandwidth allocation to maximize the throughput. The authors in [10] discussed the practical implementation of flexible resource management in realistic satellite payloads and digital video broadcasting-satellite-second generation (DVB-S2) standard, and designed a scheme of power and bandwidth allocation to reduce the capacity-demand gap and improve the fairness. Further in [83], the authors jointly optimized power and carrier assignment to minimize the number of occupied carriers and power consumption while satisfying terminals' traffic demands.

In the time domain, the major task is to optimize the scheduling of timeslots to terminals/beams. BH technique is a typical application of time-domain flexibility. In [92], practical implementation of BH was discussed and the benefits of BH were demonstrated via performance evaluation compared with several conventional resource allocation schemes. In general, the BH optimization problems involve

the decision of beam illumination, which are with challenging combinatorial properties. Considering the difficulty of optimizing beam illumination patterns, the authors in [24] proposed a genetic-based approach to maximize the capacity and minimize the power consumption. In [84], iterative algorithms based on minimal co-channel interference (MinCCI) and maximal SINR (MaxSINR) were proposed to maximize capacity. Moreover, considering the potential benefits of machine learning, the authors in [85, 86] applied DL or DRL to tackle the BH optimization problems and accelerate the decision of beam scheduling. The advantages of learning-assisted schemes in tackling combinatorial problems were verified with the comparison of traditional optimization-based approaches.

The technique of adaptive beam patterns, with the capability of changing beam shapes, is promising to facilitate spatial-domain flexibility [93, 94] to embrace the challenges of heterogeneous traffic distribution in satellite systems. In [87, 26], the authors investigated the multiple factors that can affect the beam shapes, e.g., beamwidth, beam center position, and tilt angle, and designed footprint optimization schemes to match capacity to irregular traffic distribution. The authors in [28] proposed to adjust the beam size to support different configurations in different networks for better integration of terrestrial cellular networks and NTN. In [27], an adaptive beam control scheme was designed to minimize the co-channel interference from LEO satellites to terrestrial systems.

Compared to single-domain flexibility, resource optimization based on multiple dimensions offers more space for performance enhancement but is more complicated with the intrinsic mutual influence among techniques in different domains. The sophisticated duality between frequency- and time-domain flexibilities was analyzed in [88]. In [89], the authors studied the optimization trade-off between beam size and transmit power. However, the interplay among different domains is not easy to reveal through conventional optimization-based approaches. Learning might be an alternative to ease the problem solving by viewing the input/output relationships as a black box and exploiting useful information from empirical data. In [90], multi-agent deep reinforcement learning was applied to jointly optimize beam hopping and bandwidth allocation. To accommodate flexibilities in power, bandwidth, and spatial domains, the authors in [91] applied multi-agent deep reinforcement learning to solve a multi-objective problem to minimize the capacity-demand gap, effective isotropic radiated power (EIRP), and occupied bandwidth.

2.2 NOMA-Based Resource Allocation in Terrestrial Systems

NOMA is superior to conventional OMA in many aspects, e.g., providing enhanced spectral efficiency, supporting massive connectivity, reduced transmission latency and signaling cost, etc. [32, 31], which attract investigations on NOMA-based resource allocation in terrestrial systems.

NOMA-based optimization problems are generally related to power allocation and user grouping (or scheduling). In the early attempts, power allocation strategy is designed simple. Power can be split based on a pre-determined policy [95], e.g., fairness-aware fraction transmit power control (FTPC) strategy [96]. These power allocation strategies can provide performance benchmarks for NOMA-based resource optimization design. Regarding user grouping, the authors in [97] provided preliminary insights on user pairing strategies in NOMA, where two typical scenarios were discussed, i.e., fixed power allocation NOMA (F-NOMA) and cognitive-radio-inspired NOMA (CR-NOMA). It was shown that F-NOMA would follow the best-worst pairing policy whereas CR-NOMA tends to pair the best-channel user with the second-best-channel user. In [98], the rate-maximization problem was decomposed into two subproblems: user grouping and power allocation. The low-complexity strategies of user grouping in uplink and downlink NOMA were further analyzed. Intuitively, the best-worst pairing policy is deemed as a beneficial method to facilitate NOMA in some simple scenarios since large channel gain difference can augment the performance gap between NOMA and OMA [99]. For its simplicity, best-worst pairing is

one of the widely-adopted strategies to simplify the problem solving or to be viewed as a benchmark for performance comparison.

To exploit more performance gain, joint optimization of user scheduling and power allocation is further investigated. Dealing with NOMA-based resource optimization problems is challenging due to the nonconvex expression of the rate functions and combinatorial properties of the user scheduling (decision-making) part. In some cases, the NP-hardness of the problems has been proven [42, 100, 43]. The optimal solutions to these problems in general cases cannot be obtained in polynomial time unless P=NP. In [101], the convexity of the resource allocation problems in single-cell NOMA scenarios was revealed by transforming the rate function into an equivalent power function. To achieve the near-optimum, the authors in [42] proposed an efficient power and subchannel allocation scheme based on Lagrangian duality and dynamic programming. In [43], the authors reformulated the subchannel-user scheduling subproblem as a many-to-many matching problem and designed a swap-matching-based strategy. The authors in [102] developed the optimal solution of joint power and subcarrier allocation problems in full-duplex multi-carrier systems via monotonic optimization. To reduce the complexity, an iterative CSA-based approach was proposed. In [52], the authors went deeper in this direction and provided theoretical algorithmic designs of optimal, approximate, and heuristic schemes to solve these NP-hard problems.

Apart from general NOMA systems, researchers studied NOMA applications in multi-antenna scenarios and fathomed the interplay between NOMA and MIMO/MISO techniques [103]. In [104, 102, 105, 106], NOMA was employed to exploit spatial-dimension flexibility. The synergy of NOMA and precoding techniques in non-overloaded systems was investigated, where the number of users is smaller than that of transmit antennas. In such systems, NOMA can bring performance gain but the applicability is limited when the number of users is large due to the potential error propagation and complexity issues in the SIC process. NOMA is not good at exploiting spatial-domain flexibility compared to MIMO/MISO techniques [103]. However, NOMA seems more suitable to support the transmission in overloaded systems where users are more than transmit antennas. In this context, NOMA is applied to enhance the power-domain flexibility within each beam to multiplex more than one user and mitigate intra-beam interference whereas precoding is employed among beams to alleviate inter-beam interference, which is a widely-adopted approach [35, 36, 37, 38, 39, 40]. The joint optimization of NOMA strategies (involving power allocation and user grouping/pairing) is challenging in multi-beam systems. To simplify the decision-making process, the idea of grouping/pairing users with highly-correlated channels and large channel gain difference is widely used [35, 37, 38, 40, 107], which can efficiently reduce inter-beam interference while guaranteeing performance gain in each beam over OMA.

As discussed in Chapter 1, terrestrial-NOMA schemes may not be directly applied to satellite-NOMA systems due to the distinctive features of satellite systems. Different channel propagation models call for the specific design of satellite-NOMA resource allocation. For instance, the authors in [41] found that, in multi-beam satellite systems, pairing terminals with highly correlated channels and smallest channel gain difference outperforms the other two schemes, i.e., pairing terminals with lowest Euclidean distance and pairing terminals with highly correlated channels and largest channel gain difference. This result may not be consistent with terrestrial-NOMA systems. When the number of terminals in each beam exceeds two and terminals request heterogeneous traffic demand, the grouping strategies would be more sophisticated. Besides, distinctive constraints and targeted metrics bring new challenges, e.g., the objective related to the matching between offered capacity and requested traffic is unusual in terrestrial systems but practical in SatCom.

2.3 NOMA-Based Resource Allocation in SatCom

The potential applicability and performance improvement of NOMA in satellite systems have been analyzed in many works [108, 109, 34, 33, 110, 111]. The authors in [108] analyzed the performance evaluated by general metrics, e.g., ergodic capacity, energy efficiency, outage probability, and average symbol error rate, in a NOMA-based satellite system. The numerical results verified the performance gain compared to conventional OMA. In [109], the authors discussed the practical implementation of NOMA in the DVB-S2X standard. Besides, considering that the performance of NOMA in SatCom could be limited by inevident channel gain difference within the beam coverage, the work demonstrated that the heterogeneity in terminals' antennas could be advantageous to performance improvement. In [34], the applicability of NOMA in multi-beam satellite systems was analyzed. The authors also envisioned some open challenges of NOMA schemes coordinated with precoding and frequency reuse patterns. In [33], NOMA applications in several typical scenarios, e.g., cognitive satellite-terrestrial systems and cooperative satellite/terrestrial relay systems, were discussed. In [110], NOMA was introduced to an integrated satellite-terrestrial system with dual satellites to improve capacity and fairness. Furthermore, a realistic NOMA-based satellite system for delivering mMTC services was described in [111]. The implementation of NOMA in practical SatCom was demonstrated and the bright future of satellite-NOMA systems was envisioned.

With proven power-domain enhancement, researchers started to focus on resource optimization in NOMA-enabled satellite systems to embrace the requirements of high throughput and massive connectivity for next-generation HTS. We summarize the related works of satellite-NOMA resource allocation in Table 2.2. In multi-beam satellite systems, especially the ones with the full frequency reuse (FFR) pattern and over-loaded transmission, co-channel interference could largely deteriorate the system performance. NOMA can be applied in each beam to reduce part of intra-beam interference and accommodate more terminals. Towards this end, the authors in [112] and [47] optimized power allocation to maximize capacity and the number of associated terminals, respectively, while guaranteeing the quality of service (QoS) requirements. To achieve the network stability, the authors in [113] designed a particle swarm optimization based approach to optimize power allocation for NOMA-based satellite internet of things (IoT) services. But more generally, NOMA is coordinated with precoding for additional performance gain, where NOMA and precoding target at intra-beam and inter-beam interference mitigation, respectively. In [41], the authors discussed strategies of terminal scheduling when NOMA is coordinated with precoding and found that scheduling strategies in SatCom could be different from that in terrestrial systems. To tackle the issues of imperfect channel state information (CSI), robust design of precoding schemes were studied in [114] and [48]. Considering practical SatCom scenarios with multiple gateways, the authors in [115] proposed a distributed strategy to optimize precoding and power allocation. In [45], precoding vectors and power allocation were optimized for rate maximization in a NOMA-based massive MIMO satellite system.

With the trend of satellite-terrestrial integration in future beyond 5G and 6G, NOMA is also widely studied in hybrid/integrated satellite-terrestrial networks. In [107, 116, 117], the authors optimized precoding vectors, power allocation, and user pairing/association for NOMA-based satellite-terrestrial integrated networks. In [118], the authors focused on completion time minimization in NOMA-based LEO satellite-terrestrial integrated networks. In the above works, the satellite served as a supplemental component to terrestrial systems where NOMA was not applied in the satellite part. Considering NOMA at both terrestrial and satellite sides, NOMA was designed to cooperate with bandwidth compression in satellite-terrestrial integrated systems in [119]. To alleviate severe co-channel interference, the authors designed a novel NOMA scheme with iterative SIC and symmetrical coding. In [120], joint optimization of power allocation, user association, and bandwidth assignment was investigated in an uplink NOMA-

Table 2.2: Related works of NOMA-based resoure allocation in SatCom

Ref.	Scenario	Target
[112]	Satellite IoT (further integrated with terrestrial IoT)	Power allocation to max capacity with QoS guarantee
[47]	Satellite systems	Joint power allocation and admission control to max the number of associated terminals
[113]	LEO Satellite IoT	Joint network stability and power allocation to max long-term network utility
[41]	Satellite systems	Terminal scheduling to max capacity
[114]	LEO satellite IoT	Robust beamforming design to min power for long-term QoS
[48]	Satellite systems	Robust beamforming design to max α-fairness for long-term QoS
[115]	Multi-gateway multi-beam satellite systems	Distributed approach to power allocation, terminal scheduling, and precoding design
[45]	LEO satellite systems with massive MIMO	Joint precoding design and power allocation to max sum rate
[107]	Satellite-terrestrial integrated networks (NOMA in terrestrial part)	Precoding design, user pairing, and power allocation to max total capacity
[116]	Satellite-terrestrial integrated networks (NOMA in terrestrial part)	User pairing design and joint optimization of precoding and power allocation to max total capacity
[117]	Satellite-terrestrial integrated networks (NOMA in terrestrial part)	Precoding design, user pairing, and power allocation to max energy efficiency
[118]	LEO satellite-terrestrial integrated networks (NOMA in terrestrial part)	Jointly optimizing power allocation, cooperative data, and subcarrier assignment to min completion time
[119]	Hybrid satellite-terrestrial networks	NOMA cooperates with bandwidth compression to mitigate interference and improve spectral efficiency
[120]	Satellite-terrestrial integrated networks	Jointly optimizing power allocation, user association, and bandwidth assignment to max capacity and min cross-tier interference

based satellite-terrestrial integrated system with caching. Furthermore, NOMA applications have been extended to space-air-ground integrated networks, e.g., [121] and [122].

Considering the difficulty of satellite-NOMA resource optimization, learning techniques enrich the methodology in solution development. In [123], DL was applied in satellite-IoT systems to approximate the implicit mapping between queue size + channel gain and decoding order and predict the optimal decoding order for the SIC process in NOMA. To deal with the nonconvexity in the formulated problem, the authors in [124] employed DRL to speed up the optimization of power allocation. Besides, support vector machine (SVM) was adopted to tackle the issues raised by imperfect CSI and achieve high efficiency in user pairing [125].

We summarize the limitations of recent works on satellite-NOMA resource allocation schemes:

- As discussed in Chapter 1, the performance metrics and targeted objectives for practical satellite systems are different from those widely-used in terrestrial systems. Objective metrics like sum-rate maximization [42, 100, 43], power minimization [101], and energy efficiency [126] have already

been fully discussed in terrestrial networks, which, however, neglect the influence of capacity-demand mismatch in satellite systems. This may cause severe waste and low utilization of on-board resources. Metrics specific for SatCom, e.g., OCTR and capacity-demand gap, should be considered in the design of satellite-NOMA schemes. However, in the literature, the study on NOMA-based resource allocation to optimize these practical SatCom metrics is limited.

- Resource optimization problems for satellite-NOMA systems are difficult in general, especially the ones with combinatorial properties. Most of the related works focused on algorithmic design based on optimization theory, e.g., the ones summarized in Table 2.2. In [123, 124, 125], machine learning was employed to assist the problem solving, which demonstrated the efficiency of the learning-assisted method. However, how learning helps to solve problems in satellite-NOMA systems and deliver an efficient solution has not been fully investigated yet. A challenging issue is to fathom how to guarantee the feasibility of the predicted integer solutions to a complicated satellite-NOMA resource optimization problem.

- The exploitation of multi-dimension flexibilities has been discussed for many years, e.g., joint optimization for power- and frequency-domain flexibilities. Besides, the cooperation of NOMA in the power domain and bandwidth compression in the frequency domain was investigated in [119]. But the synergy investigation of NOMA and SatCom techniques, e.g., BH with time-domain flexibility and adaptive beam patterns with spatial-domain flexibility, is in the stage of early attempt. How to accommodate multi-dimension flexibilities and design efficient resource optimization schemes is an open challenge.

Chapter 3

Resource Optimization based on Power-Domain Flexibility

This chapter provides a resource optimization paradigm for general NOMA-enabled multi-beam satellite systems, where NOMA is adopted to enhance power-domain flexibility. We investigate whether NOMA can help to improve the matching between offered capacity and requested demand and how much gain can be obtained when NOMA is applied. Towards this end, we formulate a problem of jointly optimizing power allocation, decoding orders, and terminal-timeslot assignment to maximize the worst OCTR among terminals. To solve the challenging problem, we design an algorithmic framework to jointly allocate power and decide decoding orders, with the guarantee of optimality and convergence. Based on the framework, a heuristic scheme is proposed to solve the original joint problem, which iteratively updates terminal-timeslot assignment and precoding vectors to further enhance the minimum OCTR. Numerical results demonstrate the convergence of the algorithmic framework and the advantages of the proposed NOMA schemes in matching offered capacity to traffic demand compared to the conventional OMA scheme. Besides, we verify the applicability of the proposed NOMA schemes in some practical scenarios.

3.1 Introduction

A multi-beam satellite system provides wireless services to wide-range areas. On the one hand, traffic distribution is typically asymmetric among beams [12]. On the other hand, satellite capacity is restricted by practical aspects, e.g., payload design, limited flexibility in resource management, and tended to be fixed before launch [2]. The asymmetric traffic and the predesigned capacity could result in mismatches between requested traffic and offered capacity [127], i.e., hot beams with unmet traffic demand or cold beams with unused capacity [10]. Both cases are undesirable for satellite operators, which motivates the investigation of flexible resource allocation to reduce the mismatches for future multi-beam satellite systems.

In terrestrial systems, NOMA has demonstrated its superiority, e.g., in throughput, energy, fairness, etc., [128, 31], over OMA. By performing superposition coding at the transmitter side, more than one terminal's signal can be superimposed with different levels of transmit power and broadcast to co-channel allocated terminals. At the receiver side, SIC is performed. In this way, NOMA is capable of alleviating co-channel interference, accommodating more terminals, and improving spectral efficiency [31].

The authors in [110, 41, 34, 33] analyzed the applicability of integrating NOMA to satellite sys-

tems. In [110], NOMA was applied in satellite-terrestrial integrated systems to improve capacity and fairness. NOMA was considered in multi-beam satellite systems in [41, 34], where precoding, power allocation, and user grouping schemes were studied to maximize the capacity. In [33], the authors provided an overview for applying NOMA to satellite networks. Under a single-beam scenario, the authors in [108, 129] analyzed outage performance for satellite-NOMA. In [108], a comprehensive study on outage probability, capacity, and energy efficiency for a NOMA-based land mobile satellite network was provided. In [129], the outage performance of a NOMA-based satellite network was investigated in the cases of perfect and imperfect SIC.

In the literature, resource optimization for NOMA-enabled multi-beam satellite systems is studied to a limited extent. First, the study of integration between NOMA and the satellite is limited, e.g., [107, 116], where the satellite is functioned as a supplemental component. In both works, NOMA was applied to the terrestrial systems but not to the satellite component. Second, the previous satellite-NOMA works commonly adopted general terrestrial-oriented metrics, e.g., capacity [110, 41], fairness [110], and outage probability [108, 129]. Nevertheless, practical and featured metrics for multi-beam satellite systems, e.g., mismatches between requested traffic and offered capacity, have not been fully discussed. Third, for NOMA-enabled multi-beam satellite systems, how to derive an appropriate decoding order which is coupling with the beam-power variations, needs to be addressed. The authors in [112] studied power optimization to reduce the traffic-capacity mismatch for NOMA-based multi-beam satellite systems, with adopting a predefined and fixed decoding order, thus simplifying the power allocation. In practical scenarios, decoding orders may change when beam power is adjusted [130]. Therefore, it is important to optimize decoding orders for multi-beam satellite systems since an inappropriate decoding order can result in unsuccessful SIC and thus performance degradation. In this chapter, we consider a full frequency reuse system, where inter-beam interference is mitigated via precoding while NOMA is applied to reduce intra-beam interference within a beam.

3.1.1 Challenges and Contributions

In general, resource allocation schemes for terrestrial multi-antenna NOMA systems may not be directly applied to multi-beam satellite systems [2, 34]. For instance, terminals with highly correlated channels and large channel-gain difference are favorable to be grouped to mitigate inter-beam and intra-beam interference by precoding and NOMA, respectively [38, 35, 40]. Such desired terminal groups or pairs can be observed in terrestrial-NOMA systems but might not be easily obtained in satellite scenarios. In addition, channel models, payload design, and on-board limitations could render resource optimization in satellite-NOMA systems more challenging than terrestrial-NOMA systems [21].

In the literature, how NOMA can help to improve the performance of the practical metric, OCTR [10], has not been fully studied. In this chapter, we focus on jointly optimizing power, decoding orders, and terminal-timeslot assignment in multi-beam satellite systems to improve the performance of OCTR. The main contributions are summarized as follows:

- We formulate a max-min resource allocation problem to jointly optimize power allocation, decoding orders, and terminal-timeslot assignment, such that the lowest OCTR among terminals can be maximized. The problem falls into the domain of combinatorial non-convex programming, which brings more performance gain in OCTR but is more challenging compared to our previous work [131].

- Unlike previous studies, we develop a simple approach to circumvent the difficulties in jointly optimizing undetermined optimal decoding order and undetermined rate-function expressions based on the derived theoretical analysis.

- By fixing the terminal-timeslot assignment, we augment the power-tune solution in [131] and propose a PF theory based approach to solve the remaining problem, i.e., jointly optimizing power allocation and decoding orders (JOPD). We also provide theoretical results to prove that the approach is with guaranteed fast convergence to the optimum. The fixed terminal-timeslot assignment is determined by grouping the terminals with maximum channel correlation (MaxCC).

- We provide a complete algorithmic solution for the considered joint optimization problem. Under the framework of JOPD, we develop a heuristic algorithm to jointly optimizing power allocation, decoding orders, and terminal-timeslot scheduling (JOPDT), which iteratively updates terminal-timeslot assignment and precoding vectors, and improves the overall OCTR performance. JOPDT aims at providing benchmarks and upper bounds for JOPD.

- The numerical results, firstly, verify the fast convergence of JOPD. Secondly, we show the OCTR performance gain of NOMA over OMA in the two proposed NOMA-based schemes, i.e., JOPD + MaxCC (with lower complexity) and JOPDT (with higher complexity). Thirdly, we compare the performance of the max-min OCTR objective with another widely-used objective. Lastly, we evaluate the OCTR performance in the scenarios with practical consideration, e.g., atmospheric-fading effects and SIC imperfection, to demonstrate the applicability of the proposed algorithms to more practical scenarios.

3.2 System Model

3.2.1 A Multi-Beam Satellite System

We consider the forward-link transmission in a multi-beam satellite system, where a geostationary earth orbit (GEO) satellite is equipped with an array-fed reflector antenna to generate B spot beams. The satellite provides fixed services to ground terminals. Each terminal is equipped with a single antenna. We denote $\mathcal{B} = \{1, \ldots, B\}$ as the set of the beams. One feed per beam is implemented in the system and the index of a feed is assumed to be consistent with that of the beam it serves. We follow a typical scenario in satellite systems, e.g., [12, 2, 10, 41], as shown in Fig. 6.3. The motivation is to facilitate our investigation on how NOMA-enabled resource optimization performs in an aggressive frequency-reuse scenario for addressing a practical issue, i.e., to overcome the mismatch effect between requested traffic and offered capacity. The gateway with the co-located resource management unit connects the core network and the satellite payload. The gateway collects terminals' feedbacks, e.g., channel conditions and traffic demand, via the return link. The resource manager is responsible for generating optimized decisions, and the outcome is communicated to the gateway and then to the payload. The satellite plays as a transparent transceiver to relay data from the gateway to ground terminals.

Let $\mathcal{U}_b$ be the set of all the fixed ground terminals located within the service area of the b-th beam. For each scheduling period, K_b terminals from $\mathcal{U}_b$ are selected for transmission. Denote $\mathcal{K}_b = \{1, \ldots, K_b\}$ as the set of the selected terminals in beam b, where $\mathcal{K}_b \subseteq \mathcal{U}_b$. We focus on resource allocation during a scheduling period consisting of C timeslots. Let $\mathcal{C} = \{1, \ldots, C\}$ be the set of the timeslots.

As we consider fixed ground terminals, the channel gains vary over scheduling periods but keep static during a scheduling period. Define $\mathbf{h}_{bk} = [h^1_{bk}, \ldots, h^i_{bk}, \ldots, h^B_{bk}]^T \in \mathbb{C}^{B\times 1}$ as the channel vector of the k-th terminal in beam b at timeslot c. The i-th element of the vector, h^i_{bk}, denotes the channel coefficient from the i-th feed to the k-th terminal in beam b, where $i \in \mathcal{B}$. The channel coefficient can be expressed as

$$h^i_{bk} = e^{\mathrm{j}\vartheta_{bk}} \sqrt{\frac{G^{\mathrm{Sat}}_{ibk} L_{bk} G^{\mathrm{Rx}}_{bk}}{\kappa T B_W}}, \tag{3.1}$$

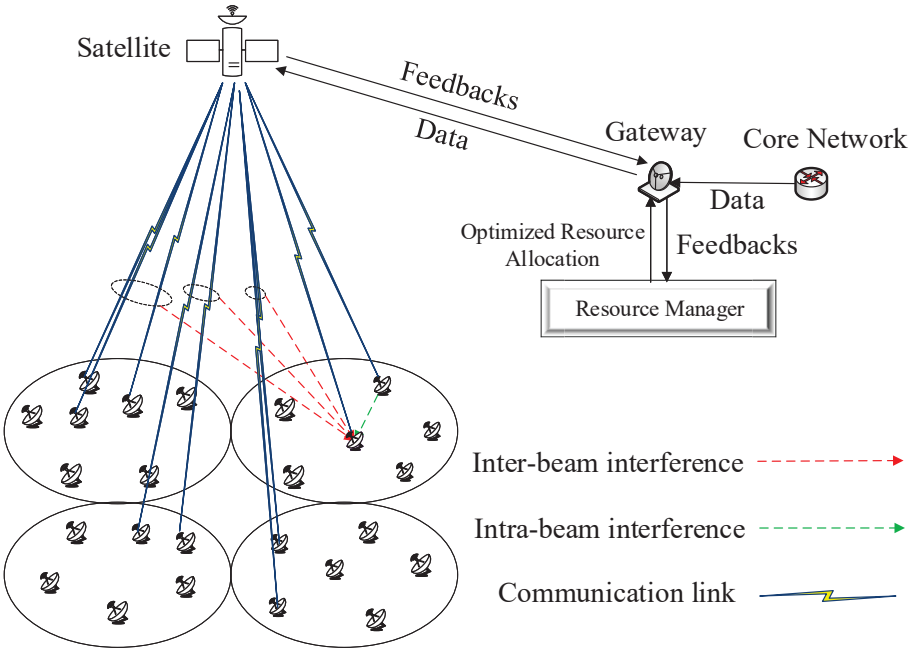

Figure 3.1: An illustrative scenario of the NOMA-enabled multi-beam satellite system, where all the beams share the same frequency band.

where G_{ibk}^{Sat} is the transmit antenna gain corresponding to the off-axis angle between the beam center and the terminal. Let L_{bk} denote the free-space propagation loss from the GEO satellite to the k-th terminal in beam b, which is calculated by,

$$L_{bk} = (\frac{v}{4\pi f_{\text{freq}} d_{bk}})^2, \tag{3.2}$$

where v, f_{freq}, and d_{bk} represent the propagation speed, the frequency, and the distance between the GEO satellite and the k-th terminal in beam b, respectively. G_{bk}^{Rx} is the receiver antenna gain. $\kappa T B_W$ is the noise distribution, where κ, T, and B_W denote the Boltzmann constant, the receiver noise temperature, and the occupied bandwidth, respectively. $e^{\text{j}\vartheta_{bk}}$ denotes the phase variation due to the long propagation paths to each terminal, where ϑ_{bk} is uniformly distributed between 0 and 2π. The channel model has been widely adopted in the literature, e.g., [41, 132, 133]. By introducing NOMA and precoding to mitigate interference, 1-color frequency-reuse pattern is adopted, where all the beams share the same frequency band [2]. In terms of payload, the on-board payload is equipped with the module of multi-port amplifier (MPA) such that power can be flexibly distributed across different beams.

3.2.2 Precoding and NOMA

To alleviate inter-beam interference, we adopt a linear precoding scheme, minimum mean square error (MMSE), which has been widely considered in satellite systems, e.g., [12, 2, 134, 135]. Compared to dirty-paper coding which can attain the maximum capacity with unaffordable computational complexity, MMSE can achieve a good trade-off between high spectral efficiency and low computational complexity [41]. On the other hand, MMSE can achieve better performance in addressing both inter-beam interference and noise than zero-forcing and maximum ratio transmission schemes [136]. In the system model, we assume that CSI is available at the gateway so that precoding and resource optimization can be performed. In practice, a CSI estimation procedure can be performed first by using pilot-assisted approaches, which is facilitated by the DVB-S2X standard and its superframe structure [137].

Denote $\mathbf{w}_{bc} = [w_{bc}^1, \ldots, w_{bc}^i, \ldots, w_{bc}^B]^T \in \mathbb{C}^{B\times 1}$ as the precoding vector for the b-th beam at timeslot c. The i-th element of the vector, w_{bc}^i, represents the precoding coefficient of the i-th feed for the b-th beam, where $i \in \mathcal{B}$. The received signal can be expressed as:

$$y_{bkc} = \underbrace{\mathbf{h}_{bk}^H \mathbf{w}_{bc}\sqrt{p_{bkc}}s_{bkc}}_{\text{desired signal}} + \underbrace{\sum_{l\in\mathcal{K}_b\setminus\{k\}} \mathbf{h}_{bk}^H \mathbf{w}_{bc}\sqrt{p_{blc}}s_{blc}}_{\text{intra-beam interference}} + \underbrace{\sum_{b'\in\mathcal{B}\setminus\{b\}}\sum_{j\in\mathcal{K}_{b'}} \mathbf{h}_{bk}^H \mathbf{w}_{b'c}\sqrt{p_{b'jc}}s_{b'jc}}_{\text{inter-beam interference}} + \underbrace{n_{bkc}}_{\text{noise}}, \tag{3.3}$$

where s_{bkc}, p_{bkc}, and $n_{bkc} \sim \mathcal{CN}(0, \sigma^2)$ are the signal with unit power, power scaling factor, and the complex circular symmetric independent identically distributed additive white gaussian noise with zero mean and variance σ^2, respectively. The transmit power of the b-th beam (or feed) is $\rho_{bc}\sum_{k\in\mathcal{K}_b} p_{bkc}$, $\forall c \in \mathcal{C}$, where $\rho_{bc} = [\sum_{i\in\mathcal{B}} \mathbf{w}_{ic}\mathbf{w}_{ic}^H]_{b,b}$ denotes the power radiated by the b-th feed for precoding [132].

To implement MMSE, we construct $\mathbf{H} \in \mathbb{C}^{B\times B}$ as the channel matrix, where the b-th row represents the channel vector of the terminal with $\max_{k\in\mathcal{K}_b} \|\mathbf{h}_{bk}\|$ [40]. The precoding matrix reads,

$$\mathbf{W} = \beta\mathbf{H}^H(\mathbf{H}\mathbf{H}^H + \sigma^2\mathbf{I}_B)^{-1}, \tag{3.4}$$

where $\mathbf{I}_B$ is the identity matrix with the dimension B by B. β is a scaling factor to normalize the precoding matrix as $[\mathbf{W}\mathbf{W}^H]_{b,b} \leq 1, \forall b \in \mathcal{B}$. The scaling factor can be determined as

$$\beta^2 = \frac{1}{\max\{\text{diag}((\mathbf{H}^H\mathbf{H})^{-1})\}}. \tag{3.5}$$

Note that the regularization factor before $\mathbf{I}$ is fixed to σ^2 in this work.

Within a beam, NOMA is applied to mitigate intra-beam interference among terminals. The signal-to-interference-plus-noise ratio (SINR) γ_{bkc} is expressed as,

$$\gamma_{bkc} = \frac{|\mathbf{h}_{bk}^H \mathbf{w}_{bc}|^2 p_{bkc}}{\sum\limits_{l\in\mathcal{K}_b\setminus\{k\}} \phi_{bklc}|\mathbf{h}_{bk}^H \mathbf{w}_{bc}|^2 p_{blc} + \sum\limits_{b'\in\mathcal{B}\setminus\{b\}} |\mathbf{h}_{bk}^H \mathbf{w}_{b'c}|^2 \sum\limits_{j\in\mathcal{K}_{b'}} p_{b'jc} + \sigma^2}, \tag{3.6}$$

where $\phi_{bklc} \in \{0, 1\}$ indicates decoding order, where $k \neq l$. Let g_{bkc} denote the ratio between channel gain and inter-beam interference plus noise,

$$g_{bkc} = \frac{|\mathbf{h}_{bk}^H \mathbf{w}_{bc}|^2}{\sum\limits_{b'\in\mathcal{B}\setminus\{b\}} |\mathbf{h}_{bk}^H \mathbf{w}_{b'c}|^2 \sum\limits_{j\in\mathcal{K}_{b'}} p_{b'jc} + \sigma^2}. \tag{3.7}$$

In the system model, we adopt a descending order of g_{bkc} as the decoding order in SIC, which is a proper decoding order and widely used in the literature for NOMA, e.g., [31, 130, 38, 131, 138]. By the definition, $g_{bkc} > g_{blc}$ means that terminal k decodes the signal of l before decoding its own signal. Otherwise, terminal k treats l's signal as noise when $g_{bkc} < g_{blc}$. To ease the presentation, we assume the decoding order is consistent with the terminal index, i.e., $g_{b1c} \geq g_{b2c} \geq \cdots \geq g_{bK_bc}$, unless otherwise stated.

The throughput of terminal k in beam b at timeslot c is,

$$R_{bkc} = B_W \log(1 + \gamma_{bkc}). \tag{3.8}$$

Hence the offered capacity of that terminal is derived as,

$$R_{bk} = \sum_{c \in \mathcal{C}} R_{bkc}. \tag{3.9}$$

We remark that, in this work, we assume perfect SIC (as well as CSI) to explore an upper-bound performance of NOMA over OMA. The performance can be served as benchmarks for the cases with various imperfections. In practice, there are a set of approaches being developed, and can be applied to facilitate successful SIC. For instance, one can group terminals with large channel-gain difference and significant power disparity such that the terminals are able to distinguish the intended signal and more likely to perform successful SIC [139]. In addition, some advanced techniques, e.g., soft-in soft-out decoding [140] and multi-branch SIC [141], can help to alleviate the performance degradation caused by imperfect SIC, and keep the error ratio of imperfect SIC at low levels.

3.3 Problem Formulation

We formulate a max-min fairness problem to improve the OCTR performance by power, decoding-order, and terminal-timeslot optimization. We define the variables and formulate the max-min fairness problem $\mathcal{P}_0$ as follows:

$$\begin{aligned}
&p_{bkc} \geq 0, \quad \text{allocated power for terminal } k \text{ in beam } b \text{ at timeslot } c,\\
&\phi_{bklc} = \begin{cases} 0, & \text{in beam } b, \text{ terminal } k \text{ decodes } l\text{'s signal at timeslot } c \text{ before decoding its own signal},\\ 1, & \text{terminal } k \text{ does not decode } l\text{'s signal and treat it as noise}, \end{cases}\\
&\alpha_{bkc} = \begin{cases} 1, & \text{terminal } k \text{ in beam } b \text{ is scheduled to timeslot } c,\\ 0, & \text{otherwise}, \end{cases}
\end{aligned} \tag{3.10a}$$

$$\mathcal{P}_0 : \max_{p_{bkc}, \phi_{bklc}, \alpha_{bkc}} \min_{b \in \mathcal{B}, k \in \mathcal{K}_b} \frac{R_{bk}}{D_{bk}} \tag{3.11a}$$

$$\text{s.t.} \sum_{b \in \mathcal{B}} \rho_{bc} \sum_{k \in \mathcal{K}_b} p_{bkc} \leq P_{tot}, \forall c \in \mathcal{C}, \tag{3.11b}$$

$$\rho_{bc} \sum_{k \in \mathcal{K}_b} p_{bkc} \leq P_{b,\max}, \forall b \in \mathcal{B}, \forall c \in \mathcal{C}, \tag{3.11c}$$

$$\rho_{bc} \sum_{k \in \mathcal{K}_b} p_{bkc} = \rho_{bc'} \sum_{k \in \mathcal{K}_b} p_{bkc'}, \forall b \in \mathcal{B}, \forall c, c^{'} \in \mathcal{C}, c \neq c^{'}, \tag{3.11d}$$

$$\sum_{k \in \mathcal{K}_b} \alpha_{bkc} \leq \bar{K}, \forall b \in \mathcal{B}, \forall c \in \mathcal{C}, \tag{3.11e}$$

$$\sum_{c \in \mathcal{C}} \alpha_{bkc} = 1, \forall b \in \mathcal{B}, \forall k \in \mathcal{K}_b, \tag{3.11f}$$

$$p_{bkc} \leq \hat{P} \alpha_{bkc}, \forall b \in \mathcal{B}, \forall c \in \mathcal{C}, \forall k \in \mathcal{K}_b, \tag{3.11g}$$

$$g_{blc} - g_{bkc} \leq A \phi_{bklc}, \forall b \in \mathcal{B}, \forall c \in \mathcal{C}, \forall k, l \in \mathcal{K}_b, k \neq l, \tag{3.11h}$$

$$\phi_{bklc} + \phi_{blkc} = 1, \forall b \in \mathcal{B}, \forall c \in \mathcal{C}, \forall k, l \in \mathcal{K}_b, k \neq l. \tag{3.11i}$$

In the objective, we focus on the OCTR improvement and fairness enhancement at the terminal level [133]. The OCTR metric for terminal k in beam b is defined as $\frac{R_{bk}}{D_{bk}}$, where R_{bk} and D_{bk} are the offered capacity and requested traffic demand, respectively. The optimization task is to maximize the worst OCTR among terminals in $\mathcal{K}_b$, such that the mismatch and the fairness issues can be addressed. In (4.7d), the total power is less than a budget P_{tot}, due to the limited on-board power supply. Constraints (3.11c) state that the allocated power for each beam should be restricted by the power constraint, $P_{b,\max}$. Constraints (3.11d) denote that, the power allocated to each beam is identical across timeslots, considering the practical issues in waveform design, dynamic range of the signal, and non-linearities of the amplifier [2, 21, 72]. For each beam, the number of terminals simultaneously accessing the same timeslot is no more than $\bar{K}$ in (3.11e). In (3.11f), each terminal is limited to be scheduled once during a scheduling period to avoid imbalanced timeslot assignment among terminals, which is important for serving a large number of terminals. Constraints (3.11g) connect two sets of variables, p_{bkc} and α_{bkc}, where $\hat{P}$ is no smaller than the maximal p_{bkc}, e.g., $\hat{P} = P_{tot}$. If $\alpha_{bkc} = 0$, p_{bkc} is zero. If $\alpha_{bkc} = 1$, $\hat{P} \geq p_{bkc} > 0$ since the option $\alpha_{bkc} = 1$ and $p_{bkc} = 0$ is clearly not optimal, thus will be excluded from the optimum. Constraints (3.11h) and (3.11i) confine variables ϕ_{bklc} to perform SIC by the descending order defined in (3.7), where A is no smaller than the maximum value of g_{bkc}. If $g_{bkc} > g_{blc}$, $\phi_{bklc} = 0$ which means that terminal k decodes the signal of l before decoding its own signal, and terminal l treats k's signals as noise. If $\phi_{bklc} = 1$, it implies $g_{bkc} < g_{blc}$, then terminal k does not decode l's signal and treat it as noise. Note that due to the constraints $\phi_{bklc} + \phi_{blkc} = 1$ in (3.11i), $\phi_{bklc} = 1$ also implies $\phi_{blkc} = 0$ and $g_{blc} > g_{bkc}$ in the mean time.

$\mathcal{P}_0$ is a mixed-integer non-convex programming due to the binary variables, α_{bkc} and ϕ_{bklc}, and the non-convexity of R_{bkc}. Solving mixed-integer non-convex programming is in general challenging. A typical way to address a max-min problem is to check whether it can be reformulated as a monotonic constrained max-min utility (MCMU) problem, where the objective functions and constraints are competitive utility functions (CUFs) and monotonic constraints (MCs), respectively [55]. If yes, PF can be applied with fast convergence. The general MCMU is expressed as:

$$\mathcal{P}_{PF}: \max_{\mathbf{Q}} \quad \min_{j=1,\ldots,J} \quad f_j(\mathbf{Q}) \tag{3.12a}$$

$$\text{s.t.} \quad F_m(\mathbf{Q}) \leq \bar{F}_m, m = 1, \ldots, M. \tag{3.12b}$$

In $\mathcal{P}_{PF}$, $\mathbf{Q} = [Q_1, \ldots, Q_j, \ldots, Q_J]$ is the vector collecting all the Q-variables. $f_j(\mathbf{Q})$ represents the objective function. $F_m(\mathbf{Q})$ and $\bar{F}_m$ are the constraint functions and upper-bound parameters, respectively. The properties of CUF and MC are presented in Definition 1 and Definition 2, respectively.

Definition 1. The objective function $f_j(\mathbf{Q})$ in $\mathcal{P}_{PF}$ is CUF if the following properties are satisfied:

- *Positivity: $f_j(\mathbf{Q}) > 0$ if $\mathbf{Q} \succ \mathbf{0}$; $f_j(\mathbf{Q}) = 0$ if and only if $\mathbf{Q} = \mathbf{0}$.*
- *Competitiveness: $f_j(\mathbf{Q})$ strictly monotonically increases in Q_j but decreases in $Q_{j'}$, where $j' \neq j$.*
- *Directional Monotonicity: For $\zeta > 1$ and $\mathbf{Q} \succ \mathbf{0}$, $f_j(\zeta\mathbf{Q}) > f_j(\mathbf{Q})$.*

Definition 2. The constraints, $F_m(\mathbf{Q}) \leq \bar{F}_m$, $\forall m = 1, \ldots, M$, are MCs if the following properties are satisfied:

- *Strict Monotonicity: $F_m(\mathbf{Q}_1) > F_m(\mathbf{Q}_2)$ if $\mathbf{Q}_1 \succ \mathbf{Q}_2$, $\forall m$.*
- *Validity: If $\mathbf{Q} \succ \mathbf{0}$, $\exists \zeta > 0$ such that $F_m(\zeta\mathbf{Q}) \geq \bar{F}_m$ for some m.*

MCMU and PF may not be directly applied to solve $\mathcal{P}_0$ due to the following reasons:

- The solutions for MCMU (e.g., [55, 142, 143]) are derived for a specific scenario, e.g., one terminal per cell or per beam. When the scenario of multiple users per beam, along with undetermined decoding orders and binary variables, is considered in this work, the satisfiability of Definition 1 and Definition 2 no longer holds for original $\mathcal{P}_0$.
- In $\mathcal{P}_0$, determining decoding orders is coupled with beam power allocation. Optimizing beam power could result in changes of decoding orders. As a consequence, the function of R_{bk} in $\mathcal{P}_0$ becomes undetermined (corresponding to the objective function in $\mathcal{P}_{PF}$), which is an obstacle in analyzing the applicability of MCMU and PF.
- Precoding vectors are decided based on the terminal-timeslot assignment. The coupling between precoding vectors and terminal-timeslot assignment could result in undetermined $|\mathbf{h}_{bk}\mathbf{w}_{bc}|^2$ in the objective function (4.7a) while optimizing α_{bkc}.

To solve $\mathcal{P}_0$, the following issues should be tackled. First, the applicability of MCMU and PF for different special cases of $\mathcal{P}_0$ should be analyzed. Second, the challenges to deal with the combinatorial and non-convex components in $\mathcal{P}_0$ need to be addressed. Towards these ends, we first discuss the optimization of power allocation and decoding orders with the fixed terminal-timeslot assignment. Then we focus on solving the whole joint optimization problem.

3.4 Optimal Joint Optimization of Power Allocation and Decoding Orders

With fixed α_{bkc} in $\mathcal{P}_0$, we formulate the remaining power and decoding-order optimization problem in $\mathcal{P}_1$.

$$\mathcal{P}_1: \max_{p_{bkc}>0,\phi_{bklc}} \min_{b\in\mathcal{B},k\in\mathcal{K}_b} \frac{R_{bk}}{D_{bk}} \tag{3.13a}$$

$$\text{s.t.} \quad (4.7\text{d}), (3.11\text{c}), (3.11\text{d}), (3.11\text{h}), (3.11\text{i}). \tag{3.13b}$$

Note that prior to optimization, we have pre-processed p_{bkc} according to the fixed variables α_{bkc}. That is, only positive p-variables, i.e., $p_{bkc} > 0$ (resulted by $\alpha_{bkc} = 1$), retain in $\mathcal{P}_1$ and to be optimized. $\mathcal{P}_1$ is complicated due to the coupled power and decoding-order optimization. From $\mathcal{P}_1$, we can observe that if the decoding orders can be determined by temporarily fixing the beam power, the remaining power allocation problem resembles P_{PF}. This enables us to take advantages of the PF method in fast convergence and optimality guarantee. In this section, we first discuss the strategy of fixing the terminal-timeslot assignment. Next, we discuss the solution of $\mathcal{P}_1$, and the applicability of MCMU and PF.

3.4.1 Terminal-Timeslot Scheduling

Terminal-timeslot scheduling or terminal grouping is significant for NOMA and precoding. In the literature, the grouping strategies are either optimal or suboptimal. The former is to find the optimal terminal groups but with prohibitively computational complexity, e.g., an optimal scheme for joint precoding and terminal-subcarrier assignment in [102]. For the latter, some heuristic approaches are developed for terrestrial-NOMA systems but might not be directly applied to satellite NOMA. For example, the strategy of grouping terminals with highly correlated channels and large channel gain difference is widely used in terrestrial-NOMA systems [38, 35, 40]. However, in satellite systems, neighboring terminals may have highly correlated channels but small channel gain difference [34], whereas terminals far away from each other may have non-correlated channels.

Considering the trade-off between interference reduction and computational complexity, we apply MaxCC strategy to select terminals with the largest correlation [132]. The reasoning behind this strategy is that the precoder should be able to mitigate inter-beam interference more effectively whenever the terminals grouped within the same beam have highly correlated channel vectors. The procedure is summarized in the following. In a timeslot, we select one terminal, say $k^{'}$, randomly from $\mathcal{U}_b$. Then we calculate its correlation factors (or cosine similarity metric) with all the other terminals, i.e., $\theta = \frac{|\mathbf{h}_{bk^{'}}^H \mathbf{h}_{bj}|}{\|\mathbf{h}_{bk^{'}}\| \|\mathbf{h}_{bj}\|}$ [41], where $j \in \mathcal{U}_b \setminus \{k^{'}\}$. The terminal with the largest θ is scheduled with $k^{'}$ to the same timeslot. The selected terminals are deleted from $\mathcal{U}_b$ and added to $\mathcal{K}_b$. The above procedure is performed for each timeslot one by one until all the timeslots are processed or $\mathcal{U}_b$ becomes empty.

3.4.2 Terminal Power Optimization with Fixed Beam Power

We define $\mathbf{P} = [P_1, \ldots, P_b, \ldots, P_B]$ as the vector collecting all the beam power. With fixed α_{bkc} and temporarily fixed $\mathbf{P}$, the terminal power allocation is independent among beams. Thus $\mathcal{P}_1$ can be decomposed to B subproblems. The b-th subproblem, $\mathcal{P}_1(b)$, corresponds to the terminal power optimization in beam b. Let $\bar{\mathbf{P}}_b$ collect all the beam power except the b-th beam's power, i.e., $\bar{\mathbf{P}}_b = [P_1, \ldots, P_{b-1}, P_{b+1}, \ldots, P_B]$. In (3.7), g_{bkc} can be considered as a function of $\bar{\mathbf{P}}_b$, which is defined as,

$$g_{bkc} = \hat{f}_{bkc}(\bar{\mathbf{P}}_b). \tag{3.14}$$

The decoding order variables ϕ_{bklc} are determined when $\mathbf{P}$ is fixed. Thus, constraints (3.11h) and (3.11i) do not apply in $\mathcal{P}_1(b)$.

$$\mathcal{P}_1(b): \max_{p_{bkc}} \min_{k \in \mathcal{K}_b} \frac{R_{bk}}{D_{bk}} \tag{3.15a}$$

$$\text{s.t.} \quad \rho_{bc} \sum_{k \in \mathcal{K}_b} p_{bkc} = P_b, \forall c \in \mathcal{C}, \tag{3.15b}$$

where (3.11d) is equivalently converted to (3.15b) and denotes that the sum of terminals' power in each beam across timeslots is equal to the beam power. By introducing an auxiliary variable t_b, $\mathcal{P}_1(b)$ can be equivalently transformed to a maximization problem:

$$\mathcal{P}_1(b): \max_{p_{bkc}, t_b} \quad t_b \tag{3.16a}$$

$$\text{s.t.} \quad \text{(3.15b)}, \quad t_b D_{bk} - R_{bk} \leq 0, \forall k \in \mathcal{K}_b. \tag{3.16b}$$

To better reveal the convexity of $\mathcal{P}_1(b)$, we express p_{bkc} by a function of R_{bkc} based on (4.5) [130]. Then the power variables p_{b1c}, ..., p_{bK_bc} read,

$$\begin{aligned}
p_{b1c} &= \frac{e^{\frac{R_{b1c}}{B_W}} - 1}{g_{b1c}}, \\
p_{b2c} &= \frac{e^{\frac{R_{b2c}}{B_W}} - 1}{g_{b2c}} (g_{b2c} p_{b1c} + 1), \\
&\ldots \\
p_{bK_bc} &= \frac{e^{\frac{R_{bK_bc}}{B_W}} - 1}{g_{bK_bc}} (g_{bK_bc} \sum_{j=1}^{K_b - 1} p_{bjc} + 1).
\end{aligned} \tag{3.17}$$

The constraints in (3.15b) can be equivalently written as:

$$\sum_{k=1}^{K_b}\left(\frac{1}{g_{bkc}}-\frac{1}{g_{b(k-1)c}}\right)e^{\sum\limits_{j\geq k}\frac{R_{bjc}}{B_W}}-\frac{1}{g_{bK_bc}}=\frac{P_b}{\rho_{bc}},\forall c\in\mathcal{C}, \tag{3.18}$$

where $\frac{1}{g_{b0c}}=0$. Then $\mathcal{P}_1(b)$ is equivalently converted to $\mathcal{P}_2(b)$ by treating R_{bkc} as variables:

$$\mathcal{P}_2(b):\max_{R_{bkc},t_b}\quad t_b \tag{3.19a}$$

$$\text{s.t.}\quad (3.18),(4.7b). \tag{3.19b}$$

Note that constraints (3.18) are not affine. We further relax the equality constraints in (3.18) to inequality in (4.9c), leading to a convex exponential-cone format,

$$\sum_{k=1}^{K_b}\left(\frac{1}{g_{bkc}}-\frac{1}{g_{b(k-1)c}}\right)e^{\sum\limits_{j\geq k}\frac{R_{bjc}}{B_W}}-\frac{1}{g_{bK_bc}}\leq\frac{P_b}{\rho_{bc}},\forall c\in\mathcal{C}. \tag{3.20}$$

We then conclude the equivalence between (3.18) and (4.9c) at the optimum, thus concluding the convexity of $\mathcal{P}_2(b)$ and $\mathcal{P}_1(b)$.

Proposition 1. The optimum of $\mathcal{P}_2(b)$, i.e., t_b^*, which is located on timeslot c^*, can be obtained by the following equation:

$$\sum_{k=1}^{K_b}\left(\frac{1}{g_{bkc^*}}-\frac{1}{g_{b(k-1)c^*}}\right)e^{\sum\limits_{j\geq k}\frac{t_b^*D_{bj}}{B_W}}-\frac{1}{g_{bK_bc^*}}=\frac{P_b}{\rho_{bc^*}}. \tag{3.21}$$

Proof. We can obtain the optimum of the relaxed problem based on KKT conditions. The corresponding Lagrangian dual function is:

$$\begin{aligned}&\mathcal{L}(R_{bkc},t_b;\lambda_c,\mu_k)=\\&-t_b+\sum_{c\in\mathcal{C}}\lambda_c\left(\sum_{k=1}^{K_b}\left(\frac{1}{g_{bkc}}-\frac{1}{g_{b(k-1)c}}\right)e^{\sum\limits_{j\geq k}\frac{R_{bjc}}{B_W}}-\frac{1}{g_{bK_bc}}-\frac{P_b}{\rho_{bc}}\right)+\sum_{k=1}^{K_b}\mu_k(tD_{bk}-R_{bk}),\end{aligned} \tag{3.22}$$

where $\lambda_c\geq 0$ and $\mu_k\geq 0$ are Lagrangian multipliers for constraints (3.18) and (4.7b), respectively. The KKT conditions can be derived as

$$\frac{\partial\mathcal{L}}{\partial R_{bkc}}=\lambda_c\sum_{n=1}^{k}\left(\frac{1}{g_{bnc}}-\frac{1}{g_{b(n-1)c}}\right)e^{\sum\limits_{j\geq n}\frac{R_{bjc}}{B_W}}-\mu_k=0,\forall c\in\mathcal{C},k\in\mathcal{K}_b, \tag{3.23a}$$

$$\frac{\partial\mathcal{L}}{\partial t}=-1+\sum_{k=1}^{K_b}\mu_kD_{bk}=0, \tag{3.23b}$$

$$\lambda_c\left(\sum_{k=1}^{K_b}\left(\frac{1}{g_{bkc}}-\frac{1}{g_{b(k-1)c}}\right)e^{\sum\limits_{j\geq k}\frac{R_{bjc}}{B_W}}-\frac{1}{g_{bK_bc}}-\frac{P_b}{\rho_{bc}}\right)=0,\forall c\in\mathcal{C}, \tag{3.23c}$$

$$\mu_k(t_bD_{bk}-R_{bk})=0,\forall k\in\mathcal{K}_b. \tag{3.23d}$$

At the optimum of $\mathcal{P}_1(b)$, at least one constraint in (4.7b), say the k^*-th constraint/terminal, will be active, i.e., the equality holds, whereas the others keep inequalities [50]. The optimal value t_b^* is then achieved

at the equality $t_b^* D_{bk^*} - R_{bk^*} = 0$ [143, 50]. In (3.23d), for the inequality terms $t_b^* D_{bk} - R_{bk} < 0$, the corresponding μ_k must be zero, while for the equality term $t_b^* D_{bk^*} - R_{bk^*} = 0$, $\mu_{k^*} > 0$ instead of zero since (3.23b) cannot hold for all-zero μ_k. Hence, the optimal t_b^* is associated with positive μ_k^*. The positive μ_k^* in (3.23a) results in positive λ_c which leads to $\sum_{k=1}^{K_b}(\frac{1}{g_{bkc}} - \frac{1}{g_{b(k-1)c}})e^{\sum_{j\geq k}\frac{R_{bjc}}{B_W}} - \frac{1}{g_{bK_bc}} - \frac{P_b}{\rho_{bc}} = 0$ in (3.23c). Thus the conclusion. □

Proposition 1 establishes the equivalence between (3.18) and (4.9c) at the optimum. The convexity of $\mathcal{P}_1(b)$ and $\mathcal{P}_2(b)$ is concluded. We define a function $t_b^* = f_b(\mathbf{P})$ in an inexplicit way in (3.21) by moving t_b^* to the left side of the equality and the remaining to the right, where $f_b(\mathbf{P})$ denotes the function of the optimal OCTR of beam b when beam power is $\mathbf{P}$.

3.4.3 Beam Power Optimization

Given $\mathbf{P}$, the optimal power allocation among terminals can be obtained from KKT conditions. Next, we optimize the beam power allocation. The problem is formulated in $\mathcal{P}_3$,

$$\mathcal{P}_3: \max_{\mathbf{P}} \quad \min_{b\in\mathcal{B}} \quad f_b(\mathbf{P}) \tag{3.24a}$$

$$\text{s.t.} \quad \sum_{b\in\mathcal{B}} P_b \leq P_{tot}, \tag{3.24b}$$

$$P_b \leq P_{b,\max}, \forall b \in \mathcal{B}, \tag{3.24c}$$

where the objective $f_b(\mathbf{P})$ is the function of the optimal OCTR of the b-th beam with $\mathbf{P}$ and can be equivalently converted from (3.21). The expression of $f_b(\mathbf{P})$ depends on $\mathbf{P}$ and the decoding order. Next, we prove $\mathcal{P}_3$ is an MCMU. Constraints (3.24b) and (3.24c) are linear, which satisfy the MC conditions. The CUF conditions of $f_b(\mathbf{P})$ are analyzed in Lemma 1 and Lemma 2.

Lemma 1. The objective function $f_b(\mathbf{P})$ in $\mathcal{P}_3$ is a CUF for any decoding orders.

Proof. Given any $\mathbf{P}$ and the corresponding decoding order, according to Definition 1, we check the three conditions for $f_b(\mathbf{P}), \forall b \in \mathcal{B}$.

Positivity: Rewrite (3.21) equivalently as:

$$\sum_{k=1}^{K_b-1} \frac{1}{g_{bkc^*}} e^{\sum\limits_{j>k}\frac{t_b^* D_{bj}}{B_W}} (e^{\frac{t_b^* D_{bk}}{B_W}} - 1) + \frac{1}{g_{bK_bc^*}}(e^{\frac{t_b^* D_{bK_b}}{B_W}} - 1) = \frac{P_b}{\rho_{bc^*}}. \tag{3.25}$$

The right-hand side is positive, then the term $e^{\frac{t_b^* D_{bk}}{B_W}} - 1$ in the left-hand side has to keep positive. Hence t_b^* is positive.

Competitiveness: By deriving the partial derivatives of $f_b(\mathbf{P})$, i.e., $\frac{\partial f_b}{\partial P_b}$ and $\frac{\partial f_b}{\partial P_{b'}}$ in (3.26) and (3.27), respectively, we observe $\frac{\partial f_b}{\partial P_b} > 0$ and $\frac{\partial f_b}{\partial P_{b'}} < 0$, which means that $f_b(\mathbf{P})$ monotonically increases with beam b's power P_b but decreases with any other beam's power $P_{b'}$.

$$\frac{\partial f_b}{\partial P_b} = \frac{1}{\sum_{k=1}^{K_b}\left(\frac{1}{g_{bkc^*}} - \frac{1}{g_{b(k-1)c^*}}\right) e^{\sum_{j\geq k}\frac{t_b^* D_{bj}}{B_W}} \sum_{j\geq k}\frac{D_{bj}}{B_W}}, \tag{3.26}$$

$$\frac{\partial f_b}{\partial P_{b'}} = -\frac{\sum_{k=1}^{K_b-1} \frac{|\mathbf{h}_{bk}^H \mathbf{w}_{b'c^*}|^2}{|\mathbf{h}_{bk}^H \mathbf{w}_{bc^*}|^2 \rho_{bc^*}} e^{\sum_{j>k} \frac{t_b^* D_{bj}}{B_W}} (e^{\frac{t_b^* D_{bk}}{B_W}} - 1) + \frac{|\mathbf{h}_{bK_b}^H \mathbf{w}_{b'c^*}|^2}{|\mathbf{h}_{bK_b}^H \mathbf{w}_{bc^*}|^2 \rho_{bc^*}} (e^{\frac{t_b^* D_{bK_b}}{B_W}} - 1)}{\sum_{k=1}^{K_b} \left(\frac{1}{g_{bkc^*}} - \frac{1}{g_{b(k-1)c^*}} \right) e^{\sum_{j\geq k} \frac{t_b^* D_{bj}}{B_W}} \sum_{j\geq k} \frac{D_{bj}}{B_W}}. \quad (3.27)$$

Directional Monotonicity: Let $\zeta > 1$. We assume $f_b(\zeta \mathbf{P}) = \tau_1$ and $f_b(\mathbf{P}) = \tau_2$. From equation (3.21), τ_1 can be derived by the following equation:

$$\sum_{k=1}^{K_b-1} \frac{1}{\hat{f}_{bkc^*}(\zeta \bar{\mathbf{P}}_b)} e^{\sum\limits_{j>k} \frac{\tau_1 D_{bj}}{B_W}} (e^{\frac{\tau_1 D_{bk}}{B_W}} - 1) + \frac{1}{\hat{f}_{bK_bc^*}(\zeta \bar{\mathbf{P}}_b)} (e^{\frac{\tau_1 D_{bK_b}}{B_W}} - 1) - \frac{\zeta P_b}{\rho_{bc^*}} = 0. \quad (3.28)$$

By substituting $f_b(\mathbf{P}) = \tau_2$ into (3.21), both sides of the equation multiply ζ, i.e.,

$$\sum_{k=1}^{K_b-1} \frac{\zeta}{\hat{f}_{bkc^*}(\bar{\mathbf{P}}_b)} e^{\sum\limits_{j>k} \frac{\tau_2 D_{bj}}{B_W}} (e^{\frac{\tau_2 D_{bk}}{B_W}} - 1) + \frac{\zeta}{\hat{f}_{bK_bc^*}(\bar{\mathbf{P}}_b)} (e^{\frac{\tau_2 D_{bK_b}}{B_W}} - 1) - \frac{\zeta P_b}{\rho_{bc^*}} = 0. \quad (3.29)$$

Based on the equation in (3.7), we can derive $\frac{1}{\hat{f}_{bkc^*}(\zeta \bar{\mathbf{P}})} < \frac{\zeta}{\hat{f}_{bkc^*}(\bar{\mathbf{P}})}$ by:

$$\frac{1}{\hat{f}_{bkc^*}(\zeta \bar{\mathbf{P}})} = \frac{\sum_{b' \neq b} |\mathbf{h}_{bk}^H \mathbf{w}_{b'c^*}|^2 \zeta \frac{P_{b'}}{\rho_{b'c^*}} + \sigma^2}{|\mathbf{h}_{bk}^H \mathbf{w}_{bc^*}|^2} < \zeta \frac{\sum_{b' \neq b} |\mathbf{h}_{bk}^H \mathbf{w}_{b'c^*}|^2 \frac{P_{b'}}{\rho_{b'c^*}} + \sigma^2}{|\mathbf{h}_{bk}^H \mathbf{w}_{bc^*}|^2} = \frac{\zeta}{\hat{f}_{bkc^*}(\bar{\mathbf{P}}_b)}. \quad (3.30)$$

Based on (3.30), the terms $\frac{1}{\hat{f}_{bkc^*}(\zeta \bar{\mathbf{P}})}$ and $\frac{1}{\hat{f}_{bK_bc^*}(\zeta \bar{\mathbf{P}})}$ in (3.28) are smaller than $\frac{\zeta}{\hat{f}_{bkc^*}(\bar{\mathbf{P}}_b)}$ and $\frac{\zeta}{\hat{f}_{bK_bc^*}(\bar{\mathbf{P}}_b)}$ in (3.29), respectively. Hence, the equalities in (3.28) and (3.29) cannot hold under both cases $\tau_1 = \tau_2$ and $\tau_1 < \tau_2$. Thus $\tau_1 > \tau_2$ and $f_b(\zeta \mathbf{P}) > f_b(\mathbf{P})$. □

Based on Lemma 1, we can develop PF-based algorithm to converge if the decoding order remains under the power adjustment. However, the expression of $f_b(\mathbf{P})$ typically changes since the adjustment of $\mathbf{P}$ can result in new decoding orders. As a consequence, it is not straightforward to observe the satisfiability of CUF and the convergence when $f_b(\mathbf{P})$ varies. Next, we conclude that the objective function in $\mathcal{P}_3$ is a CUF even if the decoding order changes.

Lemma 2. $f_b(\mathbf{P})$ in $\mathcal{P}_3$ remains a CUF even if the decoding order changes.

Proof. Positivity: The positivity of $f_b(\mathbf{P})$ holds whether the decoding order changes or not according to (3.25).

Competitiveness: The decoding order in beam b depends on $\bar{\mathbf{P}}_b$. Given any two terminals k and $k^{'}$ in beam b, suppose that in beam $b^{'}$, there exist $P_{b'}$ and δ such that $P_{b'}$ leads to $g_{bkc} = g_{bk'c}$; setting $P_{b'} - \delta$ results in terminal k decoding $k^{'}$ ($g_{bkc} > g_{bk'c}$); and $P_{b'} + \delta$ changes the decoding order to $k^{'}$ decoding k ($g_{bkc} < g_{bk'c}$). $f_b(\mathbf{P})$ is competitive when the decoding order stays unchanged. When $g_{bkc} = g_{bk'c}$, $f_b(\mathbf{P})$ remains the same under both decoding orders. Thus $f_b(\mathbf{P})$ is continuous, indicating that $f_b(\mathbf{P})$ monotonically decreases in $P_{b'}$ even if the decoding order changes. The competitiveness is concluded.

Directional monotonicity: Assume that the decoding order changes from k decoding $k^{'}$ to $k^{'}$ decoding k as the beam power increases from $\mathbf{P}$ to $\zeta \mathbf{P}$, where $\zeta > 1$. There exists ζ_0, where $1 < \zeta_0 < \zeta$, such that $\zeta_0 \mathbf{P}$ corresponds to $g_{bkc} = g_{bk'c}$. As proven in Lemma 1, $f_b(\mathbf{P}) < f_b(\zeta_0 \mathbf{P})$ and $f_b(\zeta_0 \mathbf{P}) < f_b(\zeta \mathbf{P})$. Thus $f_b(\mathbf{P}) < f_b(\zeta \mathbf{P})$. □

Based on Lemma 1 and Lemma 2, the objective function in $\mathcal{P}_3$ is a CUF. Constraints (3.24b) and (3.24c) are linear and thus satisfy the MC conditions, which concludes $\mathcal{P}_3$ is an MCMU.

Algorithm 1 JOPD

Input:

Initial beam power, $\mathbf{P}^{(0)}$;
iteration index: $n = 0$;
maximum number of iterations, $N_{\max}$;
precision: $\xi_1 > 0$.

1: **repeat**
2: **for** $b = 1, \ldots, B$ **do**
3: Update and sort g_{bkc} with $\mathbf{P}^{(n)}$.
4: Determine decoding order ϕ_{bklc} based on the descending order of g_{bkc}.
5: Calculate $t_b^{*(n)} = f_b(\mathbf{P}^{(n)})$ by (3.21).
6: Update $\mathbf{P}$ by $P_b = \frac{P_b^{(n)}}{t_b^{*(n)}}$.
7: **end for**
8: Calculate $\epsilon = \max\left\{\frac{P_b}{P_{b,\max}}, \forall b \in \mathcal{B}; \sum_{b\in\mathcal{B}} \frac{P_b}{P_{tot}}\right\}$.
9: Update $\mathbf{P}^{(n+1)} = \frac{\mathbf{P}}{\epsilon}$, $n = n + 1$.
10: **until** $n > N_{\max}$ or $|t_b^{*(n+1)} - t_b^{*(n)}| < \xi_1$
11: Calculate p_{bkc} based on $\mathbf{P}^{(n)}$.

Output:

t_b^*, p_{bkc}.

3.4.4 A Fast-Convergence Approach Based on PF for Joint Power and Decoding-Order Optimization

$\mathcal{P}_3$ is an MCMU where the objective function is CUF and the constraints are MCs. We propose an iterative algorithm based on PF, i.e., JOPD, in Alg. 8 to solve $\mathcal{P}_3$. Let $\mathbf{P}^{(n)}$, $P_b^{(n)}$ and $t_b^{*(n)}$ represent the values of $\mathbf{P}$, P_b, and t_b^* at the n-th iteration, respectively. For each iteration (line 3 to line 6), decoding orders are updated according to the descending order of g_{bkc} in line 3 and line 4. Then the optimal OCTR of each beam is calculated in line 5. Beam power is adjusted inversely proportional to the value of t_b^* in line 5 [55], which suggests that power for the beams with larger t_b^* will be reduced in the next iteration, and more power is allocated to the beams with worse OCTR. In line 8, we introduce a factor ϵ to confine beam power in the domain of (3.24b) and (3.24c). The iteration breaks if either n exceeds the maximum number of iterations, $N_{\max}$, or $|t_b^{*(n+1)} - t_b^{*(n)}|$ is smaller than the tolerance ξ_1. The convergence and optimality of JOPD are concluded in Theorem 1.

Theorem 1. With any initial vector $\mathbf{P}$*, JOPD converges geometrically fast to the optimum of* $\mathcal{P}_3$*.*

Proof. At the optimum, $f_b(\mathbf{P}^*) = t^*, \forall b \in \mathcal{B}$, where $\mathbf{P}^* = [P_1^*, \ldots, P_b^*, \ldots, P_B^*]$ and t^* are the optimal beam power and the optimal OCTR value, respectively. Define function $\eta_b(\mathbf{P}) = \frac{P_b}{f_b(\mathbf{P})}, \forall b \in \mathcal{B}$. At the convergence, $\frac{P_b^*}{t^*} = \frac{P_b^*}{f_b(\mathbf{P}^*)}, \forall b \in \mathcal{B}$.

The algorithm converges geometrically fast to t^* with any initial $\mathbf{P}$ if $\eta_b(\mathbf{P})$ satisfies the following conditions [144]:

- There exist $\underline{\tau}$ and $\overline{\tau}$, where $0 < \underline{\tau} \leq \overline{\tau}$, such that $\underline{\tau} \leq \eta_b(\mathbf{P}) \leq \overline{\tau}, \forall b \in \mathcal{B}$.
- For any beam power $\mathbf{P}_1 \succ \mathbf{0}$ and $\mathbf{P}_2 \succ \mathbf{0}$, and $0 < \zeta \leq 1$, if $\zeta\mathbf{P}_1 \preceq \mathbf{P}_2$, then $\zeta\eta_b(\mathbf{P}_1) \leq \eta_b(\mathbf{P}_2)$, $\forall b \in \mathcal{B}$. For $0 < \zeta < 1$, if $\zeta\mathbf{P}_1 \prec \mathbf{P}_2$, then $\zeta\eta_b(\mathbf{P}_1) < \eta_b(\mathbf{P}_2)$, $\forall b \in \mathcal{B}$.

For the first condition, $\eta_b(\mathbf{P})$ stays between $\underline{\tau}$ and $\overline{\tau}$, which means the function could not be zero or infinite with any $\mathbf{P}$. Due to the positivity of $f_b(\mathbf{P})$, $\eta_b(\mathbf{P}) = \frac{P_b}{f_b(\mathbf{P})} > 0$, i.e., $\eta_b(\mathbf{P}) \geq \underline{\tau} > 0$. Since $\mathbf{P}$ is bounded by $P_{b,\max}$, $\eta_b(\mathbf{P})$ is finite. Thus the function is upper bounded, i.e., $\eta_b(\mathbf{P}) \leq \overline{\tau}$.

For the second condition, we prove $\zeta\eta_b(\mathbf{P}_1) \leq \eta_b(\mathbf{P}_2)$ via showing the inequality below.

$$\zeta\eta_b(\mathbf{P}_1) \leq \eta_b(\zeta\mathbf{P}_1) \leq \eta_b(\mathbf{P}_2). \tag{3.31}$$

The first inequality $\zeta\eta_b(\mathbf{P}_1) \leq \eta_b(\zeta\mathbf{P}_1)$ reads,

$$\frac{\zeta P_b}{f_b(\mathbf{P}_1)} \leq \frac{\zeta P_b}{f_b(\zeta\mathbf{P}_1)}. \tag{3.32}$$

Let $\zeta\mathbf{P}_1 = \mathbf{P}$, then $\mathbf{P}_1 = \frac{1}{\zeta}\mathbf{P}$, where $\frac{1}{\zeta} \geq 1$. According to **Lemma 1** and **Lemma 2**, $f_b(\mathbf{P})$ satisfies directional monotonicity, thus $f_b(\frac{1}{\zeta}\mathbf{P}) \geq f_b(\mathbf{P})$ and $\zeta\eta_b(\mathbf{P}_1) \leq \eta_b(\zeta\mathbf{P}_1)$ holds. For the second inequality in (3.31), $\eta_b(\zeta\mathbf{P}_1) \leq \eta_b(\mathbf{P}_2)$. Based on $\frac{\partial f_b}{\partial P_b} > 0$ and $\frac{\partial f_b}{\partial P_{b'}} < 0$ in (3.26) and (3.27), we can derive the partial derivatives of $\eta_b(\mathbf{P})$ as $\frac{\partial \eta_b}{\partial P_b} = \frac{f_b(\mathbf{P}) - P_b\frac{\partial f_b}{\partial P_b}}{f_b^2(\mathbf{P})}$, and $\frac{\partial \eta_b}{\partial P_{b'}} = -\frac{P_b\frac{\partial f_b}{\partial P_{b'}}}{f_b^2(\mathbf{P})}$, where $\frac{\partial \eta_b}{\partial P_{b'}}$ is positive. We derive $\frac{\partial^2 f_b}{\partial P_b^2} < 0$ based on (3.26), which indicates the concavity of $f_b(\mathbf{P})$ on P_b [50]. Let $\mathbf{P}_0 = [P_1, \ldots, 0, \ldots, P_B]$. According to the first-order condition of concavity [50] and $f_b(\mathbf{P}_0) = 0$, $f_b(\mathbf{P}) - f_b(\mathbf{P}_0) > (P_b - 0)\frac{\partial f_b}{\partial P_b}$, and thus $\frac{\partial \eta_b}{\partial P_b} = \frac{f_b(\mathbf{P}) - P_b\frac{\partial f_b}{\partial P_b}}{f_b^2(\mathbf{P})} > 0$. The monotonicity of $\eta_b(\mathbf{P})$ is concluded, i.e., $\eta_b(\mathbf{P})$ is an increasing function of $\mathbf{P}$. Hence $\eta_b(\zeta\mathbf{P}_1) \leq \eta_b(\mathbf{P}_2)$ holds in (3.31), and thus $\zeta\eta_b(\mathbf{P}_1) \leq \eta_b(\mathbf{P}_2)$. The result that $\zeta\eta_b(\mathbf{P}_1) < \eta_b(\mathbf{P}_2)$ if $\zeta_0\mathbf{P}_1 \prec \mathbf{P}_2$ follows analogously. □

In JOPD, the complexity of each iteration (line 3 to line 6) is mainly from sorting g_{bkc} in line 3 and deriving $t_b^{*(n)}$ by solving (3.21) in line 5. Sorting can be achieved by typical methods, e.g., heapsort [145]. The computational complexity of sorting g_{bkc} in beam b for K_b users is $\mathcal{O}(K_b \log(K_b))$ [145]. The complexity of solving the nonlinear equation in (3.21) with $t_b^{*(n)}$ bounded by $[0, 1]$ and tolerance ε_1 is $\mathcal{O}(-\log(\varepsilon_1))$ [146], where $0 < \varepsilon_1 < 1$. Deriving $t_b^{*(n)}$ for each beam in (3.21) can dominate the complexity when the pre-defined ε_1 is small enough. On the other hand, sorting could be with higher complexity when ε_1 is large. Thus, the complexity of each iteration is $\mathcal{O}(\max\{K_b \log(K_b), -\log(\varepsilon_1)\})$. With maximum $N_{\max}B$ iterations, the complexity of JOPD is $\mathcal{O}(N_{\max}B \max\{K_b \log(K_b), -\log(\varepsilon_1)\})$. Overall, the convergence is geometrically fast if there exist $0 < \varpi < 1$ and a constant $\Pi > 0$ such that $\|P_b^{(n)} - P_b^*\| \leq \Pi\varpi^n$ for all n [55], where P_b^* denotes the optimal beam power.

Next, in Corollary 1, we conclude that although the optimal beam power, coupling with decoding orders, in $\mathcal{P}_1$ is challenging to be directly obtained, the optimum of $\mathcal{P}_1$, in fact, can be achieved by solving a simple problem, i.e., $\mathcal{P}_3$.

Corollary 1. The optimum of $\mathcal{P}_1$ is equal to that of $\mathcal{P}_3$.

The reasons can be explained as follows. $\mathcal{P}_1$ and $\mathcal{P}_3$ solves de facto the same problem, i.e., with the fixed α-variables then obtain the max-min OCTR along with the optimal beam and terminal power allocation since in $\mathcal{P}_3$, when $\mathbf{P}$ is known, p_{bkc} is also known. Theorem 1 indicates that, under the same α_{bkc}, no better beam power allocation than $\mathbf{P}^*$ can be found. Thus $\mathbf{P}^*$ is optimal for $\mathcal{P}_1$ and $\mathcal{P}_3$. Given $\mathbf{P}^*$ to $\mathcal{P}_1$, the resulting max-min OCTR and terminal power allocation are therefore optimal, and thus the conclusion.

The difference between $\mathcal{P}_1$ and $\mathcal{P}_3$ is that, in $\mathcal{P}_1$, one has to deal with the issue of unconfirmed convergence and undetermined optimal R_{bk} expressions due to the decoding-order variations and the undetermined optimal decoding order. In $\mathcal{P}_3$, we circumvent these difficulties by using the established

analytical results in this section. By solving $\mathcal{P}_3$ via Alg. 1, we update beam power associated with decoding order successively, instead of obtaining the optimum directly. Guaranteed by Lemma 1, Lemma 2, and Theorem 1, this simple power-adjustment approach eventually leads to the optimal beam power and optimal decoding order for the given α-variables.

3.5 A Heuristic Algorithm for Joint Power, Decoding-Order, and Terminal-Timeslot Optimization

JOPD is limited by the one-off terminal-timeslot assignment. Based on the framework of JOPD and taking its fast-convergence advantages, we design a heuristic approach, JOPDT, to iteratively update timeslot-terminal assignment and improve the overall performance. The procedure of the heuristic approach is presented in Alg. 2.

Line 3 to line 10 present the process of implementing the JOPD framework. In line 2 and line 5, precoding vectors and decoding orders are updated based on the terminal-timeslot assignment and beam power allocation, respectively. In line 6, a joint power-allocation, decoding-order, and terminal-timeslot optimization problem is solved. The problem is constructed as follows. Analogous to JOPD, by fixing $\mathbf{P}$, $\mathcal{P}_0$ is decomposed into B subproblems, each of which represents the optimization of terminals' power allocation and terminal-timeslot assignment in the beam. The b-th subproblem is expressed as,

$$\mathcal{P}_4(b): \max_{p_{bkc},\alpha_{bkc}} \quad \min_{k\in\mathcal{K}_b} \quad \frac{R_{bk}}{D_{bk}} \tag{3.33a}$$

$$\text{s.t.} \quad \rho_{bc}\sum_{k\in\mathcal{K}_b} p_{bkc} = \rho_{bc'}\sum_{k\in\mathcal{K}_b} p_{bkc'}, \forall c, c^{'} \in \mathcal{C}, c \neq c^{'}, \tag{3.33b}$$

$$\sum_{k\in\mathcal{K}_b} \alpha_{bkc} \leq \bar{K}, \forall c \in \mathcal{C}, \tag{3.33c}$$

$$\sum_{c\in\mathcal{C}} \alpha_{bkc} = 1, \forall k \in \mathcal{K}_b, \tag{3.33d}$$

$$p_{bkc} \leq \hat{P}\alpha_{bkc}, \forall c \in \mathcal{C}, \forall k \in \mathcal{K}_b. \tag{3.33e}$$

The decoding order indicators ϕ_{bklc} are determined based on $\mathbf{P}$ and g_{bkc}. Thus variables ϕ_{bklc} are therefore fixed and constraints (3.11h) and (3.11i) are no longer needed in $\mathcal{P}_4(b)$. By expressing p_{bkc} by R_{bkc}, $\mathcal{P}_4(b)$ is reformulated as:

$$\mathcal{P}_5(b): \max_{R_{bkc},\alpha_{bkc},t_b} \quad t_b \tag{3.34a}$$

$$\text{s.t.} \quad \text{(3.33c), (3.33e), (3.33d),} \tag{3.34b}$$

$$\sum_{k=1}^{K_b}\left(\frac{1}{g_{bkc}} - \frac{1}{g_{b(k-1)c}}\right) e^{\sum\limits_{j\geq k}\frac{R_{bjc}}{B_W}} - \frac{1}{g_{bK_bc}} \leq \frac{P_b}{\rho_{bc}}, \quad \forall c \in \mathcal{C}, \tag{3.34c}$$

$$t_b D_{bk} - R_{bk} \leq 0, \forall k \in \mathcal{K}_b, \tag{3.34d}$$

where the inequalities in (3.33b) are relaxed as the inequalities in (3.34c) to convert the constraints to exponential cones. Thus $\mathcal{P}_5(b)$ is identified as mixed-integer exponential conic programming (MIECP) [50], whose optimum can be solved by branch and bound or outer approximation approach.

Similar to $f_b(\mathbf{P}) = t_b^*$ in $\mathcal{P}_2(b)$, the optimal objective $\bar{t}_b^*$ in $\mathcal{P}_5(b)$ can be re-expressed by an inexplicit

Algorithm 2 JOPDT

Input:

Initial beam power, $\mathbf{P}^{(0)}$;
iteration index in the JOPD framework, $n = 0$;
iteration index, $\bar{n} = 0$;
maximum iteration in the JOPD framework, $N_{\max}$;
maximum iteration, $\bar{N}_{\max}$;
initial terminal-timeslot assignment, $\boldsymbol{\alpha}_b^{(0)}$, $\forall b \in \mathcal{B}$;
precision: $\xi_2 > 0$.

1: **repeat**
2: Update precoding vectors $\mathbf{w}_{bc}$ based on $\boldsymbol{\alpha}_b^{(\bar{n})}$.
3: **repeat**
4: **for** $b = 1, \ldots, B$ **do**
5: Update and sort g_{bkc} with $\mathbf{P}^{(n)}$.
6: Decide decoding orders ϕ_{bklc} based on the descending orders of g_{bkc}.
7: Solve $\mathcal{P}_5(b)$ and obtain $\bar{t}_b^{*(n)}$ with $\mathbf{P}^{(n)}$.
8: Update $\mathbf{P}$ by $P_b = \frac{P_b^{(n)}}{\bar{t}_b^{*(n)}}$.
9: **end for**
10: Calculate $\epsilon = \max\left\{\frac{P_b}{P_{b,\max}}, \forall b \in \mathcal{B}; \sum_{b\in\mathcal{B}} \frac{P_b}{P_{tot}}\right\}$.
11: Update $\mathbf{P}^{(n+1)} = \frac{\mathbf{P}^{(n+1)}}{\epsilon}$. $n = n + 1$.
12: **until** $n > N_{\max}$ or $|\bar{t}_b^{*(n+1)} - \bar{t}_b^{*(n)}| < \xi_2$
13: $\bar{n} = \bar{n} + 1$.
14: Update timeslot assignment $\boldsymbol{\alpha}_b^{(\bar{n})}$.
15: **until** $\bar{n} > \bar{N}_{\max}$
16: Calculate p_{bkc} based on $\mathbf{P}^{(n)}$.

Output:

$\bar{t}_b^*$, p_{bkc}, $\boldsymbol{\alpha}_b$, $\mathbf{w}_{bc}$.

function of $\mathbf{P}$, say $\bar{f}_b(\mathbf{P})$. Based on Lemma 1 and Lemma 2, the objective function $f_b(\mathbf{P})$ in $\mathcal{P}_2(b)$ is a CUF. We then conclude that $\bar{f}_b(\mathbf{P})$ is also a CUF in Corollary 2.

Corollary 2: $\bar{f}_b(\mathbf{P})$ is a CUF.

Proof. The properties of positivity and competitiveness follow analogously from Lemma 1 and Lemma 2. Regarding the directional monotonicity, given $\zeta\mathbf{P}$ and $\mathbf{P}$ to $\mathcal{P}_5(b)$, we can obtain the optimal terminal-timeslot allocation $\boldsymbol{\alpha}_1^*$ and $\boldsymbol{\alpha}_2^*$, respectively, where $\boldsymbol{\alpha}_1^*$ and $\boldsymbol{\alpha}_2^*$ collect all α-variables in beam b. Note that the difference between $\mathcal{P}_5(b)$ and $\mathcal{P}_2(b)$ is that α_{bkc} is treated as fixed parameters in $\mathcal{P}_2(b)$, whereas α_{bkc} is to be optimized in $\mathcal{P}_5(b)$ as variables. Thus, under the same $\boldsymbol{\alpha}_2^*$ in $\mathcal{P}_2(b)$, $f_b(\zeta\mathbf{P}) > f_b(\mathbf{P})$ can hold for $\zeta > 1$ according to Lemma 1 and Lemma 2. Since $\boldsymbol{\alpha}_2^*$ is the optimal outcome of using $\mathbf{P}$ in $\mathcal{P}_5(b)$, then $\bar{f}_b(\mathbf{P}) = f_b(\mathbf{P})$. Compared with $f_b(\zeta\mathbf{P})$ and $\bar{f}_b(\zeta\mathbf{P})$, $f_b(\zeta\mathbf{P})$ with a suboptimal $\boldsymbol{\alpha}_2^*$ is no higher than $\bar{f}_b(\zeta\mathbf{P})$ with its optimal $\boldsymbol{\alpha}_1^*$, thus $\bar{f}_b(\zeta\mathbf{P}) > f_b(\zeta\mathbf{P})$, and $\bar{f}_b(\zeta\mathbf{P}) > \bar{f}_b(\mathbf{P})$, then the conclusion. □

Owing to the linearity, the constraints in the formulation of $\mathcal{P}_3$ are MCs. With the properties of CUF and MC, the beam power allocation problem is an MCMU and can be tackled by the PF-based approach. By solving $\mathcal{P}_5$ in line 7, a new terminal-timeslot assignment $\alpha_b^{(\bar{n})}$ is obtained (updated in line 14), and the optimal $\bar{t}_b^*(n)$ is achieved, which is used to update beam power in line 8. The algorithm terminates

Table 3.1: Simulation Parameters

Parameter	Value
Frequency	20 GHz (Ka band)
B_W	500 MHz
Satellite location	13° E [148]
Satellite height	35,786 km [148]
Beam radiation pattern	provided by ESA [148]
Receive antenna gain	42.1 dBi
Channel model	free-space propagation loss
σ^2	-126.47 dBW
B, C	4, 5
$P_{b,\max}$, P_{tot}	120 W, 400 W [21]
$\lvert\mathcal{U}_b\rvert$	70
$\bar{K}$	2
D_{bk}	uniform distribution [149],traffic emulator in [127]
$N_{\max}$, $\bar{N}_{\max}$	15, 5

when the number of iterations (line 2 to line 14) reaches $\bar{N}_{\max}$.

In Alg. 2, there are at most $\bar{N}_{\max}N_{\max}B$ MIECPs to be solved. For each MIECP, the optimum can be obtained by branch and bound approach with exponential-time complexity [59]. For the worst-case scenario, the approach fathoms all the combinations of binary variables [147], resulting in solving 2^{K_bC} conic programmings. The complexity of solving a conic programming by interior-point method is $\mathcal{O}(-\nu \log \varepsilon_2)$ [54], where ν and ε_2 represent the self-concordant barrier parameter and precision. Thus the upper-bound complexity of Alg. 2 is $\mathcal{O}(-\bar{N}_{\max}N_{\max}\sum_{b\in\mathcal{B}} 2^{K_bC}\nu \log \varepsilon_2)$. Note that the global optimum of $\mathcal{P}_0$ is absent. Alg. 2 with exponential complexity aims at providing benchmarks and upper bounds for low-complexity algorithms.

3.6 Performance Evaluation

3.6.1 Parameter Settings

We evaluate the performance of the proposed resource allocation approaches in a NOMA-enabled multi-beam satellite system. The key parameters are summarized in Table 6.1. The parameters related to the satellite and beam radiation patterns are provided by European Space Agency (ESA) [148]. The power parameters follow the typical values in [21]. Fig. 6.5 illustrates the beam pattern we consider. In the system, NOMA is applied in a small cluster of beams ($B = 4$) which are served by an MPA. Adjacent clusters occupy orthogonal frequencies such that the inter-cluster interference can be neglected. Note that the variation of transmit antenna gain is related to the off-axis angle between the beam center and the terminal. In NOMA, since the complexity of multi-user detection increases with the number of signals to be detected by the receiver [34], $\bar{K} = 2$ is set in the simulation unless otherwise stated. The results are averaged over 1000 instances. For each instance, one terminal is randomly selected from $\mathcal{U}_b$ and the other is paired via MaxCC for each timeslot. Two NOMA-based schemes, i.e., JOPD+MaxCC with lower complexity and JOPDT with higher complexity, are compared to OMA and other benchmarks.

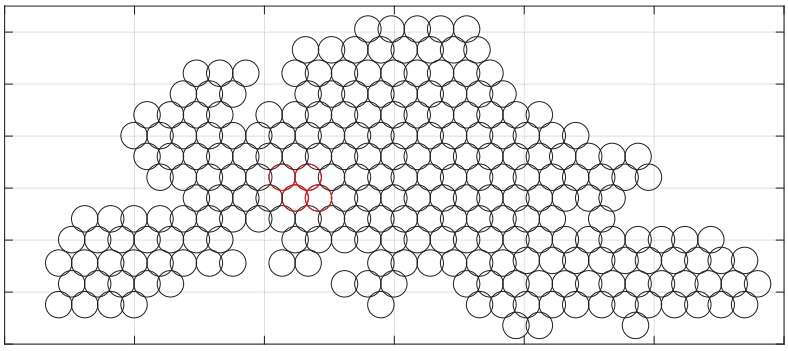

Figure 3.2: Beam pattern covering Europe provided by ESA. The figure shows an instance of four beams (highlighted in red color) served by an MPA.

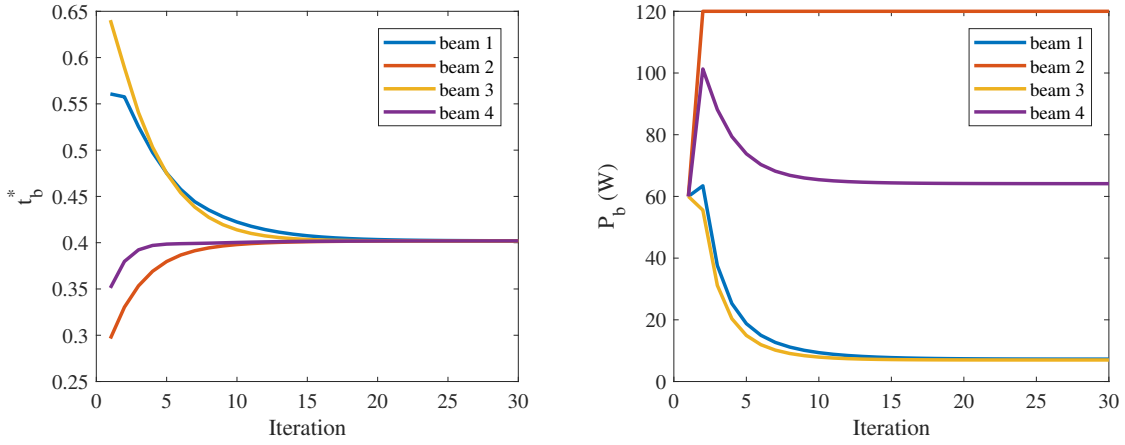

Figure 3.3: Evolutions of t_b^* and P_b over iterations in JOPD.

3.6.2 Numerical Results

Convergence performance of JOPD

We first verify the convergence performance of JOPD. Fig. 3.3 shows the evolutions of t_b^* and P_b over iterations. From the figures, we observe that beam power is adjusted based on the values of t_b^*. The power of the beams with smaller t_b^* increases while the power of the other beams decreases in each iteration. As it is proven in Theorem 1, JOPD converges, e.g., in Fig. 3.3(a) within around 15 iterations. Besides, the results verify the conclusion of Lemma 2, that is, the convergence of a CUF is not affected by the variation of decoding orders.

Comparison of max-min OCTR between NOMA and OMA

Next, we compare the max-min OCTR performance among JOPDT, JOPD+MaxCC, and OMA in Fig. 6.9 to verify the superiority of the proposed NOMA-based schemes. Different frequency-reuse patterns, i.e., 1-color, 2-color, and 4-color frequency-reuse patterns, are implemented. In 1-color frequency-reuse pattern, the entire bandwidth is shared by all the spot beams. 2-color (or 4-color) pattern refers to the scenarios that the bandwidth is equally divided into 2 (or 4) portions, each of which is occupied by one

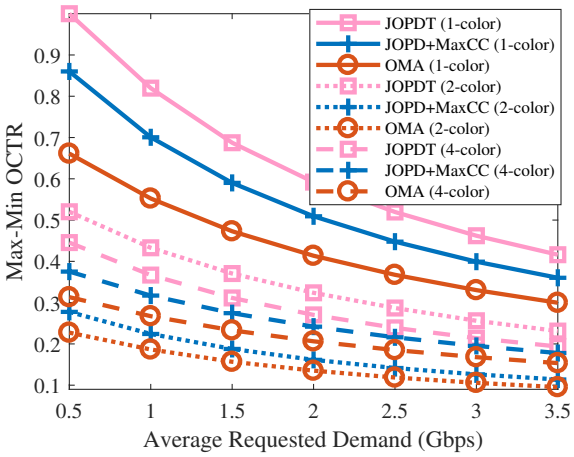

Figure 3.4: Max-min OCTR with respect to traffic demand among JOPDT, JOPD+MaxCC, and OMA.

of the 2 (or 4) adjacent beams. In OMA, the available frequency band is halved. Each half of the band is occupied by one terminal at each timeslot. Note that terminals are paired and scheduled to each timeslot by MaxCC in OMA.

In average, JOPD with MaxCC outperforms OMA with MaxCC in max-min OCTR by 24.0%, 20.0%, and 17.5% under 1-color, 2-color, and 4-color pattern, respectively. Particularly, with the implementation of 1-color pattern, the max-min OCTR in JOPD is 30.1% higher than that in OMA when the average requested demand is 0.5 Gbps. JOPD coordinated with precoding and MaxCC benefits from both reduced inter-beam and intra-beam interference compared to OMA. Remark that in 2-color pattern, both JOPD+MaxCC and OMA are worse than other frequency-reuse patterns. The reason is that compared to 2-color pattern, precoding is more effective in 1-color to mitigate strong inter-beam interference to a large extent, whereas 4-color pattern inherently receives much less inter-beam interference than that of 2-color pattern. Besides, the OCTR performance of JOPD+MaxCC is compared with JOPDT. By taking into account optimizing the terminal-timeslot assignment, JOPDT is able to improve the max-min fairness by approximately 16.2%, 98.2%, and 12.7% under 1-color, 2-color, and 4-color reuse patterns, respectively. The results validate the improvement of JOPDT over JOPD by iteratively updating the terminal-timeslot assignment.

In Fig. 3.5(a), we present the OCTR performance among JOPD+MaxCC, JOPDT, and OMA, with respect to $P_{b,\max}$. By using higher beam power $P_{b,\max}$, the max-min-OCTR value in all the three algorithms can be improved, but not significant. This might suggest that, to improve the worst-OCTR terminal's performance in practice, developing advanced user-scheduling and power-allocation schemes would be the key rather than simply increasing beam power.

In Fig. 3.5(b), we show the OCTR performance with various $\bar{K}$ for the proposed two algorithms. The max-min OCTR in two NOMA schemes increases effectively when $\bar{K}$ grows from 2 to 3. The growth becomes slow when 4 to 5 terminals are multiplexed on each slot. As we mentioned before, higher $\bar{K}$ might not necessarily bring significant improvement but imposes more complexity to multi-user detection and SIC at the receiver side. Thus, in the simulation, we set $\bar{K} = 2$ for the trade-off between performance gain and complexity.

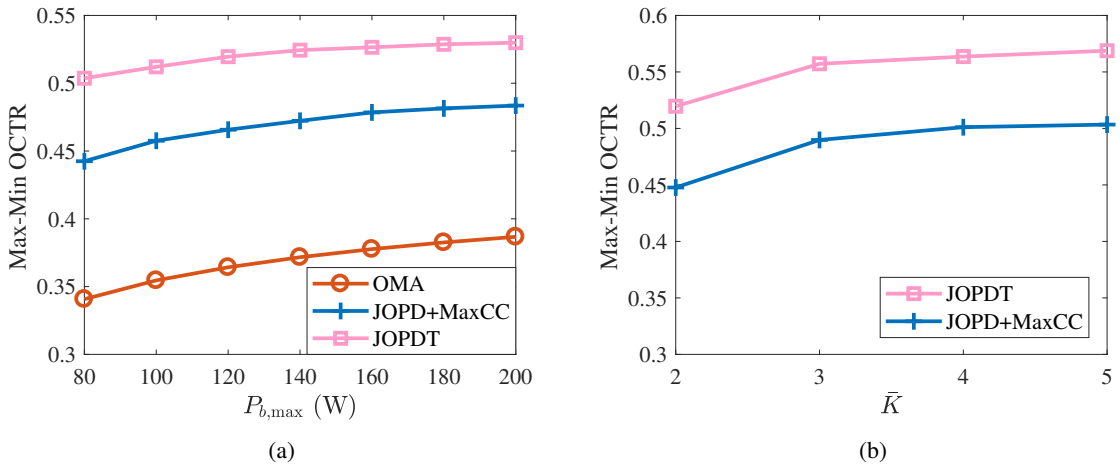

Figure 3.5: Max-min OCTR with respect to: (a), $P_{b,\max}$; (b), $\bar{K}$, among JOPDT, JOPD+MaxCC, and OMA.

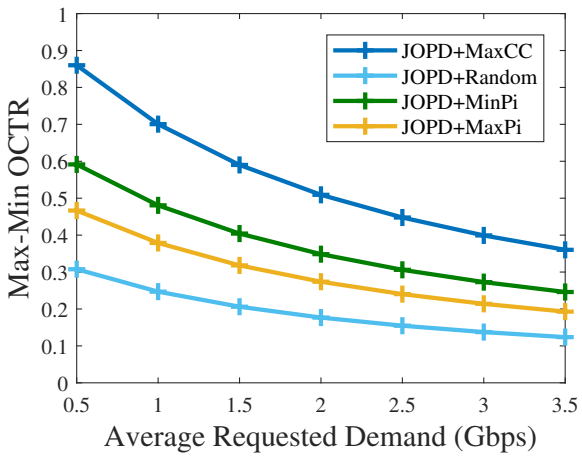

Figure 3.6: Max-min OCTR with respect to traffic demand among different terminal-timeslot assignment approaches.

Comparison of max-min OCTR among different terminal-timeslot allocation approaches

Different strategies of terminal-timeslot scheduling are compared in Fig. 6.10 in order to illustrate the advantages of MaxCC with NOMA in improving OCTR performance. The basis of MaxCC is to allocate each timeslot to terminals with highest-correlation channels without considering the gap of $\|\mathbf{h}_{bk}\|$. The benchmarks are listed as follows:

- MaxPi [41]: Allocate each timeslot to terminals with highly correlated channels and the largest gap of $\|\mathbf{h}_{bk}\|$,
- MinPi [41]: Allocate each timeslot to terminals with highly correlated channels and the smallest gap of $\|\mathbf{h}_{bk}\|$,
- Random: Allocate each timeslot to terminals randomly.

Note that in MaxPi and MinPi, terminals with the largest and smallest gain difference, respectively, are

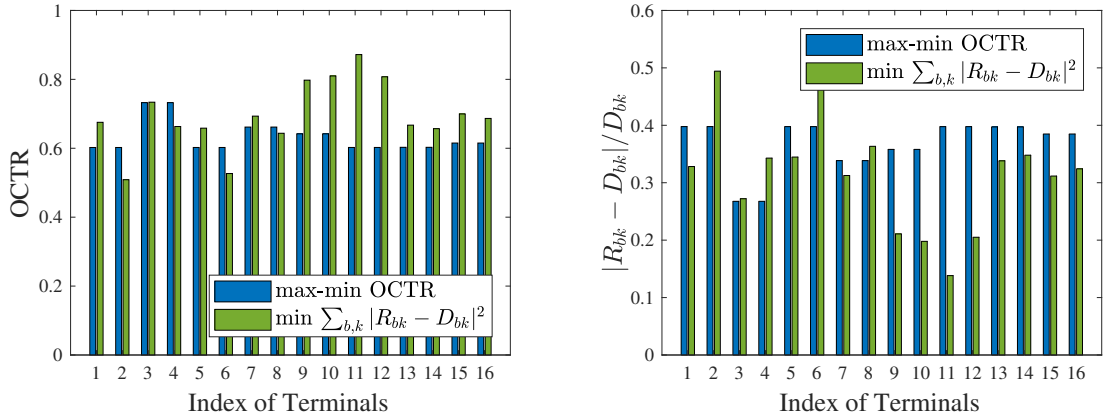

(a) (b)

Figure 3.7: An illustration of the distribution of (a) OCTR; (b) Ratio $|R_{bk} - D_{bk}|/D_{bk}$ among terminals achieved by max-min OCTR and min $\sum_{b,k} |R_{bk} - D_{bk}|^2$.

selected from those with correlation factor $\theta > 0.9$.

From Fig. 6.10, JOPD+MaxCC brings the largest gain compared to other benchmarks. In MaxCC, the terminals with the highest channel correlation are selected. Hence MaxCC can effectively reduce the inter-beam interference and exploit the synergy of NOMA with precoding. Besides, the OCTR performance is sensitive to inter-beam interference. The non-highest correlated channels in MinPi and MaxPi introduce a considerable amount of inter-beam interference and thus degrade the performance to a certain extent.

Comparison of objective functions between "max-min OCTR" and "min $\sum_{b,k} |R_{bk} - D_{bk}|^2$"

Fig. 3.7(a) presents the distribution of OCTRs among terminals achieved by JOPD+MaxCC, compared with NOMA to minimize $\sum_{b,k} |R_{bk} - D_{bk}|^2$. Previous works, e.g., [21, 44], focus on reducing the sum of the gap between offered capacity and requested traffic demand, i.e., "min $\sum_{b,k} |R_{bk} - D_{bk}|^2$". The approach proposed in [138] is adopted to solve the problem with the objective of "min $\sum_{b,k} |R_{bk} - D_{bk}|^2$". We can observe that the max-min operator compromises the performance of high-capacity terminals, e.g., terminals 9 to 12, to compensate terminals with low OCTRs, e.g., terminals 2 and 6. The average OCTR in "max-min OCTR" is lower than that in "min $\sum_{b,k} |R_{bk} - D_{bk}|^2$" by 8.82%, but the minimum OCTR increases by 18.4% in "max-min OCTR".

We evaluate the performance of "max-min OCTR" and "min $\sum_{b,k} |R_{bk} - D_{bk}|^2$" by another metric, $\frac{|R_{bk} - D_{bk}|}{D_{bk}}$, in Fig. 3.7(b). The performance in "min $\sum_{b,k} |R_{bk} - D_{bk}|^2$" achieves 14.78% higher average performance but loses of 19.54% in the worst $\frac{|R_{bk} - D_{bk}|}{D_{bk}}$ than "max-min OCTR". In addition, by adopting the Jain fairness index [10], i.e., $(\sum_{b,k} \frac{R_{bk}}{D_{bk}})^2 / ((\sum_b K_b) \sum_{b,k} (\frac{R_{bk}}{D_{bk}})^2)$, the performance in both functions "max-min OCTR" and "min $\sum_{b,k} |R_{bk} - D_{bk}|^2$" leads to satisfactory fairness values 0.99 and 0.98, respectively.

Evaluation in the scenarios with pracitcal factors

In Fig. 3.8, we evaluate the max-min OCTR among the three algorithms when practical factors are considered. The performance achieved by the three schemes over the channels with free-space propaga-

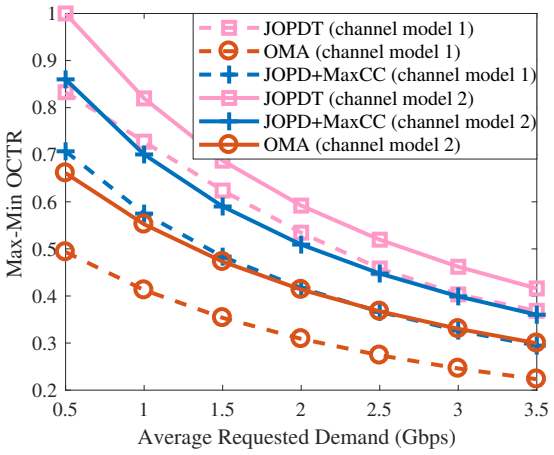

(a)

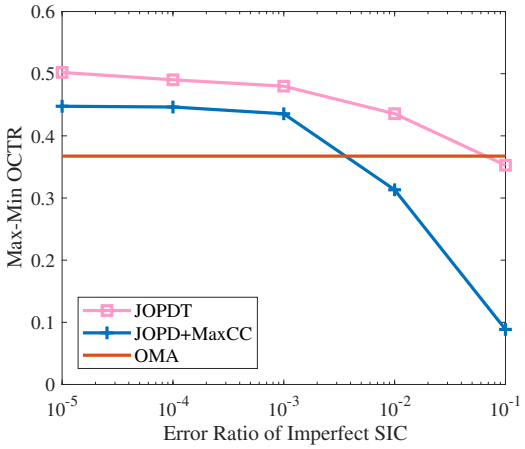

(b)

Figure 3.8: Max-min OCTR comparison: (a) by adopting two channel models: 1, atmospheric-fading model based on ITU-R P.1853-2, 2, free-space model; (b) considering error ratio of imperfect SIC.

tion loss and with atmospheric fading is compared in Fig. 3.8(a). The channel model with atmospheric fading (consisting of long-term effects and rain effects) is emulated based on Recommendation ITU-R P.1853-2 [150]. From the results, firstly, we observe that the performance improvement of the proposed two NOMA schemes, i.e., JOPDT and JOPD+MaxCC, over OMA is consistent in both channel models. Secondly, the benefits of adopting NOMA in the atmospheric-fading model over OMA are even more significant than that in the free-space cases.

In Fig. 3.8(b), we investigate the OCTR performance under imperfect-SIC conditions. We adopt an approach proposed in [139] which uses an error ratio to represent the residual intra-beam interference due to error propagation of imperfect SIC. With a lower error ratio, e.g., from 10^{-5} to 10^{-3}, the performance of both NOMA schemes slightly decreases, but keeps considerable performance gain over OMA. However, as the error ratio increases, this performance gain can be diminished because a non-negligible residual interference has to be taken into account in NOMA but this type of interference does not present in OMA. The NOMA performance can be lower than that of OMA when error ratios are very high, e.g., 10^{-2} and 10^{-1}. This suggests that to maintain the advantages of NOMA in practice, the error ratio of

SIC has to be confined at low levels, otherwise OMA might be a more favorable option. In addition, we observe that JOPDT is more robust than JOPD+MaxCC in against imperfect SIC. This is because that when the error ratio and the resulting interference become non-negligible, JOPDT is able to properly update the terminal groups iteratively whereas JOPD+MaxCC has to keep the fixed terminal-timeslot assignment.

3.7 Conclusion

This chapter has introduced NOMA into multi-beam satellite systems to facilitate aggressive frequency reuse and enhance power-domain flexibility. We have provided a resource optimization framework for general NOMA-enabled SatCom. A max-min problem of jointly optimizing power, decoding orders, and terminal-timeslot assignment has been formulated to improve the worst OCTR among terminals. We have proposed a PF-based algorithmic framework JOPD to jointly allocate power and decide decoding orders by fixing terminal-timeslot assignment with the guarantee of fast convergence. Based on the framework of JOPD, a heuristic approach JOPDT has been developed to iteratively update the terminal-timeslot assignment and improve the overall OCTR performance. The superiority of the proposed algorithms in max-min fairness over OMA has been demonstrated.

Chapter 4

Learning-Assisted Approaches for Resource Optimization in NOMA-Satellite Systems

In this chapter, we move from optimization to machine learning and provide learning-assisted resource optimization frameworks for general NOMA-enabled satellite systems. We investigate a problem to minimize the transmission time by jointly optimizing power allocation and terminal-timeslot assignment for accomplishing a transmission task. The problem appears non-linear/non-convex with integer variables and can be equivalently reformulated in the format of MICP. Conventional optimal or near-optimal iterative methods may be applied but at the expenses of high computational complexity. Towards an efficient solution, we train DNN to perform fast and high-accuracy predictions to tackle the difficult combinatorial parts, i.e., determining the minimum consumed timeslots and terminal-timeslot scheduling. Conventional end-to-end learning directly predict the integer solutions, which, however, may encouter the feasibility issue when the problem is complex. To provide feasible power allocation, we develop a low-complexity post procedure to process the predicted outcomes. For further enhancement of feasibility, we propose a dual-DNN assisted approach, where the first learning task is to predict the integer variables while the second task is to guarantee the feasibility of the solutions. Numerical results show that the proposed learning-assisted algorithms outperform benchmarks in terms of average computational time, transmission time performance, and feasibility guarantee. In the end, we discuss the pros and cons of optimization-based and learning-assisted schemes.

4.1 Introduction

SatCom has drawn growing attention owing to the advantages in providing wide coverage and high throughput [2]. However, due to the long distance between satellites and ground terminals, large transmission time restricts the performance of satellite systems, especially in the context of delivering services with latency restrictions [2], which motivates studies on resource optimization for satellite delay-constrained services [151, 152, 153, 118]. The authors in [151] and [152] focused on delay-constrained resource allocation problems in satellite multi-beam and satellite-backhauling systems, respectively. In [153] and [118], the authors investigated completion time minimization problem in LEO satellite assisted uplink IoT networks. To embrace future trends of SatCom, new applications, e.g., satellite-backhauling and content delivery, require more sophisticated design in terms of latency reduction.

Due to the capability of multiplexing more co-channel users and enhancing spectral efficiency than OMA, power-domain NOMA has the potentials to further reduce delay for satellite systems. Satellite-

NOMA has already proven its performance gains in capacity [108], outage performance [108], and OCTR [154] compared to conventional satellite-OMA systems. However, resource allocation for transmission delay minimization in NOMA-enabled satellite systems has not been fully investigated yet. Delay is considered in the constraints of resource optimization in NOMA-based multi-beam satellite systems in [112]. In [118], the objective of the resource allocation problem is to minimize the completion time for LEO-satellite-assisted Internet of things systems. However, NOMA is applied in the terrestrial part but not in satellite transmission. It is unknown how satellite-NOMA schemes perform in transmission delay reduction compared to conventional satellite-OMA schemes. To the best of our knowledge, this is the first work to investigate resource optimization of transmission time minimization for NOMA-enabled satellite systems.

Another factor that influences the delivery of satellite delay-constrained services is the computational complexity of resource allocation algorithms. High-complexity algorithms may cause processing delays and thus fail to satisfy terminals' demands before deadlines [2]. A majority of resource allocation problems in satellite systems fall into the domain of constrained combinatorial optimization [151, 152, 153, 118, 93, 154, 155]. Conventional algorithms for solving such problems may consume a large amount of computational efforts and time in attaining the optimum or near-optimum, and with limited capability to well balance optimality and computational complexity [101]. In comparison to model-based optimization, data-driven learning techniques can exploit useful information from empirical data first, and then approximate optimal decisions with less computational complexity [156].

Applying DL techniques to resource optimization in satellite systems has been studied from various aspects, e.g., predicting the optimal decoding order for NOMA-based satellite systems [123], assisting beam-timeslot scheduling for beam hopping satellite systems [85], compensating for the non-linear distortion at receivers in LEO satellite systems [157], etc. Applying DL to address constrained combinatorial problems is, however, studied to a limited extent in the literature. Directly applying end-to-end learning may not achieve desired performance due to the feasibility issue [158]. In addition, RL/DRL-based approaches are prone to address the unconstrained problems or with few constraints due to the feasibility issue. RL/DRL requires a Markov process to guarantee a satisfactory performance [68]. However, for addressing the practical combinatorial optimization problems, the Markov process might not be satisfied and the problems could be complicated with numerous constraints. These can result in difficulties in reward function design, infeasibility issues, and thus potential degradation in the overall performance. The challenges of designing a DL-based solution lie in how to apply DL to obtain a solution of constrained combinatorial optimization with low complexity, and at the meantime, achieve satisfactory approximating performance and guarantee a feasible solution by meeting all the constraints.

In this chapter, a DL-assisted approach is designed to minimize the transmission time in NOMA-enabled satellite systems. The main contributions are summarized as follows.

- We formulate a mixed-integer non-linear programming (MINLP) problem to minimize the transmission time via power allocation and timeslot-terminal assignment in a NOMA-based satellite system. With the identified convexity, we reformulate the primal problem as MICP, whose optimum or near optimum can be achieved by applying mature optimization methods in spite of high complexity. By doing so, optimal labels in (supervised) training can be obtained through well-established optimization approaches.

- As mentioned above, simply applying end-to-end learning may not provide a near-optimal solution and guarantee the feasibility in terminal-timeslot-power allocation for the considered MICP. We design two learning-assisted schemes, i.e., hybrid solution with DL and post-process optimization (DPO) and hybrid solution with dual DNNs and convex optimization (DDCO), which are combined with data-driven learning and model-based optimization approaches.

- The core idea of DPO is to tackle the high-complexity part in discrete optimization by relying on DNN predictions and a low-complexity post-process procedure to provide feasible power allocation, such that the overall algorithm can avoid a time-consuming iterative process meanwhile is able to maintain the satisfactory performance.
- To further improve the feasibility of the predicted binary solution, we adopt another DNN to identify its feasibility in power allocation after the integer solution prediction of the first DNN. Both solution prediction and feasibility-check identification are classification-like tasks and suited to be learned by DNN. With the obtained terminal-timeslot allocation, the remaining power allocation problem is optimally and efficiently solved by convex optimization.
- The numerical results demonstrate the superiority of the proposed learning assited algorithms in computational time reduction, near-optimality approaching, and feasibility guarantee, compared with state-of-the-art optimal and suboptimal solutions.

4.2 System Model

We consider resource allocation for forward-link transmission in a GEO satellite system. In the system, four-color frequency-reuse pattern is implemented, where the bandwidth is equally segmented into two portions and each portion makes use of vertical and horizontal polarizations. Each color is occupied by one of the neighboring four beams, such that any two adjacent beams can access to different orthogonal resources [2]. Hence, inter-beam interference has limited impacts on other beams and can be viewed as fixed. Resource optimization can be therefore decoupled into each beam. In this work, we focus on the algorithmic design of resource allocation for the single-beam scenario. For practical implementation, the proposed algorithm can be executed parallelly in the resource manager at the gateway side for multiple beams.

We consider that the satellite system provides services to K fixed ground terminals within a beam. Terminals' requested demands need to be satisfied by allocating power and scheduling timeslots to terminals before the deadline. We define that the number of available timeslots is up to T timeslots. In conventional OMA-based satellite systems, each timeslot can only be assigned to one terminal. In NOMA-enabled satellite systems, however, more than one terminal is allowed to access to each timeslot. The higher resource utilization in NOMA may enable the less duration in delivering deadline-constrained services compared to conventional OMA schemes.

According to the basis of NOMA, terminals' signals are superimposed at the gateway and transmitted to the satellite and then to the corresponding ground terminals. Having received the signals, terminals perform the SIC process to eliminate part of the co-channel interference. We denote the channel gain of terminal k as G_k, which is derived by,

$$G_k = G_k^{\mathrm{Tx}} L_k G_k^{\mathrm{Rx}}. \tag{4.1}$$

Here, G_k^{Tx} denotes the satellite transmit antenna gain depending on the off-axis angle between terminal k and the corresponding beam center. G_k^{Rx} is the receive antenna gain of terminal k. L_k represents the free-space path loss from the satellite to the k-th terminal. The path loss is computed by,

$$L_k = \left(\frac{c}{4\pi f d_k}\right)^2, \tag{4.2}$$

where c, f, and d_k denote the light speed, the frequency, and the distance between the satellite and terminal k, respectively. In a GEO satellite system with fixed ground terminals, the channel gains are

assumed to stay unchanged with large coherence time. The decoding order is determined based on the descending order of the channel gains. For presentation simplicity, we define that terminals' indices keep the same with the decoding order, i.e.,

$$G_1 > G_2 > \cdots > G_K. \tag{4.3}$$

The signal-to-interference-plus-noise ratio (SINR) of terminal k at timeslot t is expressed as,

$$\mathrm{SINR}_{kt} = \frac{G_k P_{kt}}{\sum_{j=1}^{k-1} G_k P_{jt} + I_k + \sigma^2}, \tag{4.4}$$

where P_{kt} denotes the transmit power of terminal k at timeslot t. I_k is the empirical expectation of the inter-beam interference to terminal k. σ^2 is the noise power. In (4.4), terminal k is unable to decode terminal j's signal when $j < k$, and terminal j's signal is thus treated as interference at terminal k's receiver. For $j > k$, terminal k performs SIC to decode and remove j's signal such that the inter-terminal interference can be reduced. Note that, if $P_{kt} = 0$, $\mathrm{SINR}_{kt} = 0$ and other terminals will not suffer the co-channel interference from the k-th terminal. The allocated capacity for terminal k at timeslot t can be derived as,

$$C_{kt} = W \log\left(1 + \mathrm{SINR}_{kt}\right), \tag{4.5}$$

where W is the occupied bandwidth. Thus, the achievable offered capacity of terminal k is derived as

$$C_k = \sum_{t=1}^{T} C_{kt}. \tag{4.6}$$

4.3 Problem Formulation and Analysis

We formulate a resource optimization problem to minimize the transmission time of accomplishing a task for delivering requested services to ground terminals. The variables are defined as follows:

$$0 \le P_{kt} \le P_{\max}, \text{ transmit power of terminal } k \text{ at timeslot } t;$$

$$a_{kt} = \begin{cases} 1, \text{ terminal } k \text{ is scheduled at timeslot } t, \\ 0, \text{ otherwise;} \end{cases}$$

$$b_t = \begin{cases} 1, \text{ timeslot } t \text{ is assigned by any terminal,} \\ 0, \text{ otherwise.} \end{cases}$$

We define vectors $\mathbf{a}$, $\mathbf{b}$, and $\mathbf{P}$ to collect all the a_{kt}, b_t, P_{kt} variables, respectively. The problem is formulated as,

$$\mathcal{P}_1 : \min_{\mathbf{a},\mathbf{b},\mathbf{P}} \sum_{t=1}^{T} b_t \tau + \max_k \left\{ \frac{d_k + d^{\mathrm{GW}}}{c} \right\} \tag{4.7a}$$

$$\text{s.t. } C_k \ge D_k, \forall k = 1, \ldots, K, \tag{4.7b}$$

$$(C_k - D_k)^2 \le \Delta, \forall k = 1, \ldots, K, \tag{4.7c}$$

$$\sum_{k=1}^{K} P_{kt} \leq P_{\max}, \forall t = 1, \ldots, T, \tag{4.7d}$$

$$\sum_{k=1}^{K} a_{kt} \leq \bar{K} b_t, \forall t = 1, \ldots, T, \tag{4.7e}$$

$$b_t \geq b_{t+1}, \forall t = 1, \ldots, T-1, \tag{4.7f}$$

$$P_{kt} \leq P_{\max} a_{kt}, \forall k = 1, \ldots, K, \forall t = 1, \ldots, T. \tag{4.7g}$$

Here, τ denotes the duration of one timeslot and d^{GW} denotes the distance between the gateway and the satellite. In the objective, the transmission time includes completion time, defined as the total duration of all the occupied timeslots, and transmission delay, defined as the maximum propagation duration among terminals. To avoid unnecessary delay, constraints (4.7f) restrict that no idle timeslot appears before the transmission task is accomplished. Once the t-th timeslot is not assigned to any terminals, the timeslots after t will be no longer scheduled. Constraints (4.7b) denote that each terminal's demand D_k must be satisfied within at most T timeslots. In (4.7c), the difference between offered capacity and requested demands of each terminal should be smaller than Δ to reduce unused capacity. In (4.7d), the total consumed power at each timeslot is no more than the beam power budget $P_{\max}$. Constraints (4.7e) confine the number of scheduled terminals at each timeslot no larger than $\bar{K}$. Constraints (4.7e) also connect $\mathbf{a}$ with $\mathbf{b}$. That is $\sum_{k=1}^{K} a_{kt} = 0$ if $b_t = 0$. Note that the solution $\sum_{k=1}^{K} a_{kt} = 0$ and $b_t = 1$ is clearly not the optimal and thus is excluded from the optimum. Constraints (4.7g) confine the dependence between $\mathbf{P}$ and $\mathbf{a}$, where $P_{kt} = 0$ if $a_{kt} = 0$, and $P_{kt} \leq P_{\max}$ if $a_{kt} = 1$.

We observe that $\mathcal{P}_1$ is identified as an MINLP due to the presence of binary variables $\mathbf{a}$, $\mathbf{b}$, and non-linear function C_{kt} in (4.4) and (4.5) [50]. To reveal the convexity of the original problem, we derive P_{kt} as the function of capacity C_{kt} based on (4.4) and (4.5) via a substituting procedure [101]. Then $\sum_{k=1}^{K} P_{kt}$ reads:

$$\sum_{k=1}^{K} P_{kt} = \sum_{k=1}^{K} \left(\frac{I_k + \sigma^2}{G_k} - \frac{I_{k-1} + \sigma^2}{G_{k-1}} \right) \exp\left(\frac{\sum_{j \geq k} C_{jt}}{W} \right) - \frac{I_K + \sigma^2}{G_K}, \tag{4.8}$$

where we define $\frac{I_0 + \sigma^2}{G_0} = 0$. Substituting (4.8) into $\mathcal{P}_1$, the original problem is equivalently reformulated as,

$$\mathcal{P}_2 : \min_{\mathbf{a},\mathbf{b},\mathbf{C}} \sum_{t=1}^{T} b_t \tau + \max_{k} \left\{ \frac{d_k + d^{\mathrm{GW}}}{c} \right\} \tag{4.9a}$$

$$\text{s.t.} \quad (4.7\text{b}), (4.7\text{c}), (4.7\text{e}), (4.7\text{f}), \tag{4.9b}$$

$$\sum_{k=1}^{K} \left(\frac{I_k + \sigma^2}{G_k} - \frac{I_{k-1} + \sigma^2}{G_{k-1}} \right) \exp\left(\frac{\sum_{j \geq k} C_{jt}}{W} \right) - \frac{I_K + \sigma^2}{G_K} \leq P_{\max}, \forall t = 1, \ldots, T, \tag{4.9c}$$

$$C_{kt} \leq C_{\max} a_{kt}, \forall k = 1, \ldots, K, \forall t = 1, \ldots, T, \tag{4.9d}$$

where vector $\mathbf{C}$ collects all the capacity variables C_{kt}. The optimization variables are $\mathbf{a}$, $\mathbf{b}$, and $\mathbf{C}$. Similar to (4.7g), we confine the relationships between $\mathbf{C}$ and $\mathbf{a}$ in (4.9d), where $C_{\max} > \max_{k,t}\{C_{kt}\}$. That is, $C_{kt} = 0$ if $a_{kt} = 0$, and $C_{kt} \leq C_{\max}$ if $a_{kt} = 1$. Note that since $\mathcal{P}_1$ and $\mathcal{P}_2$ are equivalent, the solution of $\mathbf{P}$ can be computed by the expression of $\mathbf{C}$ based on the substituting procedure after solving $\mathcal{P}_2$.

The expression of (4.9c) is the sum of exponential functions, which is convex [50]. More specifically,

we recognize that the convex constraints (4.9c) are in fact in the format of non-symmetric exponential cones. Besides, constraints (4.7c) are in the convex quadratic format. Thus $\mathcal{P}_2$ is identified as an MICP problem [159]. On the one hand, optimal or near-optimal solutions of small-/medium-scale MICP problems can be obtained by conventional branch-and-bound and outer-approximation methods [160]. Some state-of-the-art solvers, e.g., MOSEK [51], can also apply. The procedure of solving a MICP problem in MOSEK follows four steps: presolve, cut generation, starting-point initialization, and iterative search [51]. The first three steps aim to pre-optimize the problem and find a good initial point. In the iterative search, the optimum is bounded and approached by branch-and-bound and outer-approximation approach. Nevertheless, the intrinsic difficulties in discrete optimization lead to exponentially increased computational complexity and time, which are unaffordable in practical scenarios. With deadline constraints, the applicability of these approaches in satellite systems may be inevitably cause the failure of accomplishing a transmission task.

On the other hand, DL has already proven satisfactory performance in several learning tasks, e.g., classification and regression, where a mapping from training inputs to outputs is learned [68]. However, DL may not be directly applicable to complicated mixed-integer optimization problems like $\mathcal{P}_2$. Direct end-to-end learning, for example, does not perform well in the prediction of optimal integer solutions [158] since imperfect prediction will lead to dissatisfaction of some constraints and thus the infeasibility issue. It is essential to identify whether the predicted solution is feasible or not and to obtain a near-optimal feasible solution efficiently. How to design a DL-based approach to appropriately address $\mathcal{P}_2$ is non-trivial, and requires careful design in a tailored way.

4.4 DPO: Hybrid Solution Combined with DNNs and a Post-Process Optimization

In this section, we design DPO to tackle $\mathcal{P}2$. A complete solution for $\mathcal{P}2$ consists of three terms, i.e., the minimum number of consumed timeslots ($b^* = \min \sum_{t\in\mathcal{T}} b_t$), the terminal-timeslot assignment on b^* slots, and the corresponding capacity/power allocation. The procedure of DPO is illustrated in Fig. 4.1 and Alg. 3, where three DNNs work parallelly to predict different variables.

As an input to DPO, the first DNN directly learns the mapping between channel-demand parameters and b^*. We adopt a widely-used Softmax function as the activation function in the output layer, which normalizes the outputs to a categorical distribution [68]. For example, the t-th element in the output vector, b_t, represents the probability of consuming t timeslots, which is derived by

$$b_t = \frac{\exp(\tilde{b}_t)}{\sum_{t'\neq t} \exp(\tilde{b}_{t'})}, \tag{4.10}$$

where $\tilde{b}_t$ denotes the output at t-th node in the last hidden layer. The predicted $\hat{b}$ is obtained by selecting the highest probability from output nodes, i.e.,

$$\hat{b} = \max_{t\in\mathcal{T}} \{b_t\}. \tag{4.11}$$

For training, we use a tuple $\{\mathbf{G}, \mathbf{D}; \mathbf{b}^*\}_n,\ n = 1, \ldots, N$ to represent the n-th training set, where the input channel-coefficient vector is $\mathbf{G} = [G_1, \ldots, G_K]$ (real values) and demand vector is $\mathbf{D} = [D_1, \ldots, D_K]$. The corresponding optimal binary label is organized in $\mathbf{b}^* = [b_1, \ldots, b_T]$.

The second and third DNN-based predictions output estimated terminal-timeslot assignment $\hat{\mathbf{a}}$ and power (or rate) splitting ratios $\hat{\mathbf{r}}$, with trained by two sets of tuples $\{\mathbf{G}, \mathbf{D}; \mathbf{a}^*\}_n$ and $\{\mathbf{G}, \mathbf{D}; \mathbf{r}^*\}_n$, re-

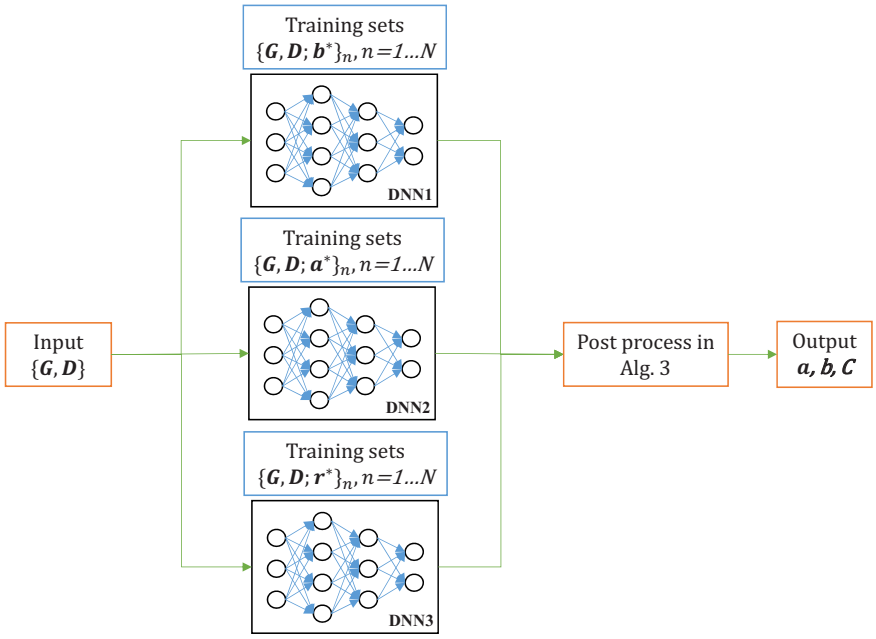

Figure 4.1: Illustration of the proposed DPO

spectively. The optimal labels in $\mathbf{a}^*$ are binary, and the labels in vector $\mathbf{r}^*$ are prepared by

$$r_{kt}^* = \frac{P_{kt}^*}{\sum_{k=1}^{K} P_{kt}^*}, \forall r_{kt}^* \in \mathbf{r}^*. \tag{4.12}$$

The predicted $\hat{\mathbf{a}}$ and $\hat{\mathbf{r}}$ may not be feasible for $\mathcal{P}2$ since imperfect predictions may cause constraint violation. However, the predicted $\hat{\mathbf{a}}$ carries the information of which users with high probability to be scheduled on each timeslot. In addition, the approximated ratios in $\mathbf{r}^*$ gives more flexibility in post-processing and performance scaling, compared to directly learning power values. We then rely on $\hat{\mathbf{a}}$, $\hat{\mathbf{r}}$, and $\hat{b}$ as useful guidance and develop a post-processing approach in line 2 to line 14. In line 2, to enable a higher successful rate in delivering feasible solutions, we introduce an integer offset δ as a scaling parameter to provide more chance to find a feasible power solution since with more timeslot resources, e.g., $\hat{b}+\delta$, all the terminals' demands can be satisfied more easily than using fewer timeslots, e.g., $\hat{b}$. There are two inaccurate cases, $\hat{b} < b^*$ or $\hat{b} > b^*$. In the first case, $\hat{b} < b^*$ directly results in infeasible power allocation, then δ provides more tolerance for the inaccurate $\hat{b}$ and finding feasible solution. In the second case, we confine δ to be small, e.g., $\delta = 1$ or 2, in case of large performance degradation. In line 3 to line 4, by sorting $\hat{\mathbf{a}}$, we select up to $\bar{K}$ highest-probability users on each time slot to satisfy constraints (4.7e), saying users $1, \ldots, \bar{K}$ for simplicity. Based on the user allocation, we assign power in line 5 to meet P_{max} in constraints (4.7d). We check if all the users' demands are delivered in line 9 to ensure constraints (4.7b). The algorithm terminates when $\hat{\mathcal{K}} = \varnothing$ or $\hat{b}+\delta$ is reached.

The complexity of a fully-connected DNN mainly comes from the operations of matrix multiplication, vector addition, and activation functions [68]. The number of floating-point operations (FLOPs) of a hidden layer is $(2N_l^{\text{in}}+1)N_l^{\text{out}}$ [68], where N_l^{in} and N_l^{out} denote the number of input and output nodes at the l-th hidden layer, respectively. In line 1, the complexity for 3 DNNs in the testing phase is $\mathcal{O}(3\sum_{l=1}^{N^{\text{h}}}(2N_l^{\text{in}}+1)N_l^{\text{out}})$, where N^{h} is the number of hidden layer. In the post-process, the complexity is dominated by line 3 and 7. In line 3, sorting K elements in $\hat{\mathbf{a}}$ on each TS costs $\mathcal{O}(K\log(K))$ complex-

Algorithm 3 DPO

Input:
Trained DNNs by $\{\mathbf{G}, \mathbf{D}; \mathbf{b}^*\}_n$, $\{\mathbf{G}, \mathbf{D}; \mathbf{a}^*\}_n$ and $\{\mathbf{G}, \mathbf{D}; \mathbf{r}^*\}_n,\ n = 1, \ldots, N$.
Initialize unfinished-terminal set $\hat{\mathcal{K}} = \mathcal{K}$ and offset δ (integer).

1: Given a test set to the DNNs and obtain $\hat{b}$, $\hat{\mathbf{a}}$, $\hat{\mathbf{r}}$.
2: **for** $t = 1$ to $\hat{b} + \delta$ **do**
3: Sort $\hat{a}_{1t}, \ldots, \hat{a}_{Kt} \in \hat{\mathbf{a}}$ by a descending order.
4: Select up to $\bar{K}$ highest-probability users $\{1, \ldots, \bar{K}\} \cap \hat{\mathcal{K}}$ according to $\hat{a}_{1t}, \ldots, \hat{a}_{Kt}$.
5: Power allocation $P_{kt} = P_{max} \times \hat{r}_{kt},\ \forall \hat{r}_{kt} \in \hat{\mathbf{r}},\ \forall k \in \{1, \ldots, \bar{K}\} \cap \hat{\mathcal{K}}$
6: **for** $k = 1$ to $\bar{K}$ **do**
7: Calculate delivered capacity C_{kt} by (4.5) and (4.4).
8: Update residual demand $D_k = D_k - C_{kt}$
9: **if** $D_k \leq 0$ **then**
10: $\hat{\mathcal{K}} = \hat{\mathcal{K}} \backslash \{k\}$.
11: **end if**
12: **end for**
13: Break if $\hat{\mathcal{K}} = \varnothing$.
14: **end for**

Output: Power-terminal allocation

ity [145]. In line 7, the FLOPs number of SINR calculation for the selected L users is $(1 + \bar{K})\bar{K}$. Thus the complexity of DPO can be expressed as $\mathcal{O}(\max\{3\sum_{l=1}^{N^{\mathrm{h}}}(2N_l^{\mathrm{in}} + 1)N_l^{\mathrm{out}},\ TK\log(K) + T\bar{K}(\bar{K} + 1)\})$.

4.5 DDCO: Hybrid Solution Combined with Dual DNNs and Convex Optimization

To further improve the feasibility performance, in this section, we propose DDCO to tackle $\mathcal{P}_2$. The idea is that we rely on the fast prediction in dual DNNs to tackle the most difficult and time-consuming part in MICP, i.e., optimizing discrete variables $\mathbf{a}$ and $\mathbf{b}$, instead of performing iterative searching algorithms. The remaining power (or capacity) allocation can be solved by efficient convex optimization approaches. Overall, DDCO is expected to reap advantages from learning and optimization, and thus to enable an efficient, feasible, and near-optimal solution. The procedure is illustrated in Fig. 4.2.

In DDCO, we extract two classification-like tasks from $\mathcal{P}_2$, and let dual DNNs train and learn from optimal labels to provide a promising terminal-timeslot allocation with identified feasibility. The 1-st DNN is used to predict the binary elements in $\mathbf{a}$, i.e., learning the mapping from the input of channel-gain vector $\mathbf{G} = [G_1, \ldots, G_K]$ and demand vector $\mathbf{D} = [D_1, \ldots, D_K]$ to optimal terminal-timeslot allocation $\mathbf{a}^*$. We use a tuple $\{\mathbf{G}, \mathbf{D}; \mathbf{a}^*\}_n$ to represent the n-th training-testing set, where the input vectors $\mathbf{G}$ and $\mathbf{D}$ are generated from the n-th realization in an emulator, and the corresponding optimal label $\mathbf{a}^*$ can be obtained by solving $\mathcal{P}_2$ offline. The predicted $\mathbf{a}$ from the 1-st DNN may not necessarily be binary, a threshold η is then introduced to round the fractional elements to binary.

Ideally, the predicted $\mathbf{a}$ should lead to a feasible terminal-timeslot allocation. That is, satisfying $\sum_{t=1}^{T} a_{kt} \geq 1$, $\forall k = 1, \ldots, K$, i.e., each terminal is scheduled to at least one timeslot to satisfy constraints (4.7b), and no violation for constraints (4.7e) and (4.7f). However, these feasibility conditions cannot be always guaranteed because of DL's imperfect prediction. To deal with this issue, we per-

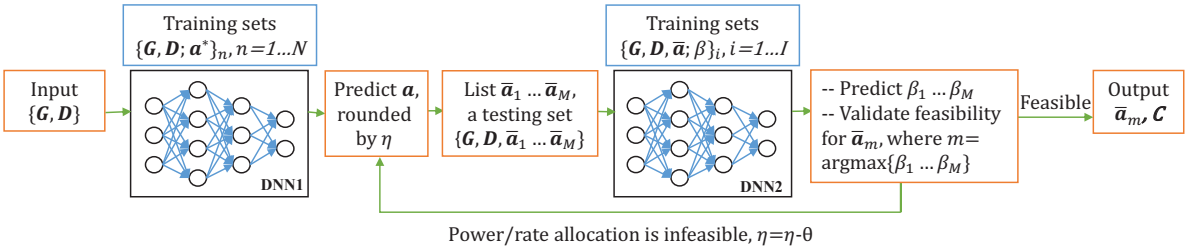

Figure 4.2: Illustration of the proposed DDCO

form a post-process for the predicted $\mathbf{a}$ to list M feasible and promising terminal-timeslot allocation $\bar{\mathbf{a}}_1, \ldots, \bar{\mathbf{a}}_M$. We use an example with $K = 4$, $T = 4$, $\bar{K} = 2$ to illustrate the process. After rounding, the predicted $\mathbf{a}$ reads,

$$[\underbrace{1,1,1,0}_{a_{11},\ldots,a_{41}}, \underbrace{1,0,1,1}_{a_{12},\ldots,a_{42}}, \underbrace{0,0,0,0}_{a_{13},\ldots,a_{43}}, \underbrace{1,0,1,0}_{a_{14},\ldots,a_{44}}]. \tag{4.13}$$

This allocation consumes 3 timeslots but the completion time is 4 timeslots, which violates constraints (4.7f), and schedules 3 terminals on the first two timeslots, which violates constraints (4.7e). To satisfy (4.7f), we move the terminals scheduled at timeslot 4 to timeslot 3 and leave timeslot 4 idle. To meet (4.7e), we select $\bar{K} = 2$ terminals from 3 for the 1-st and 2-nd timeslots, giving 9 combinations $\left(\binom{3}{2} \times \binom{3}{2}\right)$ in total. Filtered by constraints $\sum_{t=1}^{T} a_{kt} \geq 1, \forall k = 1, \ldots, K$, 4 out of 9 feasible terminal-timeslot allocations $\bar{\mathbf{a}}_1, \ldots, \bar{\mathbf{a}}_4$ are generated.

A follow-up question is that whether a feasible power (or capacity) allocation (satisfying constraints (4.7b), (4.7c), (4.9c), and (4.9d)) exists under these feasible terminal-timeslot allocations. One may notice that once $\mathbf{a}$ is fixed in $\mathcal{P}_2$, then $\mathbf{b}$ is determined. The remaining power (or capacity) optimization problem becomes a decision-version problem, that is providing a yes-or-no answer to the existence of feasible power (or capacity) allocation under the certain $\mathbf{a}$ and $\mathbf{b}$. This feasibility-check problem is presented as,

$$\mathcal{P}_3 : \text{Find } \mathbf{C}, \text{ s.t. (4.7b), (4.7c), (4.9c), (4.9d),} \tag{4.14}$$

which amounts to solving a convex optimization problem.

In general, the complexity for answering a problem's feasibility is of the same magnitude as solving the corresponding optimization problem. Thus in order to identify at least one feasible solution from $\bar{\mathbf{a}}_1, \ldots, \bar{\mathbf{a}}_M$, in the worst case, M convex problems have to be solved, which may not be computationally affordable when M is large. We train the 2-nd DNN to enable a quick feasibility check for $\bar{\mathbf{a}}_1, \ldots, \bar{\mathbf{a}}_M$. The training sets are organized in tuples $\{\mathbf{G}, \mathbf{D}, \bar{\mathbf{a}}; \beta\}_i$, $i = 1, \ldots, I$, where $\bar{\mathbf{a}}$ is a terminal-timeslot allocation, and optimal label β, obtained by solving $\mathcal{P}_3$ via convex optimization, stands for the corresponding feasibility ($\beta = 1$) or infeasibility ($\beta = 0$) of $\bar{\mathbf{a}}$. A mapping from inputs $\mathbf{G}$, $\mathbf{D}$, $\bar{\mathbf{a}}$ to optimal label β is learned. In the testing phase, the value of the m-th output node, β_m, refers to the probability of a feasible power (or capacity) solution existing for $\bar{\mathbf{a}}_m$. We select the terminal-timeslot allocation with the highest probability, say the m-th element $\beta_m = \max\{\beta_1, \ldots, \beta_M\}$, and solve the convex optimization problem under $\bar{\mathbf{a}}_m$ in order to validate the feasibility of power (or capacity) allocation to against DNN's imperfect prediction. If no feasible power exists, we reduce threshold η by step θ to involve more feasible terminal-timeslot allocations to set $\{\bar{\mathbf{a}}_1, \ldots, \bar{\mathbf{a}}_M\}$, otherwise, DDCO outputs the feasible terminal-timeslot allocation $\bar{\mathbf{a}}_M$ and corresponding capacity (or power) allocation $\mathbf{C}$ (or $\mathbf{P}$).

Table 4.1: Simulation Parameters of Satellite Systems

Parameter	Value
Frequency	20 GHz (Ka band)
Bandwidth, W	250 MHz
Satellite location	13° E
Satellite height, d^{GW}, d_k	35,786 km
Beam radiation pattern	provided by ESA [148]
Receive antenna gain	42.1 dBi
Noise power, σ^2	-126.47 dBW
Maximum transmit power, $P_{\max}$	20 dBW
Number of time slots, T	100
Maximum multiplexed users, $\bar{K}$	2
Duration of each timeslot, τ	1 ms
Demand, D_k	325 to 750 Mbps

4.6 Performance Evaluation

In this section, we evaluate the performance of the proposed DPO and DDCO. The parameter settings are summarized in Table 6.1. Both DNNs are implemented in TensorFlow, where ReLu, Mean Square Error (MSE), and Adam algorithm are adopted as the activation function, loss function, and optimizer, respectively. The inputs $\mathbf{G}$ and $\mathbf{D}$ are generated from the adopted emulator based on the parameter settings in Table 6.1, where the beam radiation pattern is provided by ESA in the context of [148]. We set the following approaches as benchmarks:

- Opt: The optimal solution is obtained by solving $\mathcal{P}_2$ with MOSEK solver [51], which is capable of tackling MICP by branch-and-cut approaches.
- BW-FTPC [98]: Terminals are grouped on the basis of best-worst (BW) pairing and power allocation is based on fractional transmit power control (FTPC) rule.
- SM-CP [43]: Terminal-timeslot assignment is iteratively updated by swap-matching (SM) approach. For each iteration, a conic programming (CP) of capacity allocation should be solved.
- SD: The single-DNN (SD) scheme follows the procedure of DDCO but without using the 2-nd DNN, instead, adopting convex optimization to verify the capacity (or power) feasibility for $\bar{\mathbf{a}}_1, \ldots, \bar{\mathbf{a}}_M$.
- OMA: Each timeslot can be only scheduled to one terminal, i.e., $\bar{K} = 1$.
- End-to-end learning [161]: The scheme directly learns and predicts power allocation.

Computational time performance

Firstly, in Table 4.3, we compare the average computational time among Opt, BW-FTPC, SM-CP, SD, DDCO, and DPO. In the optimal algorithm, the computation time increases exponentially as the problem's scale increases. In comparison, the computational time in BW-FTPC, DDCO, and DPO is significantly reduced to millisecond level while SM-CP consumes time in second level with higher magnitude. SD consumes much longer time than DDCO since the complexity for solving up to M convex problems

Table 4.2: Simulation Parameters of DNN

Parameter	**Value**
Number of hidden layers	5
Nodes per hidden layer	256
Activation function	Relu, Sigmoid, Softmax
Optimizer	Adam
Loss function	MSE, cross entropy
Training samples, N	6000
Testing samples, I	1000

Table 4.3: Average Computational Time (in Seconds) ($\eta = 0.2$, $\delta = 1$)

K	Opt	BW-FTPC	SM-CP	SD	DDCO	DPO
4	1.33	0.12	0.64	1.79	0.325	0.15
6	5.17	0.13	3.51	10.32	0.577	0.19
8	38.23	0.16	6.74	123.28	0.698	0.21
10	798.4	0.17	9.38	146.05	0.842	0.29

in SD remains considerable. With K increases, the proposed DDCO and DPO are capable of providing an overall computationally efficient solution.

Performance of minimizing transmission time

Secondly, in Fig. 4.3, we evaluate the performance of reducing transmission time. In Fig. 4.3(a), we compare the objective values, i.e., minimized transmission time, in the proposed learning-assisted approaches, DDCO and DPO, and benchmarks, Opt, BW-FTPC, SM-CP, and OMA. In general, the gap between optimal and suboptimal solutions increases significantly as the number of terminals grows, whereas the gap between DDCO and the optimum keeps less than 5% in average. The main reason for this near optimality is that, when M feasible terminal-timeslot allocations are generated for the 2-nd DNN, DDCO has strong capability to retain the optimal allocation $\mathbf{a}^*$ in the candidate set, i.e., $\mathbf{a}^* \in \{\bar{\mathbf{a}}_1, \ldots, \bar{\mathbf{a}}_M\}$. This is verified in Fig. 4.3(b), where DDCO hits optimal $\mathbf{a}^*$ in more than 95% testing sets in average. Recall that by design, $\bar{\mathbf{a}}_1, \ldots, \bar{\mathbf{a}}_M$ have the same objective value. As a consequence, even though DDCO's outputted allocation $\bar{\mathbf{a}}_m$ may not be necessarily as same as the optimal $\mathbf{a}^*$, the optimal objective value can be achieved when $\mathbf{a}^* \in \{\bar{\mathbf{a}}_1, \ldots, \bar{\mathbf{a}}_M\}$ holds. We can observe that the performance of DPO is close to that of SM-CP, with a gap of 0.26%, but DPO has an obvious reduction in computational time compared to SM-CP as displayed in Table 4.3. Both learning-assisted approaches can achieve a good trade-off between performance and complexity. Furthermore, DDCO outperforms DPO in minimizing transmission time. This is because, in DDCO, more potential integer solutions are considered such that the algorithm has higher possibility to hit the optimum than DPO.

Feasibility performance

Thirdly, we demonstrate the performance of DDCO and DPO in delivering feasible solutions. In Fig. 4.4, the adopted threshold $\eta = 0.2$ is suited for 4-terminal cases, i.e., leading to a feasible terminal-timeslot and capacity (or power) solutions in 99% instances. In contrast, the same threshold for 10-terminal cases fails, leading to infeasible solutions in most of the instances. Next, in Fig. 4.5, we decrease η for 10-terminal cases, and observe the significant performance improvement. The reason is that when η

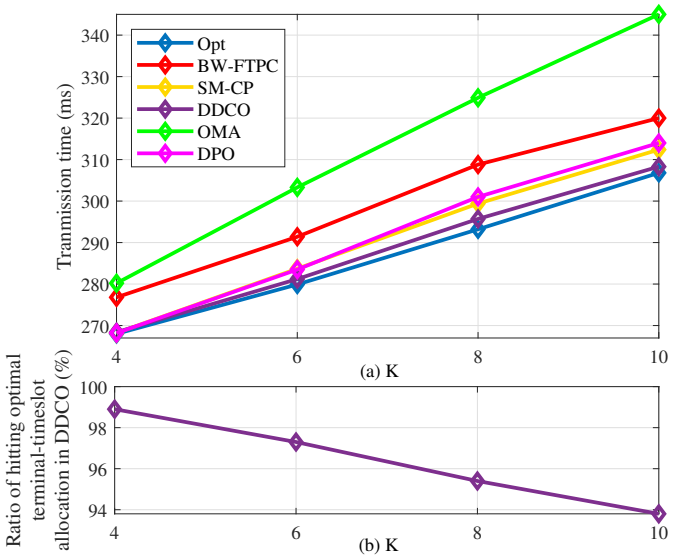

Figure 4.3: Minimized transmission time with respect to K ($\eta = 0.14$ in DDCO and $\eta = 1$ in DPO).

decreases in the 1-st DNN, the fractional elements in the predicted vector $\mathbf{a}$ are prone to be rounded to 1, then it results in more allocations in set $\{\bar{\mathbf{a}}_1, \ldots, \bar{\mathbf{a}}_M\}$. Smaller η and larger M in fact increase the probability of DDCO in obtaining a feasible capacity (or power) allocation. The results necessitate the threshold-adjustment procedure ($\eta = \eta - \theta$) in DDCO.

In 4.6, we present the performance of DPO in delivering feasible solutions with different K and δ. We can observe that, as the problem scale increases, the difficulty of finding a feasible solution grows. The feasibility rate can be improved by scaling up δ but enlarges the gap the the optimum.

To enable a fair feasibility comparison, the number of consumed timeslots is uniform for all the algorithms in Fig. 4.7. Directly applying end-to-end learning performs the worst. The ratios of BW-FTPC and SM-CP are much lower than DDCO, DPO, and SD since both algorithms require iterative operations to improve the performance. By exploiting more potential solutions and identifying their feasibility, DDCO and SD have gains in hitting feasible solution over DPO. SD performs the best as it identifies the feasibility of potential solutions by directly solving them but consumes more time than DDCO and DPC as presented in Table 4.3.

4.7 Conclusion and Discussion

In this chapter, we have provided insights on the design of learning-assisted schemes to tackle the challenging satellite-NOMA resource optimization problem. We have formulated a problem to minimize transmission time by optimizing transmit power and terminal-timeslot scheduling in a general NOMA-enabled satellite system. We have investigated how to apply DL to address a typical constrained combinatorial optimization problem. The convexity of the primal problem has been revealed by the reformulation into a MICP problem, such that the optimum/near-optimum can be obtained by conventional iterative approaches. Considering its inherent difficulty and high complexity, we have proposed DPO and DDCO to accellerate the problem solving and provide efficient, feasible, and near-optimal solutions.

In the end, we discuss the pros and cons of optimization-based and learning-assisted schemes. In optimization-based schemes, one can achieve some guaranteed performance by deriving solid analysis, e.g., monotonicity, convergence, optimality/local-optimality conditions, etc. But generally, the theoreti-

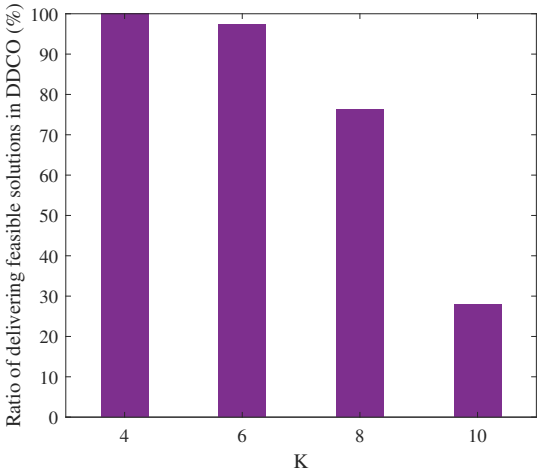

Figure 4.4: DDCO in delivering feasible solutions with respect to K ($\eta = 0.2$).

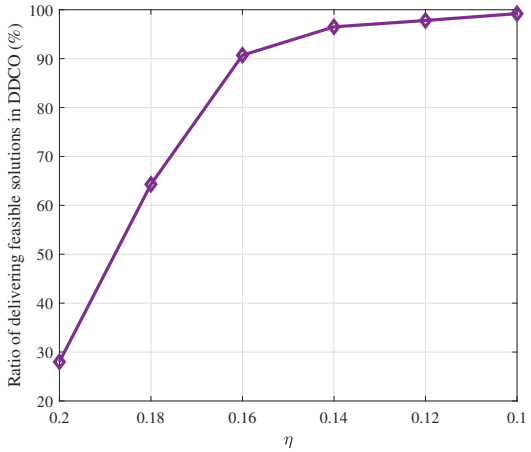

Figure 4.5: DDCO in delivering feasible solutions with respect to threshold η ($K = 10$).

cal analysis is not always easy to derive due to the challenging combinatorial and nonconvex properties of the considered problems. To attain a good result, e.g., global/local/near optimum, considerable computational efforts would be consumed, which may not be applied in practical satellite systems. For example, in some typical GEO satellite systems, algorithms with large complexity could fail to perform due to the presence of hundreds or thousands of spot beams. In more dynamic wireless environment, e.g., non-geostationary satellite systems, the algorithms should be adaptive to the variations, which requires fast decision-making process. To reduce the complexity, designing low-complexity suboptimal algorithms is an alternative choice, but with performance loss and insufficient performance guarantee.

On the other hand, learning-assisted schemes can tackle the challenging procedures in optimization problems, e.g., decision-making process, by exploiting useful information from empirical data. We can apply learning techniques to approximate the implicit mapping between input parameters and the optimal/near-optimal solution by training a learning model instead of directly solving the problem. This could reduce complexity and guarantee the performance gain if we obtain a well-trained learning model. Besides, learning can be applied to predict the demands or channel gains when considering de-

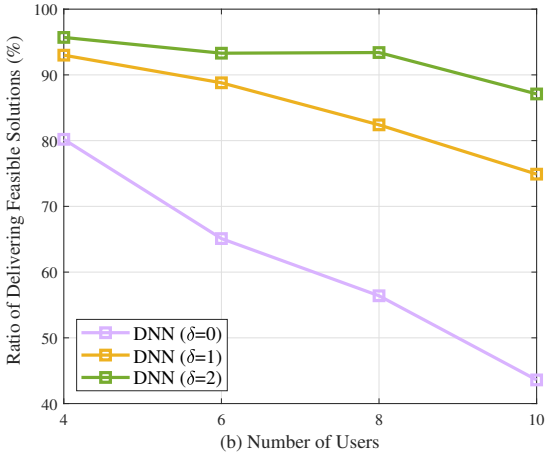

Figure 4.6: DPO in delivering feasible solutions with respect to K and δ.

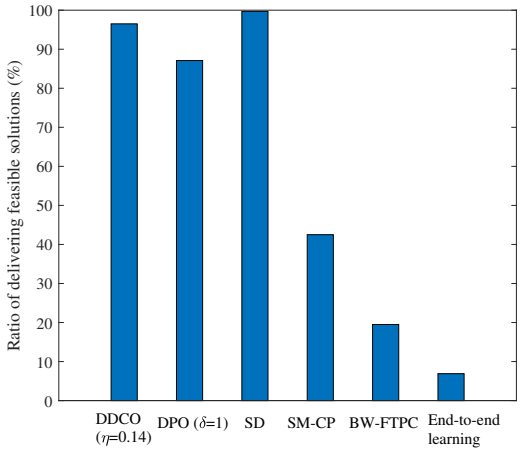

Figure 4.7: Successful ratio of delivering feasible solutions in 1000 testing sets ($K = 10$).

layed/imperfect issues. However, the performance of learning-assisted schemes may be deteriorated in the case of insufficient training data, hard-to-obtain data sets, invalidation of learning models in dynamic scenarios, etc. We cannot conclude which type of approaches is better in general. The selection of applied schemes depends on the properties of targeted scenarios and formulated problems.

Chapter 5

Joint Optimization of Power- and Time-Domain Flexibilities

This chapter starts to study resource optimization in the case of multi-dimension flexibilities in NOMA-based SatCom. Considering the advantages of BH in matching capacity to demand and alleviating co-channel interference, we exploit time-domain flexibility in multi-beam satellite systems by optimizing BH design. In this chapter, we investigate the potential synergy and mutual influence between BH and NOMA in resource optimization. In the considered system, BH is operated among beams to mitigate inter-beam interference and NOMA is employed within each beam to reduce intra-beam interference. We jointly optimize power allocation, beam scheduling, and terminal-timeslot assignment to minimize the gap between requested traffic demand and offered capacity. In the solution development, we formally prove the NP-hardness of the optimization problem. Next, we develop a bounding scheme to tightly gauge the global optimum and propose a suboptimal algorithm to enable efficient resource assignment. Numerical results demonstrate the benefits of combining NOMA and BH, and validate the superiority of the proposed BH-NOMA schemes over benchmarks.

5.1 Introduction

In conventional multi-beam satellite systems, all beams are simultaneously illuminated and on-board resources are pre-assigned before launch due to limited flexibility and capability in satellite payloads [1]. While this design is efficient for static and uniform traffic patterns, the evolution of data services leads to highly dynamic and spatially non-uniform traffic. In this case, the efficiency of resource utilization is low and the system fails to adapt to heterogeneous traffic distribution over the coverage area [2]. With the development of advanced satellite payloads, more attention has been drawn to flexible on-board resource allocation (e.g., power, bandwidth) to embrace the dramatic growth of data traffic and the uneven distribution [2, 10].

BH is a promising technique to enhance the flexibility of resource management by selectively and sequentially activating or deactivating beams [2, 24, 162]. The benefits of BH are from the following aspects. First, in a BH system, beam scheduling (or beam illumination pattern design) is optimized based on the requested traffic such that unmet and unused capacity can be reduced [24, 162]. Second, without illuminating all the beams together, the required number of radio-frequency chains is smaller, thus power consumption and payload mass are reduced [162]. Third, spatially induced co-channel interference can be alleviated by illuminating the beams that are distant from each other [17, 88]. In the DVB-S2X

standard [137], a super-frame format to facilitate BH implementation and performance enhancement has been specified. In the literature, BH has been applied in different scenarios, e.g., load balancing networks [163], cognitive satellite networks [164], and ultra-dense LEO systems [165].

To improve the performance of BH, a majority of works focus on how to design efficient approaches to decide beam-timeslot scheduling. In [24], a genetic algorithm was adopted to determine beam illumination patterns. In [164], a resource allocation problem for cognitive BH systems was studied. The authors decomposed the problem and proposed low-complexity approaches. In [84], the authors designed two iterative BH approaches based on minimum co-channel interference and maximum SINR. The authors in [166] studied resource allocation for a novel satellite system where conventional BH is combined with cluster hopping. Considering the benefits of machine learning techniques, the authors in [86] and [85] proposed resource allocation schemes assisted by deep reinforcement learning and deep learning, respectively.

Compared to conventional OMA, NOMA can achieve higher spectral efficiency and serve more terminals [33]. Beyond terrestrial systems, it is natural to investigate how NOMA can help to improve the performance for multi-beam satellite systems, e.g., [34, 154, 167, 113]. The authors in [34] studied the cooperation between NOMA and precoding in a multi-beam satellite system. In [154], joint optimization of power allocation, decoding orders, and terminal-timeslot assignment in NOMA-enabled multi-beam satellite systems was studied. To mitigate channel-phase uncertainty effects, two robust beamforming schemes were provided in [167] to minimize power consumption for delivering satellite internet-of-things services. In [113], the authors jointly optimized power allocation and network stability to maximize long-term average capacity for NOMA-based satellite internet-of-things systems. NOMA has shown superiorities in enhancing spectral efficiency and improving the performance of practical metrics for multi-beam satellite systems in the literature.

Considering the individual benefits from BH and NOMA, we are motivated to investigate how to exploit the joint advantages of these two techniques and optimize resource allocation for BH-NOMA systems. In the literature, the joint scheme of BH and NOMA is studied to a limited extent. The potential synergies of NOMA and BH were firstly studied in our previous work [168], where we considered a simplified problem without joint optimization, and focused on performance evaluation in order to verify the initial synergy between BH and NOMA.

5.1.1 Motivations and Contributions

In general, joint resource optimization for BH-NOMA systems typically leads to a combinatorial optimization problem. In some cases, the optimum might not be achievable for large-scale instances due to unaffordable complexity and time, e.g., branch-and-bound approach in solving large-scale integer linear programming problems [85, 93]. For some difficult problems, the optimum might even be unknown for small or medium cases, e.g., unknown optimum in solving MINCP problems [168]. It is therefore of importance to: 1) Identify how difficult the resource optimization problem is; 2) Provide a tight bound for the optimum; 3) Properly benchmark the developed suboptimal solutions.

In this work, we investigate joint optimization for the considered BH-NOMA scheme to enhance the performance gain by optimizing power allocation, beam scheduling, and terminal-timeslot assignment. We apply BH to selectively and sequentially activate beams over timeslots. NOMA is then implemented within each active beam to further improve the spectral efficiency. Recap that in Chapter 3, we focus on maximizing the worst OCTR performance among terminals such that the fairness of terminals with heterogeneous traffic demand can be improved. In this case, even terminals with extremely small demand could be served to improve the worst capacity-to-demand ratio. To fathom the influence of NOMA to various practical metrics in SatCom, we try to study resource optimization from different angles to enrich the findings and results in this thesis. In this chapter, we move from max-min OCTR to another

objective function, minimizing the gap between capacity and demand. Different from max-min OCTR, the capacity-demand gap concentrates more on the whole system's rate-matching performance but the performance of terminals with small demand might be sacrificed.

Beyond state-of-the-art and compared to [168], the main contributions are summarized as follows:

- We formulate a resource allocation problem to minimize the gap between offered capacity and requested traffic, leveraging by BH and NOMA. The work, together with [168], provides an early-attempt investigation for BH-NOMA systems.
- We formally prove the NP-hardness for the joint BH-NOMA optimization problem, and outline the mutual influence between BH and NOMA. We investigate the problem's insights by developing theoretical analysis.
- To gauge the unknown global optimum, we design an effective bounding scheme. In the upper-bound approach (UBA), we develop an iterative near-optimal algorithm. In the lower-bound approach (LBA), we first resolve the problem's non-convexity by simplifying the estimation of inter-beam interference. Then we construct a MICP problem to approximate the original problem.
- We design an efficient low-complexity algorithm for joint power allocation, beam scheduling, and terminal-timeslot assignment (E-JPBT) to overcome the high complexity in UBA and provide feasible solutions for large-scale instances.
- The numerical results validate the benefits of jointly considering BH and NOMA, and the tightness of the bounds in gauging optimality. We demonstrate the superiority of the proposed BH-NOMA schemes in matching offered capacity to requested traffic compared to benchmarks.

5.2 System Model

We consider a GEO satellite system which provides services to fixed ground terminals via forward links. The satellite generates B spot beams to cover the targeted area. We denote $\mathcal{B}$ as the set of the beams. Let $\mathcal{K}$ and $\mathcal{K}_b$ represent the set of terminals in the system and in the b-th beam, respectively. Note that users are assigned to beams implicitly based on their geographical coordinates [148], e.g., user k located within the 4.3 dB contour of the b-th beam's coverage area belonging to $\mathcal{K}_b$. Denote K' as the number of terminals per beam. Each terminal is equipped with a single directional antenna. All the beams share the same frequency band, i.e., 1-color frequency-reuse pattern.

The architecture of the considered multi-beam satellite system is depicted in Fig. 5.1, where the telemetry, tracking, and command (TT&C) station is part of the satellite operation center whereas the gateway and the resource manager are part of the network operation center [2]. The TT&C station is responsible for the synchronization among beams during the BH process [25]. The bent-pipe transparent satellite payload is assumed to be equipped with switching matrix and digital transparent processors to enable beam activation/deactivation and power distribution among different active beams, respectively [2, 1]. The procedure in Fig. 5.1 is described as the following: Step 1: The gateway collects information from ground terminals, e.g., traffic demand and channel status, via return links. Step 2: Based on the feedbacks, the resource manager (co-located with the gateway) executes the algorithm to optimize the beam illumination pattern and power-terminal-timeslot scheduling. The optimization outcomes are communicated to the satellite payload via the TT&C station and to the gateway [85, 2]. Step 3: Following the planned scheduling decisions, the gateway requests data from the core networks to the satellite payload. Step 4: According to the optimized beam illumination pattern, the satellite payload relies on a switching

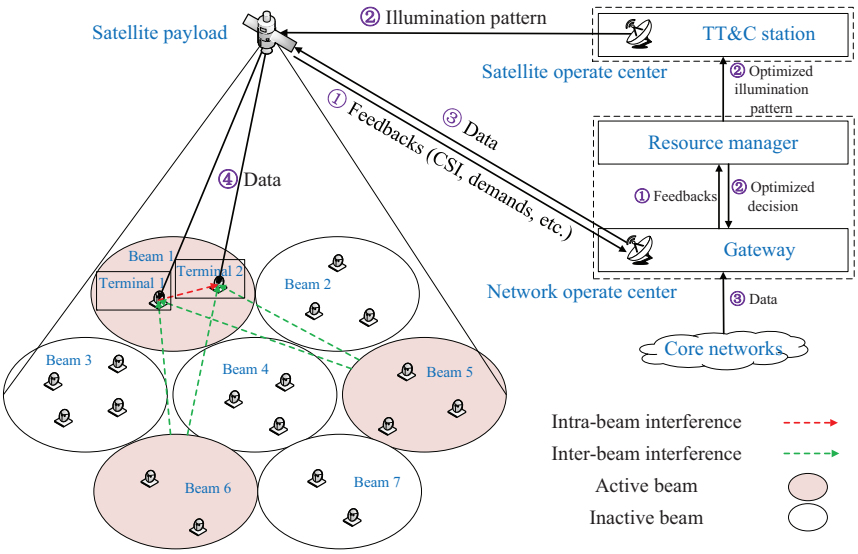

Figure 5.1: An illustrative scenario of the considered BH-NOMA system. Three beams are activated simultaneously according to the BH design. By applying NOMA in beam 1, terminal 1 at the beam center with better channel gain only receives inter-beam interference from the other two active beams, while terminal 2 at the beam edge with worse channel gain receives both intra-beam and inter-beam interference. (The numbers in the circle denote the steps of the communication procedure.)

matrix to activate the selected beams. The satellite payload delivers data to the ground terminals in active beams.

In the system, BH illuminates no more than B_0 ($B_0 < B$) beams at each timeslot due to payload architecture limitations. A scheduling period consists of T timeslots, defined as a BH window. Denote $\mathcal{T}$ as the set of the timeslots. For each beam, $\left\lceil \frac{K'}{K_0} \right\rceil$ timeslots are required such that all the terminals can be scheduled to at least one timeslot. The minimum number of timeslots to illuminate all the beams at least once is $\left\lceil \frac{B}{B_0} \right\rceil$. Thus the value of T should meet

$$T \geq \left\lceil \frac{K'}{K_0} \right\rceil \left\lceil \frac{B}{B_0} \right\rceil . \tag{5.1}$$

In an active beam, NOMA is adopted to multiplex one or more terminals in a timeslot. The signals intended for the scheduled terminals in one beam are superimposed with different power per targeted terminal. We denote p_{kt} as the transmit power for terminal k at timeslot t. The SINR of terminal k in beam b at timeslot t is derived as,

$$\gamma_{kt} = \frac{|h_{bk}|^2 p_{kt}}{\underbrace{\sum_{\substack{k' \in \mathcal{K}_b \setminus \{k\} \\ k' < k}} |h_{bk}|^2 p_{k't}}_{\text{intra-beam interference}} + \underbrace{\sum_{b' \in \mathcal{B} \setminus \{b\}} \sum_{k' \in \mathcal{K}_{b'}} |h_{b'k}|^2 p_{k't}}_{\text{inter-beam interference}} + \sigma^2}, \tag{5.2}$$

where σ^2 represents the noise power. We denote $|h_{bk}|^2$ as the channel gain from the b-th satellite antenna to the k-th terminal (assuming consistent indexes between antennas and beams). We use a widely-

adopted channel model in multi-beam satellite systems [85, 164, 17, 154, 167], which is derived as,

$$|h_{bk}|^2 = \frac{G_{bk}^{\mathrm{tx}} G_k^{\mathrm{rx}}}{\kappa T^{\mathrm{noise}} W} \left(\frac{c}{4\pi d_k f^{\mathrm{fr}}} \right)^2, \tag{5.3}$$

where G_{bk}^{tx} is the transmit antenna gain from the b-th antenna to terminal k. G_k^{rx} denotes the receive antenna gain of terminal k. The term $\kappa T^{\mathrm{noise}} W$ represents the distribution of noise, where κ, T^{noise}, and W denote the Boltzmann constant, the noise temperature of the receiver, and the carrier bandwidth, respectively. The term $\left(\frac{c}{4\pi d_k f^{\mathrm{fr}}} \right)^2$ is the free-space propagation loss, where d_k, f^{fr}, and c denote the distance between the satellite and terminal k, the frequency, and the light speed, respectively. We consider that the channel gains are static within T timeslots and updated every T timeslots.

The intra-beam interference and inter-beam interference are denoted as the first term and the second term of the denominator in (6.9), respectively. We assume consistent indexes between terminals and the descending order of channel gains, e.g., two terminals k and k' in $\mathcal{K}_b$, where $k' < k$ and $|h_{bk'}|^2 > |h_{bk}|^2$. In this case, k' performs successive interference cancellation (SIC) to decode and remove k's signals whereas k treats k''s signals as noise. We remark that, to facilitate the analysis, we assume that the channel coefficients satisfy the conditions derived in [130] (Lemma 1), such that determining the decoding order in each beam is independent of the beams' transmit power and inter-beam interference. The available rate of terminal k at timeslot t is,

$$R_{kt} = W \log_2(1 + \gamma_{kt}), \tag{5.4}$$

where W is the bandwidth for the carrier (single carrier per beam). The total offered capacity of terminal k is,

$$R_k = \sum_{t \in \mathcal{T}} R_{kt}. \tag{5.5}$$

5.3 Problem Formulation and Analysis

5.3.1 Problem Formulation

We formulate an optimization problem to minimize the gap between offered capacity and requested traffic by jointly optimizing power allocation, beam scheduling, and terminal-timeslot assignment. The variables are defined as:

$$p_{kt} \geq 0, \text{ transmit power for terminal } k \text{ at timeslot } t;$$

$$\alpha_{bt} = \begin{cases} 1, \text{ beam } b \text{ is illuminated at timeslot } t, \\ 0, \text{ otherwise;} \end{cases}$$

$$\beta_{kt} = \begin{cases} 1, \text{ terminal } k \text{ is assigned to timeslot } t, \\ 0, \text{ otherwise.} \end{cases}$$

Denote D_k as the requested traffic demand (in bps) of terminal k over a scheduling period. We apply a widely-adopted metric, $(R_k - D_k)^2$, to measure the capacity-traffic mismatch of terminal k [88, 10]. The objective function captures the average mismatch level among K terminals. The problem is formulated

as:

$$\mathcal{P}_0: \min_{\alpha_{bt},\beta_{kt},p_{kt}} \sum_{k\in\mathcal{K}} (R_k - D_k)^2 \tag{5.6a}$$

$$\text{s.t.} \quad \sum_{k\in\mathcal{K}_b} p_{kt} \leq P, \forall b \in \mathcal{B}, \forall t \in \mathcal{T}, \tag{5.6b}$$

$$\sum_{b\in\mathcal{B}} \alpha_{bt} \leq B_0, \forall t \in \mathcal{T}, \tag{5.6c}$$

$$\sum_{k\in\mathcal{K}_b} \beta_{kt} \leq K_0 \alpha_{bt}, \forall b \in \mathcal{B}, \forall t \in \mathcal{T}, \tag{5.6d}$$

$$p_{kt} \leq P\beta_{kt}, \forall k \in \mathcal{K}, \forall t \in \mathcal{T}, \tag{5.6e}$$

$$R_k \geq R_k^{\min}, \forall k \in \mathcal{K}, \tag{5.6f}$$

$$\alpha_{bt} + \alpha_{b't} \leq 1, b \neq b', \forall (b, b') \in \Omega, \forall t \in \mathcal{T}. \tag{5.6g}$$

In (6.14b), the total transmit power of terminals in each beam at each timeslot is no larger than the beam power budget P. In (6.14c), no more than B_0 beams can be illuminated at each timeslot. Constraints (6.14d) confine that no more than K_0 terminals can be allocated to a timeslot. No terminal will be scheduled in an inactive beam. Constraints (6.14f) connect p_{kt} and β_{kt}, where p_{kt} is confined to zero if $\beta_{kt} = 0$, otherwise, $p_{kt} \leq P$. In (6.14h), the rate of each terminal should meet the minimum-rate requirement to maintain a certain level of fairness among terminals. Usually, the minimum rate is smaller than the requested traffic demand, i.e., $R_k^{\min} < D_k$. In (6.14i), we introduce $\Omega \subset \mathcal{B} \times \mathcal{B}$ as a set to include all the undesired beam pairs, e.g., adjacent beams with strong interference. If a beam pair $\{b, b'\} \in \Omega$, beam b or b' can be illuminated alone or grouped with other beams, e.g., illuminating beam b and b'' in timeslot t, but beam b and b' cannot be activated together in the same timeslot because $\alpha_{bt} + \alpha_{b't} = 2$ violates (6.14i).

In $\mathcal{P}_0$, the performance and optimization decisions in BH and NOMA are coupled with each other. In general, jointly optimizing the two components is challenging. Determining NOMA resource allocation in each beam depends on the outcome of BH design, whereas achieving a high-quality BH scheme requires appropriate decisions from NOMA resource allocation. On the one hand, BH design is of importance to the resource allocation in NOMA. When a set of inappropriate beams with strong interference are activated, this can possibly result in degraded performance, e.g., low data rates per timeslot. As a consequence, each terminal might need to be assigned with more power to satisfy its demand or scheduled to more timeslots (thus suggests more timeslots consumed in total for all the terminals), which typically leads to a more complicated problem with a larger dimension and more sensitive to the feasibility issue in NOMA.

On the other hand, the decisions made in NOMA can in its turn influence the BH design. When an optimal power and terminal-timeslot allocation can be obtained in NOMA, as a result, each active beam radiates less inter-beam interference to each other compared to a suboptimal NOMA solution, and some beams can be activated with fewer timeslots due to the higher rate achieved per timeslot, which can greatly ease the BH design. Towards an overall high-quality solution for BH-NOMA systems, it is necessary to capture this mutual dependence and iteratively improve the overall performance in algorithmic design.

5.3.2 Complexity Analysis in Solving $\mathcal{P}_0$

$\mathcal{P}_0$ is an MINCP problem [50] due to the nonlinear and nonconvex functions in (5.6a) and (6.14h), and the presence of binary variables α_{bt} and β_{kt}. Solving an MINCP can be challenging in general. We further identify the intractability of $\mathcal{P}_0$ by proving the NP-completeness for its decision-version problem (or feasibility-check problem) and the NP-hardness for the optimization problem in Lemma 1 and Theorem 1, respectively. The decision-version problem of $\mathcal{P}_0$ is defined as a true-or-false problem to check if there exists a feasible solution [169]. If the decision version of $\mathcal{P}_0$ is NP-complete, then the optimization problem $\mathcal{P}_0$ is NP-hard [170], because solving $\mathcal{P}_0$ is no easier than solving its decision version. The former needs to obtain optimal solutions, whereas the latter only needs to offer a yes-or-no answer for feasibility check.

Lemma 1: The decision-version (feasibility-check) problem of $\mathcal{P}_0$ is NP-complete.

Proof. We construct a polynomial-time reduction from three-dimensional matching (3DM) problem [171], one of the typical NP-complete problems, to an instance of the decision-version problem of $\mathcal{P}_0$. Consider three different sets $\mathcal{X}$, $\mathcal{Y}$, and $\mathcal{Z}$, where $|\mathcal{X}| = |\mathcal{Y}| = |\mathcal{Z}|$. The 3DM problem is to check whether there exists a matching set $\Theta \subset \mathcal{X} \times \mathcal{Y} \times \mathcal{Z}$ such that $x_1 \neq x_2$, $y_1 \neq y_2$, and $z_1 \neq z_2$ for any two different triplets (x_1, y_1, z_1) and (x_2, y_2, z_2) in Θ. If yes, Θ is called a 3DM.

Consider a special case with one terminal per beam, i.e., $K = B$. In this case, we use terminals' indexes and beams' interchangeably. The set of beams is divided into two subsets, $\mathcal{B}_1$ and $\mathcal{B}_2$, where $\mathcal{B}_1 \cap \mathcal{B}_2 = \varnothing$ and $\mathcal{B}_1 \cup \mathcal{B}_2 = \mathcal{B}$. For any beam $b \in \mathcal{B}_i$, $\forall i = \{1, 2\}$, the channel gains satisfy the following conditions,

$$|h_{b'b}|^2 = \begin{cases} 1+\epsilon, \text{ if } b' = b, \\ 1+\frac{\epsilon}{2}, \text{ else if } b' \in \mathcal{B}_i, \\ \epsilon, \text{ else if } b' \in \mathcal{B}_j, j \neq i, \end{cases} \tag{5.7}$$

where $0 < \epsilon \leq 2^{\frac{1}{B}} - 1$. That means, for any two beams from different subsets, the inter-beam interference remains zero. We set the parameters as follows: $P = 1$, $\sigma^2 = \epsilon$, $B_0 = 2$, $T = \frac{B}{2}$, $\Omega = \varnothing$, $R_b^{\min} = 1$, and $D_b \gg 1$.

First, we prove that the instance problem is feasible if the answer to the 3DM problem is yes. We let $\mathcal{X} = \mathcal{T}$, $\mathcal{Y} = \mathcal{B}_1$, and $\mathcal{Z} = \mathcal{B}_2$. For any two triplets (t_1, b_1, b'_1) and (t_2, b_2, b'_2), the following relationships hold: $t_1 \neq t_2$, $b_1 \neq b_2$, and ${b_1}' \neq b'_2$. In this case, any two beams scheduled to the same timeslot are from different subsets and thus the inter-beam interference is zero. If beam b is illuminated at timeslot t, the rate of each beam is derived as,

$$\log_2(1 + \frac{|h_{bb}|^2 P}{|h_{b'b}|^2 P + \sigma^2}) = \log_2(1 + \frac{1+\epsilon}{\epsilon+\epsilon}) > 1 = R_b^{\min}, \tag{5.8}$$

which meets constraints (6.14b) to (6.14i). Thus the instance problem is feasible.

Next, we prove that if the instance problem is feasible, the answer to the 3DM problem is yes. Since $T = \frac{B}{2}$ and $B_0 = 2$, all beams are scheduled only once. If there exist two beams from the same subset scheduled to the same timeslot, then the rates for these two beams are,

$$\log_2(1 + \frac{|h_{bb}|^2 P}{|h_{b'b}|^2 P + \sigma^2}) = \log_2(1 + \frac{1+\epsilon}{1+\frac{\epsilon}{2}+\epsilon}) < \log_2(1+1) = 1 = R_b^{\min}, \tag{5.9}$$

which violates the minimum-rate constraint in (6.14h). To meet the constraints, the interference must be zero, requiring that any two beams scheduled to the same timeslot are from different subsets. Thus, the answer to the 3DM problem is yes. In conclusion, the yes answer to the 3DM problem is the necessary

and sufficient condition of the existence of a feasible solution of the instance problem. As the 3DM problem is NP-complete, the Lemma follows. □

Based on Lemma 1, the NP-hardness of $\mathcal{P}_0$ can be therefore concluded.

Theorem 1: $\mathcal{P}_0$ is NP-hard.

Being aware of the NP-hardness of $\mathcal{P}_0$ and the coupling effects between BH and NOMA, it is challenging to solve the original problem directly. Instead, we fix the binary variables and provide theoretical analysis of how to deal with the remaining problem.

It is worth noting that, even with the fixed binary variables α_{bt} and β_{kt}, the remaining power allocation problem, shown as in $\mathcal{P}_1$, is still non-convex [50].

$$\mathcal{P}_1 : \min_{p_{kt}} \sum_{k\in\mathcal{K}} (R_k - D_k)^2 \tag{5.10a}$$

$$\text{s.t.} \quad (6.14b), (6.14h), \tag{5.10b}$$

where $p_{kt} \geq 0$ for $\beta_{kt} = 1$ and $p_{kt} = 0$ for $\beta_{kt} = 0$. We introduce auxiliary variables δ_k and equivalently convert $\mathcal{P}_1$ as

$$\mathcal{P}_1' : \min_{p_{kt},\delta_k} \sum_{k\in\mathcal{K}} \delta_k^2 \tag{5.11a}$$

$$\text{s.t.} \quad (6.14b), (6.14h), \tag{5.11b}$$

$$-\delta_k \leq R_k - D_k \leq \delta_k, \forall k \in \mathcal{K}. \tag{5.11c}$$

At the optimum, $R_k - D_k$ is equal to either $-\delta_k$ or δ_k, $\forall k \in \mathcal{K}$, where $\delta_k \geq 0$. In the following proposition, we prove that $R_k \leq D_k$ at the optimum, which can simplify $\mathcal{P}_1'$.

Proposition 1: At the optimum of $\mathcal{P}_1$, $R_k \leq D_k$, $\forall k \in \mathcal{K}$.

Proof. The proposition can be proven by raising the contradiction that there exist some terminals with $R_k > D_k$ at the optimum. Define $\mathcal{K}_t$ as the set of the terminals scheduled to the t-th timeslot. We divide $\mathcal{K}_t$ into two subsets, $\mathcal{K}_t^+$ and $\mathcal{K}_t^-$, containing terminals with $R_k > D_k$ and $R_k \leq D_k$, respectively. Let p_{kt}^* be the optimal power. For presentation convenience, we denote $I_{k'kt}$ as the interference of terminal k caused by k' at timeslot t. We apply $0 < \zeta \leq 1$ to adjust the power of all the terminals in $\mathcal{K}_t^+$. As p_{kt}^* is optimal, $\zeta = 1$ should be optimal. For $k \in \mathcal{K}_t^+$, the SINR is expressed as,

$$\gamma_{kt} = \frac{|h_{bk}|^2 \zeta p_{kt}^*}{\sum_{k'\in\mathcal{K}_t^+\setminus\{k\}} \zeta I_{k'kt} + \sum_{k'\in\mathcal{K}_t^-} I_{k'kt} + \sigma^2}. \tag{5.12}$$

The SINR of terminals in $\mathcal{K}_t^-$ is,

$$\gamma_{kt} = \frac{|h_{bk}|^2 p_{kt}^*}{\sum_{k'\in\mathcal{K}_t^+} \zeta I_{k'kt} + \sum_{k'\in\mathcal{K}_t^-\setminus\{k\}} I_{k'kt} + \sigma^2}. \tag{5.13}$$

Given p_{kt}^*, the objective can be viewed as the function of ζ, say $\tilde{f}(\zeta; p_{kt}^*)$. We present the derivative of

$\tilde{f}(\zeta; p_{kt}^*)$ in the following,

$$\tilde{f}'(\zeta; p_{kt}^*) = \sum_{k\in\mathcal{K}_t^+} \frac{\frac{2(R_k-D_k)\gamma_{kt}}{\zeta(1+\gamma_{kt})}\left(\sum\limits_{k'\in\mathcal{K}_t^-} I_{k'kt}+\sigma^2\right)}{\sum\limits_{k'\in\mathcal{K}_t^+\setminus\{k\}}\zeta I_{k'kt}+\sum\limits_{k'\in\mathcal{K}_t^-} I_{k'kt}+\sigma^2} - \sum_{k\in\mathcal{K}_t^-} \frac{\frac{2(R_k-D_k)\gamma_{kt}}{\zeta(1+\gamma_{kt})}\sum\limits_{k'\in\mathcal{K}_t^+} I_{k'kt}}{\sum\limits_{k'\in\mathcal{K}_t^+}\zeta I_{k'kt}+\sum\limits_{k'\in\mathcal{K}_t^-\setminus\{k\}} I_{k'kt}+\sigma^2}, \tag{5.14}$$

which is obviously larger than zero since $R_k > D_k$ for terminals in $\mathcal{K}_t^+$ and $R_k < D_k$ for terminals in $\mathcal{K}_t^-$. Thus the objective can be smaller by letting $\zeta < 1$ to reduce power of the terminals in $\mathcal{K}_t^+$, which contradicts the assumption of the optimality. Thus the proposition. □

With Proposition 1, constraints (5.11c) can be converted into,

$$-\delta_k \le R_k - D_k, \forall k \in \mathcal{K}, \tag{5.15}$$

which indicates that $R_k - D_k = -\delta_k$ at the optimum. In spite of the problem conversion, we observe that solving $\mathcal{P}_1'$ remains challenging due to the nonconvexity of the logarithmic-fractional composite expressions in the R-functions [50]. A widely-adopted approach to address the fractional nonconvex function is to decouple the numerator and denominator, and transform it into a series of convex problems, e.g., Dinkelbach's transform [172], and quadratic transform [56]. Compared to conventional Dinkelbach's transform, quadratic transform has shown advantages in tackling multi-ratio fractional programming by building the equivalence of the objectives between the primal and the transformed problem [56]. Besides, quadratic transform has proven its competitiveness compared to conventional successive convex approximation method [173] in power control [56]. By applying quadratic transform [56], we convert R_{kt} from fractional format to the following,

$$\begin{aligned} f_{kt}^R(\theta_{kt}, p_{kt}) = &\log\Bigg(1 + 2\theta_{kt}\sqrt{|h_{bk}|^2 p_{kt}} \\ &-\theta_{kt}^2\left(\sum_{\substack{k'\in\mathcal{K}_b\setminus\{k\}\\ k'<k}} |h_{bk}|^2 p_{k't} + \sum_{b'\in\mathcal{B}\setminus\{b\}}\sum_{k'\in\mathcal{K}_{b'}} |h_{b'k}|^2 p_{k't} + \sigma^2\right)\Bigg), \end{aligned} \tag{5.16}$$

where $\theta_{kt} \ge 0$ is the auxiliary variable. With fixed θ_{kt}, f_{kt}^R is a concave function according to the basis of convex preservation for composite functions [50]. Then $\mathcal{P}_1'$ is rewritten as the following,

$$\mathcal{P}_2 : \min_{\theta_{kt}, p_{kt}, \delta_k} \sum_{k\in\mathcal{K}} \delta_k^2 \tag{5.17a}$$

$$\text{s.t.} \quad (6.14b), \tag{5.17b}$$

$$\sum_{t\in\mathcal{T}} f_{kt}^R(\theta_{kt}, p_{kt}) \ge R_k^{\min}, \forall k \in \mathcal{K}, \tag{5.17c}$$

$$\sum_{t\in\mathcal{T}} f_{kt}^R(\theta_{kt}, p_{kt}) - D_k \ge -\delta_k, \forall k \in \mathcal{K}. \tag{5.17d}$$

$\mathcal{P}_2$ is nonconvex in general, but can become convex when θ_{kt} is fixed, which enables an iterative approach to optimize p_{kt} with fixed θ_{kt} by solving the convex problem and updating θ_{kt} under fixed p_{kt}.

Algorithm 4 Iterative approach for power allocation

Input: feasible p_{kt} and δ_k.
1: **repeat**
2: Update θ_{kt} by (5.18).
3: Optimize p_{kt} and δ_k by solving $\mathcal{P}_2$.
4: **until** convergence
5: Calculate R_k by (6.9), (6.12), (5.5).
6: **if** there exists terminals with $R_k > D_k$ **then**
7: Solve nonlinear equations in (5.19).
8: **end if**
Output: optimized p_{kt}, δ_k.

5.4 An Iterative Approach for Upper Bound

In this section, we propose UBA algorithm to obtain an upper bound (a feasible suboptimal solution) for $\mathcal{P}_0$. In UBA, we optimize power allocation with fixed integer variables and iteratively update beam scheduling and terminal-timeslot assignment to progressively improve the performance.

5.4.1 Power Allocation with Fixed Integer Solution

The considered iterative algorithm for solving $\mathcal{P}_2$ is summarized in Alg. 4. In each iteration, line 2 and line 3 describe the procedures of alternatively update θ_{kt} and p_{kt}, respectively, where θ_{kt} is updated with fixed power allocation and p_{kt} is optimized given θ_{kt}. In the end, terminals' rates are calculated. With fixed p_{kt}, the optimal θ_{kt} is derived by [56],

$$\theta_{kt} = \frac{\sqrt{|h_{bk}|^2 p_{kt}}}{\sum\limits_{\substack{k' \in \mathcal{K}_b \setminus \{k\} \\ k' < k}} |h_{bk}|^2 p_{k't} + \sum\limits_{b' \in \mathcal{B} \setminus \{b\}} \sum\limits_{k' \in \mathcal{K}_{b'}} |h_{b'k}|^2 p_{k't} + \sigma^2}. \tag{5.18}$$

With fixed θ_{kt}, $\mathcal{P}_2$ becomes convex. The optimum can be obtained by conventional algorithms, e.g., interior-point method [54]. Based on the theoretical results in [56], we conclude that the iterative process in lines 1-4 converges to a stationary point. At the end of convergence, there may exist terminals with $\sum_{t \in \mathcal{T}} f_{kt}^R > D_k$. According to the conclusion of Proposition 1, a post process in lines 6-8 is performed for these terminals by solving the following equations,

$$R_k = D_k, \forall k \in \mathcal{K}^*, \tag{5.19}$$

where $\mathcal{K}^*$ includes the terminals with $R_k \geq D_k$. The nonlinear equations can be efficiently solved via fixed-point iteration approach [174].

The complexity of Alg. 4 mainly falls into the optimization process in line 3. For optimizing p_{kt} in line 3, we apply interior-point method to solve $\mathcal{P}_2$ with the complexity of $\mathcal{O}(\psi \log(\frac{1}{\varepsilon}))$ [54], where ψ is the self-concordant barrier parameter and ε is the precision [54]. The complexity of Alg. 4 is therefore $\mathcal{O}(N\psi \log(\frac{1}{\varepsilon}))$, where N is the maximum number of iterations.

5.4.2 Beam Scheduling and Terminal-Timeslot Assignment

Next, we jointly optimize beam scheduling and terminal-timeslot assignment to improve the performance iteratively. Some approaches, e.g., exhaustive search method, branch and bound [175], or simulated

Algorithm 5 UBA

Input: Feasible $\tilde{p}_{kt}$, $\tilde{\alpha}_{bt}$, and $\tilde{\beta}_{kt}$ (corresponding to $\tilde{\mathcal{M}}$ and $\tilde{\mathcal{N}}$).

1: **repeat**
2: Construct $\mathfrak{S}$ based on $\tilde{\alpha}_{bt}$ and (5.20).
3: **if** $\mathfrak{S} \neq \varnothing$ **then**
4: Select a swap $\mathcal{S}_{b't'}^{bt}$ and construct $\mathcal{M}$ with (b', t').
5: Optimize p_{kt} under $\mathcal{M}$ via Alg. 4.
6: **else**
7: UBA terminates.
8: **end if**
9: **if** $\tilde{\mathcal{M}}$ and $\mathcal{M}$ do not satisfy (5.21) **then**
10: Remove $\mathcal{S}_{b't'}^{bt}$ from $\mathfrak{S}$.
11: Move to line 3.
12: **end if**
13: Let $\tilde{\mathcal{M}} = \mathcal{M}$ and $\tilde{p}_{kt} = p_{kt}$ and update $\tilde{\alpha}_{bt}$, $\tilde{\beta}_{kt}$, and $\tilde{\mathcal{N}}$. Construct $\bar{\mathfrak{S}}$ based on $\tilde{\beta}_{kt}$, (5.22), and (5.23).
14: **if** $\bar{\mathfrak{S}} \neq \varnothing$ **then**
15: Select a swap $\bar{\mathcal{S}}_{k't'}^{kt}$ and construct $\mathcal{N}$ with (k', t').
16: Optimize p_{kt} under $\mathcal{N}$ via Alg. 4.
17: **end if**
18: **if** $\tilde{\mathcal{N}}$ and $\mathcal{N}$ do not satisfy (5.24) **then**
19: Remove $\bar{\mathcal{S}}_{k't'}^{kt}$ from $\bar{\mathfrak{S}}$.
20: Move to line 14.
21: **end if**
22: Let $\tilde{\mathcal{N}} = \mathcal{N}$ and $\tilde{p}_{kt} = p_{kt}$ and update $\tilde{\beta}_{kt}$.
23: **until** the number of iterations reaches N'

Output: $\tilde{p}_{kt}$, $\tilde{\alpha}_{bt}$, $\tilde{\beta}_{kt}$.

annealing [43], are capable of obtaining the optimal or near optimal integer solution but at the expense of unaffordable computational complexity. To avoid exponential-time complexity, we provide a scheme based on matching theory to decrease the capacity-demand gap iteratively.

The optimization of integer solutions can be viewed as two many-to-many matching problems [43], i.e., beam-to-timeslot matching and terminal-to-timeslot matching. Define $\mathcal{M}$ and $\mathcal{N}$ as the sets containing tuples of beam-to-timeslot and terminal-to-timeslot matching, respectively. Denote $y(\mathcal{M}, \mathcal{N})$ as the objective value obtained by Alg. 4 under $\mathcal{M}$ and $\mathcal{N}$, where $\mathcal{M}$ and $\mathcal{N}$ are constructed based on α_{bt} and β_{kt}, respectively. For instance, if $\alpha_{bt} = 1$, then $(b, t) \in \mathcal{M}$, otherwise, $(b, t) \notin \mathcal{M}$. The many-to-many matching problem can be solved via swap [43]. Consider a set $\mathcal{M}_1$ where $(b, t) \in \mathcal{M}_1$ but $(b', t') \notin \mathcal{M}_1$. We define a swap $\mathcal{S}_{b't'}^{bt}$ as the operation of converting $\mathcal{M}_1$ into $\mathcal{M}_2$ by removing (b, t) and introducing (b', t'), i.e., setting $\alpha_{bt} = 0$ and $\alpha_{b't'} = 1$. A swap happens if $\mathcal{M}_1$ and $\mathcal{M}_2$ meet the following conditions:

$$1.\ \mathcal{M}_2 \text{ satisfies constraints (6.14c) and (6.14i);} \tag{5.20}$$

$$2.\ y(\mathcal{M}_1, \mathcal{N}) > y(\mathcal{M}_2, \mathcal{N}). \tag{5.21}$$

Define $\mathfrak{S}$ as the set containing all the possible $\mathcal{S}_{b't'}^{bt}$.

Analogous to beam-to-timeslot swap, we consider a set, $\mathcal{N}_1$ where $(k, t) \in \mathcal{N}_1$ but $(k', t') \notin \mathcal{N}_1$. We define a swap $\bar{\mathcal{S}}_{k't'}^{kt}$ as the operation of converting $\mathcal{N}_1$ into $\mathcal{N}_2$ by removing (k, t) and introducing (k', t'),

i.e., setting $\beta_{kt} = 0$ and $\beta_{k't'} = 1$. A swap occurs if $\mathcal{N}_1$ and $\mathcal{N}_2$ satisfy the following conditions:

$$1.\ \mathcal{N}_2 \text{ satisfies constraints (6.14d);} \tag{5.22}$$

$$2.\ k, k^{'} \in \mathcal{K}_b \text{ and } \alpha_{bt} = \alpha_{bt'} = 1; \tag{5.23}$$

$$3.\ y(\mathcal{M}, \mathcal{N}_1) > y(\mathcal{M}, \mathcal{N}_2). \tag{5.24}$$

Define $\bar{\mathfrak{S}}$ as the set containing all the possible $\bar{\mathcal{S}}_{k't'}^{kt}$.

We summarize the procedure of UBA, in Alg. 5. Denote N' as the maximum number of iterations. Line 3 to line 13 represent the swap of beam-to-timeslot matching and line 14 to line 22 indicate the terminal-to-timeslot swap. Remark that the algorithm starts to assign terminals to timeslots once beam-to-timeslot swap is executed. The algorithm terminates when the number of iterations reaches N' or there is no more valid swap.

In UBA, the complexity for each iteration consists of two parts, i.e., beam-to-timeslot swap and terminal-to-timeslot swap. The numbers of all the possible beam-to-timeslot and terminal-to-timeslot swaps are at most $TB_0 \times T(B - B_0)$ and $B_0 \times TK_0 \times T(K' - K_0)$, respectively, where K' denotes the maximum number of terminals in each beam. For each iteration, the worst case is to optimize power for all the swaps in $\mathfrak{S}$ and $\bar{\mathfrak{S}}$ by Alg. 4. Thus the complexity of UBA is $\mathcal{O}(N'T^2B_0(B - B_0 + K_0(K' - K_0))N\psi\log(\frac{1}{\varepsilon}))$. Remark that, in practice, the complexity can be largely reduced by eliminating a certain number of swaps which do not satisfy conditions (5.20), (5.22), and (5.23).

5.5 An MICP Approximation Approach for Lower Bound

In this section, we resolve $\mathcal{P}_0$'s non-convexity by intentionally simplifying the inter-beam interference, and construct an MICP formulation to enable a lower bound for $\mathcal{P}_0$. We observe that, in some BH cases, the inter-beam interference may become negligible, e.g., illuminating two distant beams. If this interference can be ignored, $\mathcal{P}_0$ becomes an MICP problem. In this case, p_{kt} for terminals in $\mathcal{K}_b$ can be derived as follows,

$$\begin{aligned}
p_{1t} &= \left(2^{\frac{R_{1t}}{W}} - 1\right) \frac{\sigma^2}{|h_{b1}|^2}, \\
p_{2t} &= \left(2^{\frac{R_{2t}}{W}} - 1\right) \left(p_{1t} + \frac{\sigma^2}{|h_{b2}|^2}\right), \\
&\cdots \\
p_{K_bt} &= \left(2^{\frac{R_{K_bt}}{W}} - 1\right) \left(\sum_{k'=1}^{K_b-1} p_{k't} + \frac{\sigma^2}{|h_{bK_b}|^2}\right).
\end{aligned} \tag{5.25}$$

Thus (6.14b) can be rewritten in an equivalent expression as,

$$\sum_{k=1}^{K_b} \left(\frac{\sigma^2}{|h_{bk}|^2} - \frac{\sigma^2}{|h_{b(k-1)}|^2}\right) 2^{\frac{\sum_{k'=k}^{K_b} R_{k't}}{W}} - \frac{\sigma^2}{|h_{bK_b}|^2} \leq P, \forall b \in \mathcal{B}, \forall t \in \mathcal{T}, \tag{5.26}$$

where we define that $\frac{\sigma^2}{|h_{b0}|^2} = 0$. Then $\mathcal{P}_0$ becomes,

$$\mathcal{P}_3 : \min_{\alpha_{bt}, \beta_{kt}, R_{kt}, \delta_k} \sum_{k \in \mathcal{K}} \delta_k^2 \tag{5.27a}$$

$$\text{s.t.} \quad (5.26), (6.14c), (6.14d), (6.14h), (6.14i), (5.11c), \tag{5.27b}$$

$$R_{kt} \leq R^{\max}\beta_{kt}, \forall k \in \mathcal{K}, \forall t \in \mathcal{T}, \tag{5.27c}$$

where $R^{\max}$ is a constant, no smaller than all possible R_{kt}. Constraints (5.27c) connect R-variables with β-variables, where $R_{kt} = 0$ if $\beta_{kt} = 0$, otherwise, $R_{kt} \leq R^{\max}$. $\mathcal{P}_3$ is an MICP with the presence of exponential cones in (5.26) and the quadratic cones in (5.27a). The optimum of $\mathcal{P}_3$ can be achieved by branch and bound or outer approximation approach [53].

Note that, since inter-beam interference has been intentially removed, the optimum of $\mathcal{P}_3$ is no larger than that of $\mathcal{P}_0$ and thus can be viewed as a lower bound of $\mathcal{P}_0$.

Remark 1: The gap between the lower bound (the optimum of $\mathcal{P}_3$) and the optimum of $\mathcal{P}_0$ follows three cases:

- Zero gap: The optimum at $\mathcal{P}_0$ and $\mathcal{P}_3$ is equivalent if only one beam is illuminated at each timeslot, since there is no inter-beam interference in the system.
- Close-to-zero gap: $\mathcal{P}_3$ provides a close lower bound to the optimum of $\mathcal{P}_0$ if the level of inter-beam interference keeps low.
- Large gap: In some cases, the lower bound becomes loose when inter-beam interference is strong. However, due to the inherent characteristics in BH optimization, only the beams with less mutual interference are preferred to be activated at the same timeslot. Thus, this undesired issue can be avoided in a majority of cases. □

5.6 An Efficient Algorithm for Joint Optimization

UBA aims at providing a tight upper bound (or near-optimal solution) to $\mathcal{P}_0$ at the expense of high complexity. To further reduce the computational complexity, we design a low-complexity approach, i.e., E-JPBT, to provide an efficient solution for $\mathcal{P}_0$. The basic idea of E-JPBT is to divide the whole decision process of $\mathcal{P}_0$ into T stages (or timeslots) and then solve a subproblem at each stage or timeslot. To avoid directly tackling integer variables with large complexity, the subproblem for each timeslot is relaxed to a continuous problem, which can be solved by Alg. 4.

The residual demand for terminal k at timeslot t is,

$$\bar{D}_k = D_k - \sum_{\tau=0}^{t-1} R_{k\tau}, \tag{5.28}$$

where $R_{0t} = 0$. At the t-th timeslot, the resource allocation problem for the current timeslot is expressed as,

$$\mathcal{P}_0(t): \min_{\alpha_{bt},\beta_{kt},p_{kt}} \sum_{k\in\mathcal{K}} \left(R_{kt} - \bar{D}_k\right)^2 + \sum_{k\in\mathcal{K}} \phi_k \left[R_k^{\min} - R_{kt} - \sum_{\tau=0}^{t-1} R_{k\tau}\right]^+ \tag{5.29a}$$

$$\text{s.t.} \sum_{k\in\mathcal{K}_b} p_{kt} \leq 1, \forall b \in \mathcal{B}, \tag{5.29b}$$

$$\sum_{b\in\mathcal{B}} \alpha_{bt} \leq B_0, \tag{5.29c}$$

Algorithm 6 E-JPBT

Input: ϕ_k.

1: **for** $t = 1, \ldots, T$ **do**
2: Optimize $\bar{\alpha}_{bt}$ and $\bar{\beta}_{kt}$ by solving $\mathcal{P}_4(t)$ via Alg. 4.
3: Select $j^* = \arg\max_j \{\sum_{b \in \mathcal{B}_j} \bar{\alpha}_{bt}\}$.
4: Set $\alpha_{bt} = 1, \forall b \in \mathcal{B}_{j^*}$.
5: Select K_0 largest-$\bar{\beta}_{kt}$ terminals for each illuminated beam.
6: Set accordingly $\beta_{kt} = 1$.
7: Optimize p_{kt} by solving $\mathcal{P}_4(t)$ via Alg. 4 with α_{bt} and β_{kt}.
8: Update $\bar{D}_k$ by (5.28).
9: **end for**
10: Optimize p_{kt} via Alg. 4 with determined α_{bt} and β_{kt}.

Output: α_{bt}, β_{kt}, and p_{kt}.

$$\sum_{k \in \mathcal{K}_b} \beta_{kt} \leq K_0 \alpha_{bt}, \forall b \in \mathcal{B}, \tag{5.29d}$$

$$p_{kt} \leq \beta_{kt}, \forall k \in \mathcal{K}_b, \tag{5.29e}$$

$$\alpha_{bt} + \alpha_{b't} \leq 1, b \neq b', \forall (b, b') \in \Omega, \tag{5.29f}$$

where the second term of the objective is the penalty for constraints (6.14h) and $\phi_k > 0$ is the penalty factor. The objective is penalized if the rate of terminal k is lower than $R_k^{\min}$, which means more resources should be allocated to this terminal in the later timeslots.

Since $\mathcal{P}_0(t)$ is MINCP and is still challenging, we relax α_{bt} and β_{kt} into continuous variables, i.e., $0 \leq \bar{\alpha}_{bt} \leq 1$ and $0 \leq \bar{\beta}_{kt} \leq 1$. Then we convert the R-function into $f_{kt}^R(\theta_{kt}, p_{kt})$ as expressed in (5.16) via quadratic transform. $\mathcal{P}_0(t)$ can be reformulated as,

$$\mathcal{P}_4(t): \min_{\bar{\alpha}_{bt}, \bar{\beta}_{kt}, p_{kt}, \theta_{kt}} \sum_{k \in \mathcal{K}} \left(f_{kt}^R - \bar{D}_k\right)^2 + \sum_{k \in \mathcal{K}} \phi_k \left[R_k^{\min} - f_{kt}^R - \sum_{\tau=0}^{t-1} f_{k\tau}^R\right]^+ \tag{5.30a}$$

$$\text{s.t. } (5.29b), (5.29c), (5.29d), (5.29e), (5.29f), \tag{5.30b}$$

which can be solved via Alg. 4. We define $\mathcal{B}_j \subseteq \mathcal{B}$ as the j-th beam group. Note that the beam groups are constructed based on Ω. We schedule the beam group on the basis of $j^* = \arg\max_j \{\sum_{b \in \mathcal{B}_j} \bar{\alpha}_{bt}\}$. Then we select K_0 largest-$\bar{\beta}_{kt}$ terminals for each active beam. Accordingly, we decide α_{bt} and β_{kt} for the current timeslot. To update the residual demand $\bar{D}_k$, we solve the remaining of $\mathcal{P}_4(t)$ via Alg. 4 with the decided integer solution. At the end, with all determined α_{bt} and β_{kt}, we optimize p_{kt} by solving $\mathcal{P}_1$ via Alg. 4.

The procedure of E-JPBT is summarized in Alg. 6, where line 2 to line 6 are the process of determining integer variables for each timeslot. In line 2, we solve the relaxed problem via Alg. 4 and obtain continuous solution, $\bar{\alpha}_{bt}$ and $\bar{\beta}_{kt}$. The decisions of α_{bt} and β_{kt} are described in line 4 and line 6, respectively. With determined integer variables, power optimization is executed via Alg. 4 to update $\bar{D}_k$. At the end of E-JPBT, we optimize power with all the determined integer solution in line 7. The complexity of E-JPBT mainly falls into the optimization process. In conclusion, E-JPBT needs to apply Alg. 4 for $2T + 1$ times, and thus the complexity of E-JPBT is $\mathcal{O}((2T+1)N\psi \log(\frac{1}{\varepsilon}))$.

Table 5.1: Simulation parameters

Parameter	Value
Frequency, f^{fr}	20 GHz (Ka band)
Bandwidth, W	500 MHz
Satellite location	13° E
Satellite height	35,786 km
Beam radiation pattern	Provided by ESA [148]
Power budget per beam, P	20 dBW
Receive antenna gain, G_k^{rx}	42.1 dBi
Noise power, σ^2	-126.47 dBW
Number of timeslots, T	256
Number of beams, B	37
Maximum active beams, B_0	5
Number of terminals per beam, K'	5
Minimum capacity, $R_k^{\min}$	5 Mbps
Traffic demand, D_k	100 Mbps to 1.2Gbps
Error ratio of imperfect SIC	10^{-4}
Maximum multiplexed terminals, K_0	3
Maximum iterations in Alg. 4, N	20
Maximum iterations in Alg. 5, N'	100

5.7 Performance Evaluation

5.7.1 Simulation Settings and Benchmarks

In this section, we evaluate the performance of the proposed NOMA-BH scheme and the proposed algorithms in a multi-beam satellite system. The parameter settings are summarized in Table 6.1 unless stated otherwise. The beam radiation pattern is provided by European Space Agency (ESA) [148], which is depicted in Fig. 5.2. We set $T = 256$, which is larger than the minimum required number of timeslots, $\left\lceil \frac{K'}{K_0} \right\rceil \left\lceil \frac{B}{B_0} \right\rceil = 16$. In this setting, all the terminals can be scheduled to at least one timeslot. The results are averaged by 1000 instances. In NOMA, we consider a practical issue in performance evaluation, i.e., residual interference in decoding terminals' signals due to imperfect SIC [139]. Note that imperfect SIC is always considered in performance evaluation. When calculating the offered-requested data rate gap, the units of capacity and demand are unified as Mbps.

In simulation, we aim to demonstrate the applicability of the proposed BH-NOMA schemes in various satellite scenarios. We consider two typical satellite scenarios [1] (highlighted in Fig. 5.2):

- Scenario 1 (Fig. 5.2(a)): We extract a set of adjacent beams from 245 beams, where the beam illumination design is carried out within a concentrated area, e.g., covering a country. Scenario 1 refers to the systems with the presence of high-level inter-beam interference.
- Scenario 2 (Fig. 5.2(b)): We randomly select a set of non-adjacent beams from 245 beams, where BH is performed within a large area. One instance is to serve terminals in some distributed target areas, e.g., mountains or rural areas. Since no adjacent beams exist in Scenario 2, the inter-beam interference is typically smaller than that in Scenario 1.

We summarize the benchmark schemes as the following for different purposes of performance evaluation. To investigate the benefits of combining BH and NOMA, we compare the proposed BH-NOMA

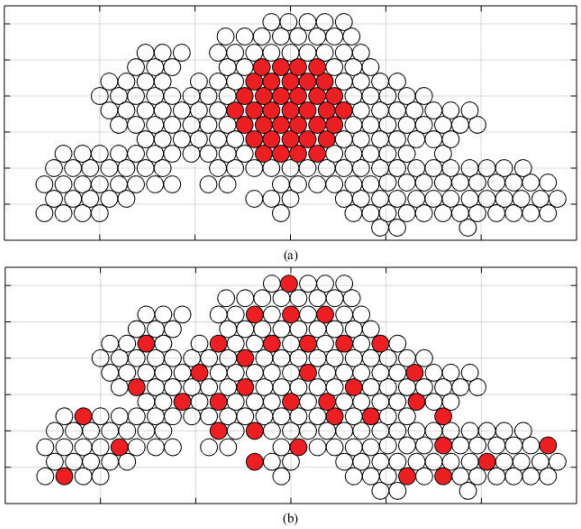

Figure 5.2: Beam pattern covering Europe provided by ESA and the adopted two scenarios, where BH is operated among the considered 37 beams (highlighted in red color).

schemes with the following standalone schemes either considering BH or NOMA (referring to Fig. 5.3 and Table II):

- BH-OMA (without NOMA): The BH-OMA problem can be formulated by simply restricting only one terminal at each timeslot, i.e., $K_0 = 1$ in $\mathcal{P}_0$, and then apply Alg. 5 to obtain the optimized result.
- 1c-NOMA (without BH): NOMA is adopted with 1-color frequency-reuse pattern (full-frequency reuse). All the beams keep illuminated without considering BH.
- 2c-NOMA (without BH): NOMA is coordinated with 2-color frequency-reuse pattern where each color represents either vertical and horizontal polarization such that adjacent two beams can occupy orthogonal resources.
- 4c-NOMA (without BH): NOMA is coordinated with 4-color frequency-reuse pattern. In the system, the frequency band is equally divided into two segments and each segment utilizes vertical and horizontal polarization. In this way, the adjacent four beams can occupy four different colors and the inter-beam interference can be reduced.

We also compare the performance achieved by the proposed algorithms with the following benchmarking schemes from the literature (referring to Fig. 5.5):

- RA: We apply the resource allocation scheme proposed in [176] to determine the number of scheduled timeslots for each beam. Then Alg. 6 is applied to decide terminal-timeslot assignment and power allocation.
- MaxSINR: An approach proposed in [88] and [84] is adopted to determine the illuminated beams at each timeslot by selecting the beams with maximum SINR. Then Alg. 6 is then adapted to optimize power allocation and terminal-timeslot assignment.
- MinCCI: An efficient approach used in [84] is applied to activate beams with the minimum inter-beam interference, then Alg. 6 is adopted analogously to MaxSINR.

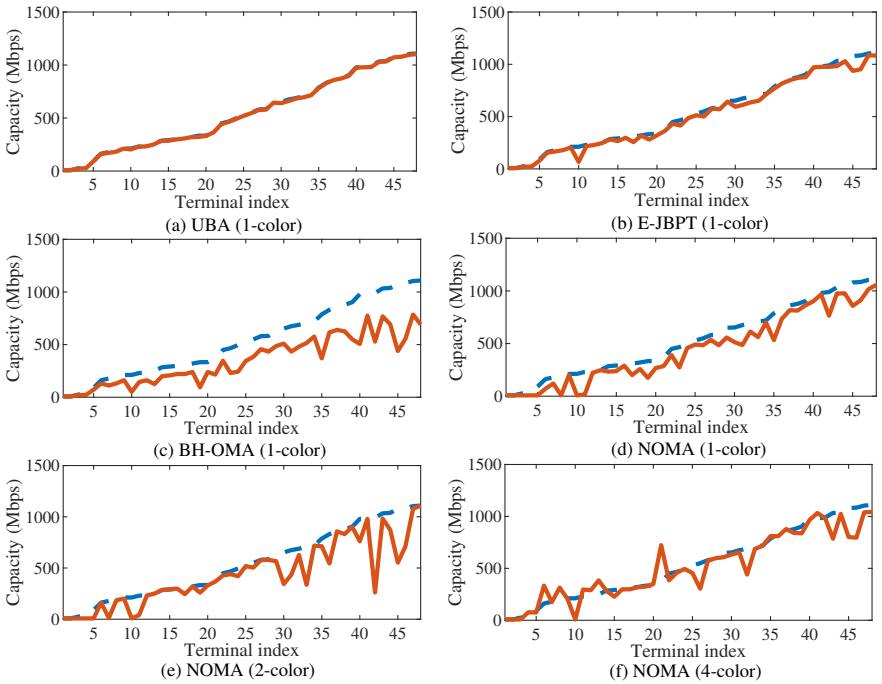

Figure 5.3: An illustration of gaps between each user's data demand (blue dashed line) and the offered capacity (red solid line) obtained in: (a) UBA, (b) E-JPBT, (c) BH-OMA, (d) 1c-NOMA, (e) 2c-NOMA, and (f) 4c-NOMA ($K = 48$, $B = 16$, $B_0 = 4$, and $K_0 = 2$).

Table 5.2: Power consumption and energy efficiency of different schemes in Fig. 5.3

Schemes	UBA	E-JPBT	BH-OMA	1c-NOMA	2c-NOMA	4c-NOMA
Power (Watts)	227.0	221.5	192.8	860.44	584.45	929.24
Energy efficiency (Mbps/Watt)	112.3	100.4	87.0	25.1	36.2	26.4

For a fair comparison with other metrics for evaluating the offered-requested data rate matching, we adapt UBA to optimize the following widely-used objective functions (referring to Table III):

- Scheme 1: The objective is to max-min offered-capacity-to-requested-traffic ratio (OCTR), i.e., $\max \min_{k \in \mathcal{K}} \frac{R_k}{D_k}$, [17, 154, 10] such that the worst capacity-traffic mismatch effects among terminals can be mitigated.
- Scheme 2: The objective aims at minimizing the total unmet capacity of terminals, i.e., $\min \sum_{k \in \mathcal{K}} [D_k - R_k]^+$, [93, 21, 10].

5.7.2 Benefits of Jointly Considering BH and NOMA

In Fig. 5.3, we discuss the benefits and evaluate the performance gains of combining BH and NOMA. The proposed BH-NOMA schemes, i.e., UBA and E-JPBT, are compared with the standalone schemes, either considering BH or NOMA. We adopt 1-color frequency-reuse pattern in UBA, E-JPBT, and BH-OMA. The gaps are large in standalone NOMA or BH schemes, i.e., Fig. 5.3(c) to Fig. 5.3(f). In contrast, by jointly optimizing BH and NOMA, the proposed BH-NOMA schemes in Fig. 5.3(a) and Fig. 5.3(b) significantly alleviate the mismatch effects, e.g., the objective value is reduced from $10^5 - 10^8$ in (Fig. 5.3(c) – Fig. 5.3(f)) to $10^2 - 10^3$ (in Fig. 5.3(a) and Fig. 5.3(b)). In Table 5.2, we further

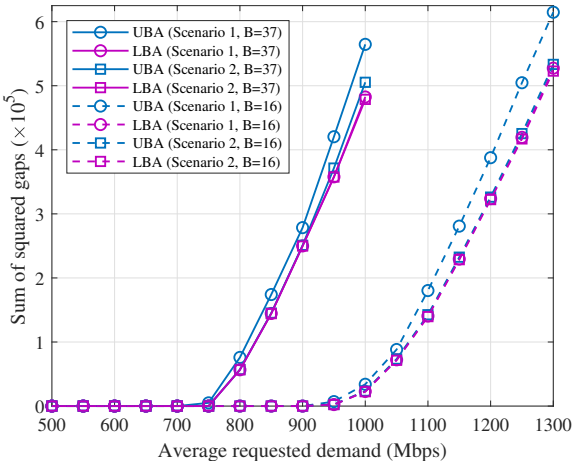

Figure 5.4: The gap performance between upper bound and lower bound, where we set 5 terminals in each beam and $K_0 = 2$.

summarize the power consumption and energy efficiency in these schemes. BH-OMA consumes the least power, slightly lower than UBA and E-JPBT, but does not perform well in capacity-demand matching and energy efficiency. Compared to 1c-NOMA, 2c-NOMA, and 4c-NOMA, the proposed UBA and E-JPBT, by augmenting both power- and time-domain flexibilities, consume much less power and achieve good trade-offs between power saving and capacity-demand mismatch reduction.

5.7.3 Performance in Bounding and Approaching the Optimum

We evaluate the tightness of upper and lower bounds in Scenario 1 and Scenario 2 with 16 or 37 beams. From Fig. 5.4, we observe that the bounding gap increases as the average demand grows. For presentation convenience, we apply the term "$\times 10^5$" in y-label as the magnitude of the values on y-axis. The proposed bounding scheme achieves near-zero gaps in Scenario 2, even for the cases with large demand. This is because the inter-beam interference can maintain at a very low level when distant beams are activated. When this small amount of inter-beam interference is intentionally neglected in LBA, it has limited impact and therefore keeps a tight lower bound for the optimum. In contrast, when Scenario 1 is considered, a larger amount of inter-beam interference is removed in LBA, thus results in larger gaps, e.g., 14.9% in 37 beams and 19.2% in 16 beams. The numerical results are consistent with the analysis in Remark 1. By our design in LBA, less interference is neglected and a tighter lower bound can be obtained. We can observe three major differences of the optimized BH solutions between Fig. 2(a) and Fig. 2(b). Firstly, the optimized BH solutions lead to smaller capacity-demand gaps, i.e., objective value, in Scenario 2 than that in Scenario 1. Secondly, in Scenario 1, the optimized BH scheme may prefer to activate a fewer number of beams per timeslot due to the presence of higher-level inter-beam interference, while more beams tend to be activated together in Scenario 2 due to the fact of distantly located beams with less mutual interference. Thirdly, the activated beams are typically non-neighboring and far away from each other in order to avoid strong inter-beam interference in Scenario 1, which may not always be the case in the optimized BH solutions of Scenario 2. This is because a beam can possibly be activated together with its nearest or neighboring beams (but geographically non-adjacent in Scenario 2) at the optimum when the interference maintains at the low level.

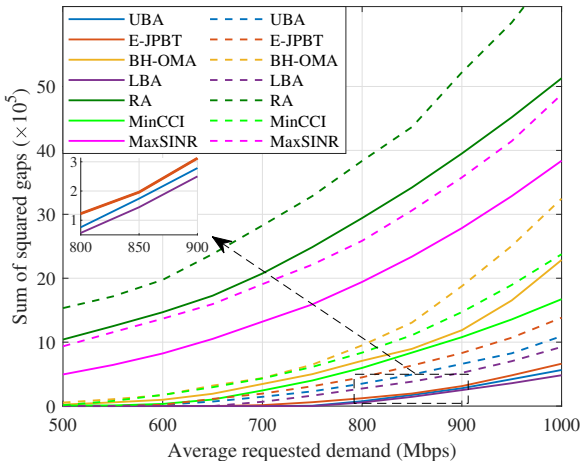

Figure 5.5: The gap performance with respect to traffic demand among the proposed schemes and benchmarks. (Scenario 1, 5 terminals per beam, $K_0 = 3$) (Solid line: under free-space channel model; Dash line: atmospheric channel model with long-term effects and rain effects.)

5.7.4 Performance Comparison between the Proposed Algorithms and Benchmarks

In Fig. 5.5, we compare the performance of the proposed UBA, LBA, and E-JPBT with BH-OMA and benchmarking schemes from the literature. We observe that the proposed schemes outperform all the four benchmarks in reducing the gap between requested and offered data rates. Firstly, due to the higher spectral efficiency in NOMA, the proposed BH-NOMA schemes outperform BH-OMA, e.g., 80.8% and 76.3% improvement in UBA and E-JPBT. Compared to RA, MaxSINR, and MinCCI, E-JPBT decreases the effect of offered-requested data mismatches by 93.2%, 90.7%, 70.4%, respectively. The proposed BH-NOMA schemes can largely reduce the mismatch effects by joint optimization of BH and NOMA compared to GA, MaxSINR, and MinCCI. We also observe that E-JPBT can achieve the cost close to the upper bound with a gap of 18.95%. Moreover, we evaluate the schemes under the channel model with atmospheric fading including long-term effects and rain effects [150]. The results verify that the advantages of the proposed UBA and E-JBPT over other benchmarks remain. The two schemes can achieve good performance in reducing the capacity-demand gaps under different channel models. The average computational time of UBA, E-JPBT, MinCCI, and MaxSINR normalized by that of RA is 14.16, 1.15, 1.10, and 1.08, respectively, where E-JPBT consumes 91.88% less time compared to UBA and maintains the same magnitude of computational time with other efficient benchmark schemes. Considering the observed performance gains, E-JPBT thus achieves a good trade-off between complexity and performance compared to other schemes.

5.7.5 The Performance of the Proposed Schemes with Different Frequency-Reuse Patterns

In Fig. 5.6, we evaluate the applicability of the proposed BH-NOMA schemes in the scenarios with the implementation of 1-color, 2-color, and 4-color frequency-reuse patterns. The performance of the proposed schemes in all the three scenarios is promising. With higher spectral efficiency, the proposed schemes in 1-color scenario can perfectly match capacity to demand when the requested demand is no larger than 650 Mbps. With less inter-beam interference, the average performance gaps between upper bound and lower bound in 2-color and 4-color scenarios are 11.23% and 2.32%, respectively, which are smaller than that in 1-color scenario. The result also verifies the conclusion in Remark 1.

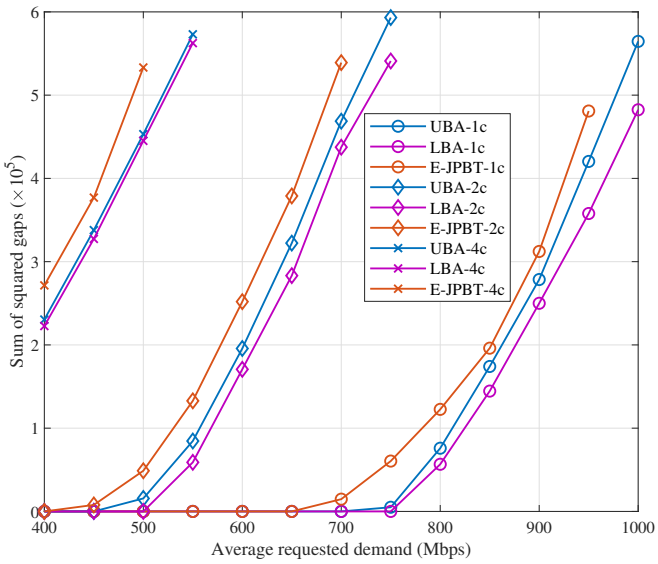

Figure 5.6: The gap performance value with respect to traffic demand of the proposed BH-NOMA schemes in different scenarios with 1-color, 2-color, adn 4-color frequency-reuse patterns.

Table 5.3: The performance comparison among different metrics

Schemes / Metrics	UBA	Scheme 1	Scheme 2
Sum squared gaps $\sum_{k\in\mathcal{K}}(R_k - D_k)^2$	1.57×10^3	3.0×10^4	1.69×10^4
The worst OCTR	0.93	0.96	0.88
Sum unmet capacity $\sum_{k\in\mathcal{K}}[D_k - R_k]^+$	218.47	1013.181	215.30

5.7.6 Comparison among Different Metrics for Evaluating the Offered-Requested Data Rate Mismatch

Next, we compare the offered-requested data mismatch performance among different metrics. In Table 5.3, we summarize the performance, where each scheme is solved by its own objective, e.g., 1.57×10^3 is obtained by UBA with the objective (5.6a) in the first row. By summarizing the obtained solutions, the results for the other two metrics can be obtained, e.g., the worst OCTR for UBA in the second row. As expected, all the three schemes perform the best with their own objectives, referring to the diagonal values, but can degrade sharply when measured with other metrics. The proposed BH-NOMA scheme shows good adaptation and generalization capabilities among different metrics, which means that UBA achieves the best performance in reducing the sum squared gaps, and slightly losses around 1% to 3% performance than the other two schemes.

5.7.7 Impact of imperfect SIC on BH-NOMA Performance

At last, we evaluate the impact of practical issues of NOMA on the performance of UBA and E-JPBT. We introduce $0 \leq \eta_k \leq 1$ to represent residual interference due to imperfect SIC [139]. Specifically, the

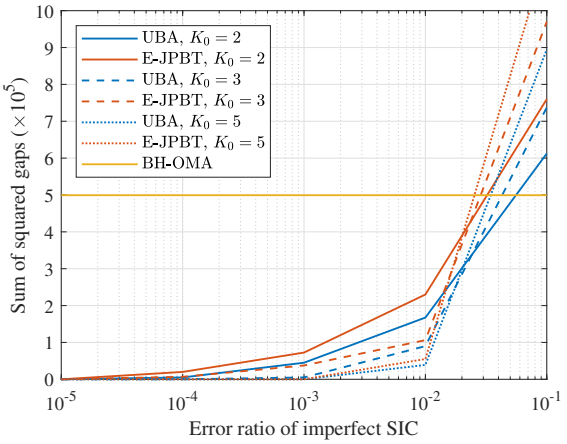

Figure 5.7: The gap performance versus error ratio of imperfect SIC of the proposed NOMA schemes.

intra-beam interference in (6.9) is rewritten as

$$\sum_{\substack{k' \in \mathcal{K}_b \setminus \{k\} \\ k' < k}} |h_{bk}|^2 p_{k't} + \sum_{\substack{k' \in \mathcal{K}_b \setminus \{k\} \\ k' > k}} |h_{bk}|^2 p_{k't} \eta_k. \tag{5.31}$$

The result in Fig. 5.7 shows the applicability of the proposed BH-NOMA schemes to imperfect-SIC scenarios. We can observe that the performance increases slowly when the error ratio of imperfect SIC is small, e.g., from 10^{-5} to 10^{-2}. When the ratio increases more than 10^{-2}, OMA might become a better choice. Besides, when the error is large, e.g., 10^{-1}, the mismatch effects in the case of $K_0 = 5$ is worse than those of $K_0 = 2$ and $K_0 = 3$. This is because the intra-beam interference caused by imperfect SIC increases with the number of co-channel terminals in the same beam.

5.8 Conclusion

In this chapter, we have investigated joint resource optimization for the coexistence of power- and time-domain flexibilities. A resource allocation problem has been formulated to minimize the gap between requested and offered data rates of terminals by jointly optimizing power allocation, beam scheduling, and terminal-timeslot assignment. We have identified the NP-hardness of the problem and proposed an effective bounding scheme, UBA and LBA, to benchmark the optimality. To reduce computational complexity, we have designed an efficient algorithm for joint optimization. In the end, we have verified the necessity of combining BH and NOMA, and demonstrated the advantages of the proposed BH-NOMA schemes compared to different benchmarks.

Chapter 6

Joint Optimization of Power- and Spatial-Domain Flexibilities

In this chapter, we continue exploiting multi-dimension flexibilities in satellite systems. Compared to conventional fixed beam pattern, adaptive beam patterns can adjust the footprint to meet irregular traffic distribution and mitigate co-channel interference. In this chapter, we study the implicit synergy between adaptive beam patterns and NOMA and investigate resource optimization in the context of power- and spatial-domain flexibilities in a multi-LEO satellite system. The formulated problem is to jointly opotimize power allocation, beam pattern selection, and terminal association to minimize the effects of capacity-demand mismatch. To tackle the challenging issues raised by discrete variables and non-convexity, we derive a joint optimization framework. Considering the complexity of the framework, we reveal the underlying relationships between beam pattern selection and NOMA optimization, based on which we design an efficient approach to achieve a good trade-off between performance and complexity. In simulation, we discuss the synergy between adaptive beam patterns and NOMA and demonstrate the superiority of the proposed schemes over benchmarks in different scenarios.

6.1 Introduction

Considering the advantages of offering high-throughput transmission and extending coverage to the space, LEO satellite systems are envisioned as one of the promising solutions to the upcoming beyond 5G (B5G) and 6G era [3]. To deliver exponentially growing traffic and support ubiquitous connectivity, the industry is motivated to develop projects on the deployment of hundreds or thousands of LEO satellites in the space [177], e.g., SpaceX Starlink. However, with densely-deployed LEO satellites, terminals may receive considerable interference from neighboring satellites [178, 179]. Besides, due to the heterogeneity of traffic distribution, resource allocation in LEO satellite systems needs to be more adaptive [15]. How to mitigate co-channel interference and provide high-quality services is challenging, which calls for the introduction of more flexibilities in resource allocation.

In conventional satellite systems, beam patterns are pre-determined and the projected beam shapes (or footprints) are fixed [1]. When LEO satellites are densely deployed and traffic demands are irregularly distributed, this fixed footprint plan may limit the performance improvement. With the development of flexible payloads, beam shapes can be altered by changing beam patterns via BFN without mechanically moving antennas [1, 180, 94]. By adjusting beam patterns, satellite transmission can be more adaptive to non-uniform traffic distribution [89, 26, 87]. Besides, the integration to terrestrial systems

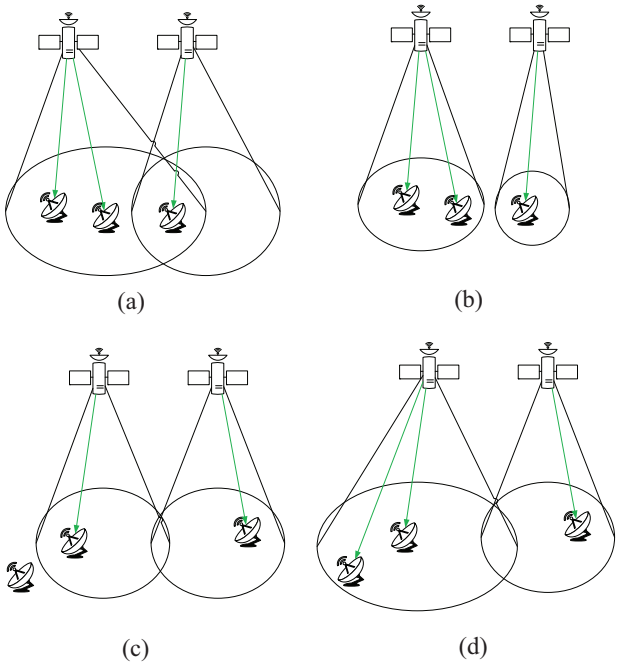

Figure 6.1: Illustrative examples of adaptive beam patterns.

can be improved by adapting footprints to mitigate co-channel interference to terrestrial systems [27] and satisfying different configuration requirements [28]. We provide illustrative instances of adaptive beam patterns in Fig. 6.1. When a terminal is located in the area covered by two adjacent satellite beams, e.g., in Fig. 6.1(a), the terminal may suffer from strong inter-satellite interference. To reduce the interference, both satellites could select patterns with smaller but more concentrated beams to cover the associated terminals, as depicted in Fig. 6.1(b). Another typical example is to change patterns with larger radiated beams to cover terminals beyond the beam edge but with high demand, e.g., from Fig. 6.1(c) to Fig. 6.1(d).

Considering the advantages in traffic adaptation and interference mitigation, adaptive beam pattern has received growing attention. The authors in [89] jointly optimized beamwidth and transmit power to adapt to varying traffic. Besides beamwidth, more factors affecting the beam shape, e.g., beam center and rotation angle, were taken into account and the footprint planning was designed to match irregular traffic distribution in [26]. In both works, regular beam shapes (e.g., circular or elliptical) are applied. The expressions of transmit antenna gain w.r.t. configuration parameters (e.g., beamwidth, beam center, rotation angle) are sophisticated in general, even in the cases of regular beam shapes. Directly optimizing footprints is difficult for practical implementation and may not be applied to irregular beam shapes [1]. Alternatively, multiple candidate beam patterns can be designed in advance for various possible scenarios and a suitable beam pattern can be selected from the candidate set depending on traffic distribution and interference. Beam pattern selection can be applied to all kinds of footprints and candidate patterns can be easily updated when necessary. In [87], the authors optimized beam pattern selection to meet irregular traffic distribution and discussed its implementation in practical satellite payloads. The above works focused on optimizing rate matching to traffic distribution over an area instead of traffic demands of specific terminals. In this work, we study beam pattern selection to alleviate capacity-demand mismatch at the terminal level.

To facilitate the accommodation of multiple terminals in each beam, NOMA is applied. By superposition coding at the transmitter side and SIC at the receiver side, spectral efficiency can be enhanced

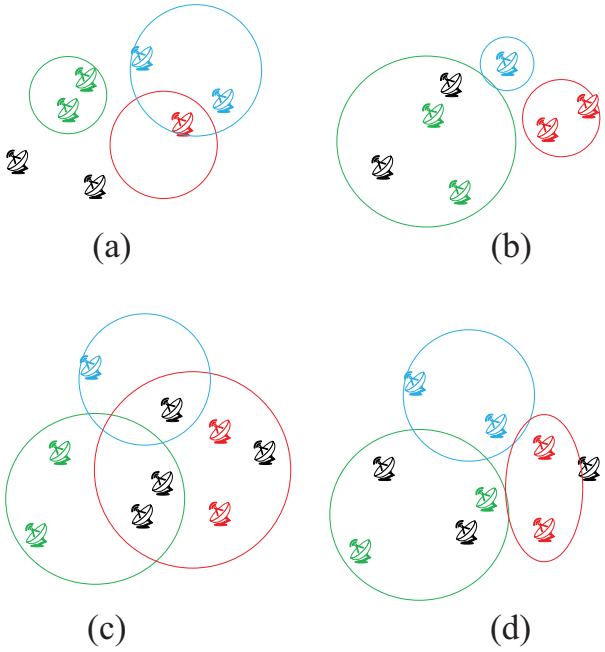

Figure 6.2: Illustrative instances of the coupling between adaptive beam patterns and NOMA. The terminals and their associated satellite are depicted in the same color.

compared to OMA [33]. NOMA has proven its advantages in LEO satellite systems, e.g., supporting massive connectivity [114] and assisting file delivery [181]. In this work, we study resource allocation in LEO satellite systems where NOMA is applied in each satellite beam to reduce intra-beam interference and facilitate multi-terminal access whereas adaptive beam pattern is adopted to mitigate inter-satellite interference and adapt to irregular traffic distribution.

6.1.1 Motivations and Contributions

Due to the coupling between beam pattern selection and NOMA (involving power allocation and terminal scheduling), resource management in the targeted LEO satellite systems is challenging. On the one hand, selecting different beam patterns could lead to the adjustment of NOMA strategies. For instance, from Fig. 6.2(a) to Fig. 6.2(b), as the green beam is enlarged, more terminals are covered, resulting in more possible combinations of terminal scheduling in this beam. On the other hand, different NOMA solutions could influence the choice of beam patterns. In Fig. 6.2(c), the green beam chooses to schedule terminals on the left to avoid large inter-satellite interference. But if the demand of the terminal in the area covered by two satellite beams grows, that terminal should be scheduled. In this case, the red beam needs to select a beam pattern with a smaller size, as depicted in Fig. 6.2(d), such that the inter-satellite interference can be reduced. The relationship between beam pattern selection and NOMA is more complicated than the instances. However, the underlying synergy and the corresponding optimization of NOMA strategies and beam pattern selection are still unknown in the literature.

As an early attempt, we are motivated to provide an investigation on resource management of beam pattern selection and NOMA in multi-LEO-satellite systems, where each satellite selects one beam pattern from multiple candidates whereas NOMA is applied in each satellite beam to accommodate multiple terminals. The main contributions are summarized as follows:

- We formulate a joint optimization problem of power allocation, beam pattern selection, and termi-

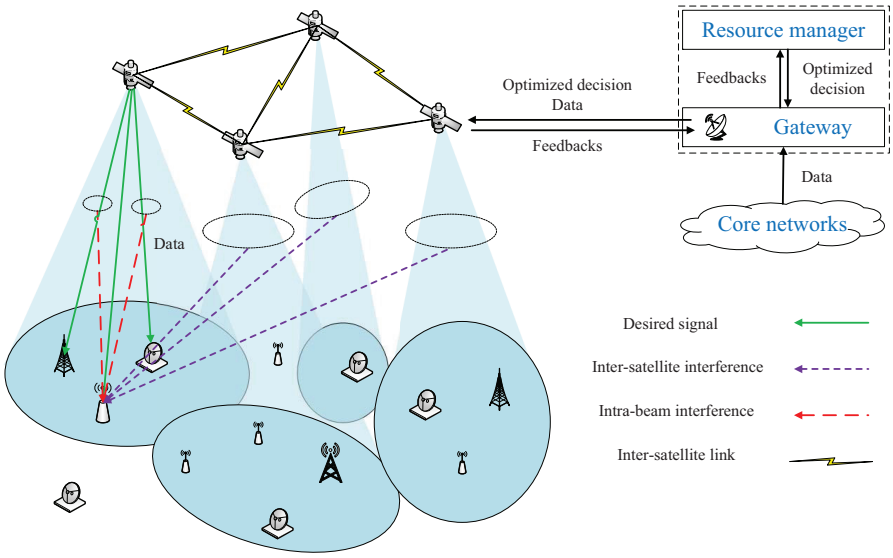

Figure 6.3: An illustrative scenario of the considered LEO satellite system. Adaptive beam patterns are adopted to adjust the beam shapes and NOMA is applied in each beam to serve multiple terminals.

nal scheduling in a multi-LEO-satellite system to minimize the capacity-demand gap. The problem falls into the category of MINCP.

- Considering the difficulty in MINCP, we provide theoretical insights on how to tackle the non-convexity and combinatorial properties in the formulated problem. Based on this, we design a joint optimization framework to allocate power, select beam patterns, and schedule terminals to timeslots/satellites (JPST).

- We analyze the implicit connection between beam pattern selection and NOMA via a special case. Based on the analysis, we design a low-complexity scheme to decide the solution of pattern selection and terminal-satellite association first and then optimize terminal-timeslot scheduling and power allocation (LC-PST).

- Numerical results show the advantages of jointly optimizing beam pattern selection and NOMA over conventional systems with OMA and fixed beam pattern.

6.2 System Model

We consider downlink transmission in a multi-LEO-satellite system, as depicted in Fig. 6.3. S satellites fly over the area of interest, where the coverages may overlap partially with neighboring satellite beams. Denote $\mathcal{S}$ as the set of the satellites and $\mathcal{K}_s$ as the set of the terminals associated to the s-th satellite. As an early-attempt study, we consider that each satellite generates one beam. In the system, all the satellites access the same frequency band. The communication procedure is described as follows: First, messages containing terminals' status, e.g., channel conditions, traffic demand, terminals' positions, etc., are feedbacked to the gateway via return links. Then the resource manager co-located with the gateway executes the resource optimization algorithm to generate optimized decisions. Next, the gateway informs optimal decisions to satellites and delivers data from the core networks to satellites. At last, satellites transmit data to targeted terminals.

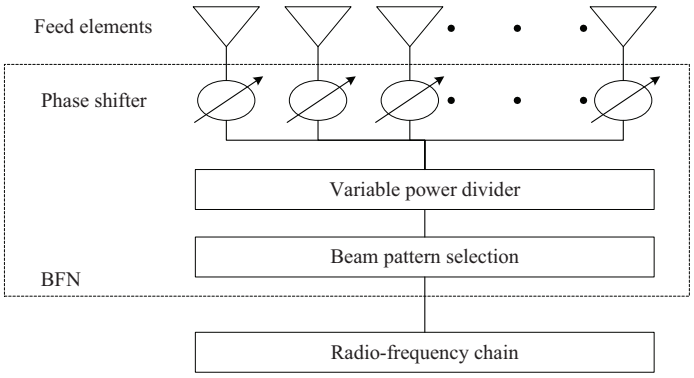

Figure 6.4: The shaped beam antenna with BFN.

6.2.1 Adaptive Beam Patterns

Denote $\mathcal{N}_s$ as the set of the candidate beam patterns of satellite s. Each pattern refers to one specific beam shape. With optimized decisions informed by the gateway, one beam pattern is selected out of $\mathcal{N}_s$. Remark that beam patterns change on a frame-by-frame basis and resource allocation is targeted for one frame. Denote $\mathcal{T}$ as the set of the T timeslots in one frame. We assume that satellites stay static within each frame. The beam pattern is generated by the BFN on the satellite payload, as depicted in Fig. 6.4. By BFN controlling phase shifters and variable power dividers to alter phases and amplitudes, each feed element generates an elementary beam and the shaped beam is constructed by these elementary beams [1]. The resulted beam shape is defined as the coverage within the φ-dB contour [1].

The relationship between the transmit antenna gain of a beam pattern and the corresponding configuration parameters is sophisticated and may not be captured by explicit expressions, especially for patterns with irregular beam shapes [1, 26, 87]. For better illustration, we use circular beam as an example to abstract the beam pattern model. The transmit antenna gain of satellite s under beam pattern n regarding terminal k is expressed by,

$$G_{snk}^{\mathrm{Tx}} = G_{s,\max}^{\mathrm{Tx}} \left(\frac{J_1(u_{snk})}{2u_{snk}} + 36 \frac{J_3(u_{snk})}{u_{snk}^3} \right)^2, \tag{6.1}$$

where $J_1(\cdot)$ and $J_3(\cdot)$ are Bessel functions of the first kind of order one and three, respectively. $G_{s,\max}^{\mathrm{Tx}}$ is the peak transmit antenna gain of satellite s. The notation u_{snk} is expressed as,

$$u_{snk} = 2.07123 \frac{\sin\theta_{sk}}{\sin\theta_{sn,\mathrm{3dB}}}, \tag{6.2}$$

where θ_{sk} denotes the off-axis angle between the s-th satellite's beam center and the k-th terminal. $\theta_{sn,\mathrm{3dB}}$ denotes the 3-dB angular beamwidth of pattern n radiated by satellite s. The beam pattern model in (6.1) is widely adopted, e.g., a simplified Bessel function was adopted in 3GPP TR 38.811 [182]. An example of transmit antenna gain with different beamwidth is presented in Fig. 6.5. With a large beamwidth, the beam can cover a wider area but the resulted inter-satellite interference is stronger. On the other hand, the decrease of beamwidth causes a smaller coverage, but the directivity is more concentrated on the beam center with less interference outwards.

For other types of beam shapes, the expression could be more complicated, e.g., the transmit antenna gain for elliptical beams depends on beam center position, beamwidth (including the major and minor axises), and tilt angle [1, 26]. Remark that this work only focuses on beam pattern selection, where

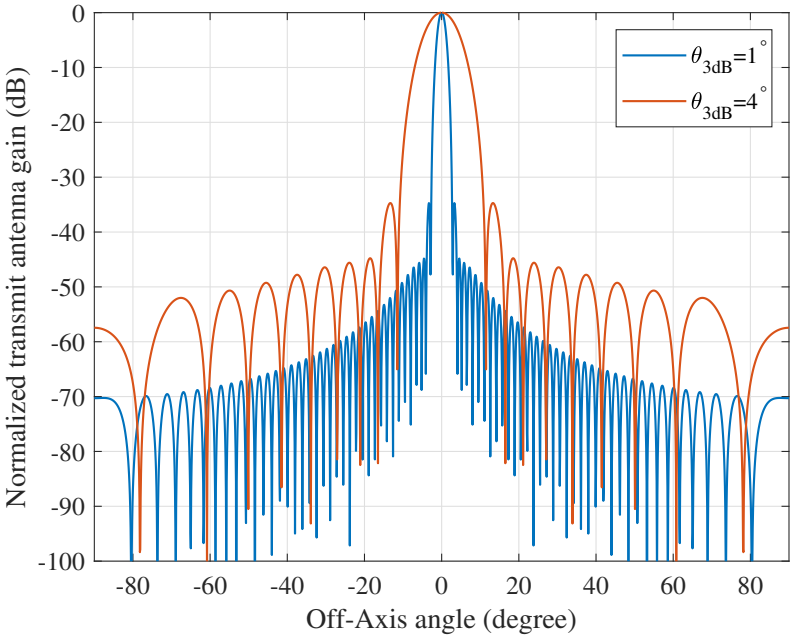

Figure 6.5: Transmit antenna gain pattern with beamwidth 1° and 4°.

the candidate patterns are pre-designed and can be updated easily when necessary. Thus the methods discussed in this work can be applied to any kind of footprint.

6.2.2 Channel Model

The channel loss from satellite s to terminal k is [182],

$$[L_{sk}^{\text{total}}] = [L_{sk}^{\text{ba}}] + [L_{sk}^{\text{ga}}] + [L_{sk}^{\text{sc}}] + [L_{sk}^{\text{ra}}], \tag{6.3}$$

where L_{sk}^{ga}, L_{sk}^{sc}, and L_{sk}^{ra} are gaseous, scintillation, and rain attenuation exceeded for $\rho\%$ of an average year, respectively. Here, the operator $[\cdot]$ converts the value into dB. L_{sk}^{ba} is the basic path loss, which is derived by,

$$[L_{sk}^{\text{ba}}] = [L_{sk}] + [L_{sk}^{\text{sf}}], \tag{6.4}$$

where L_{sk}^{sf} denotes shadow fading following log-normal distribution. L_{sk} denotes the free-space path loss, expressed by,

$$L_{sk} = 32.45 + 20\log_{10}(f^{\text{freq}}) + 20\log_{10}(d_{sk}), \tag{6.5}$$

where d_{sk} is the distance from satellite s to terminal k, and f^{freq} is the frequency. The channel gain from satellite s to terminal k under beam pattern n is expressed as,

$$|h_{skn}|^2 = G_{skn}^{\text{Tx}} G_k^{\text{Rx}} / L_{sk}^{\text{total}}, \tag{6.6}$$

where G_k^{Rx} is the receive antenna gain of terminal k. The channel gain from satellite s to terminal k is derived as,

$$|h_{sk}|^2 = \sum_{n \in \mathcal{N}_s} y_{sn} |h_{skn}|^2, \tag{6.7}$$

where $y_{sn} \in \{0, 1\}$ indicates beam pattern selection, where satellite s selects the n-th pattern if $y_{sn} = 1$ and not otherwise.

6.2.3 NOMA

By employing NOMA, each satellite can multiplex at most $\bar{K}$ terminals with different power levels at the same frequency-time resource unit. We use $\phi_{slk}[t]$ to indicate the decoding order between terminal k and l served by satellite s at timeslot t. If $\phi_{slk}[t] = 0$, terminal k performs SIC to decode l's signal and remove it. If $\phi_{slk}[t] = 1$, terminal k views l's signal as noise. Denote $p_{sk}[t]$ as the transmit power of terminal k assigned by satellite s at timeslot t. We apply one of the most widely-adopted rules to decide decoding orders, where the decoding order is identical to the ascending order of $\omega_{sk}[t] = \frac{\sum_{s' \in \mathcal{S} \setminus \{s\}} |h_{s'k}|^2 \sum_{k' \in \mathcal{K}_{s'}} p_{s'k'}[t] + \sigma^2}{|h_{sk}|^2}$ [154], i.e.,

$$\phi_{slk}[t] = \begin{cases} 0, \text{ if } \omega_{sk}[t] \leq \omega_{sl}[t]; \\ 1, \text{ otherwise.} \end{cases} \tag{6.8}$$

The signal-to-interference-plus-noise ratio (SINR) of terminal k associated to satellite s at timeslot t is derived as,

$$\gamma_{sk}[t] = \frac{|h_{sk}|^2 p_{sk}[t]}{I_{sk}^{\text{intra}}[t] + I_{sk}^{\text{inter}}[t] + \sigma^2}, \tag{6.9}$$

where

$$I_{sk}^{\text{intra}}[t] = \sum_{l \in \mathcal{K} \setminus \{k\}} |h_{sk}|^2 \phi_{slk}[t] p_{sl}[t], \tag{6.10}$$

$$I_{sk}^{\text{inter}}[t] = \sum_{s' \in \mathcal{S} \setminus \{s\}} |h_{s'k}|^2 \sum_{k' \in \mathcal{K} \setminus \{k\}} p_{s'k'}[t], \tag{6.11}$$

are intra-beam and inter-satellite interference, respectively. σ^2 is the noise power. The available rate of terminal k allocated by satellite s at timeslot t is,

$$R_{sk}[t] = B \log(1 + \gamma_{sk}[t]), \tag{6.12}$$

where B is bandwidth. Thus the offered capacity of terminal k is,

$$R_k = \sum_{t \in \mathcal{T}} \sum_{s \in \mathcal{S}} R_{sk}[t]. \tag{6.13}$$

6.3 Problem Formulation

We formulate a resource allocation problem to jointly optimize power allocation, beam-pattern selection, and terminal scheduling. The optimization variables are listed as follows,

$p_{sk}[t] \geq 0$, satellite s allocates transmit power to terminal k at timeslot t;

$$x_{sk}[t] = \begin{cases} 1, \text{ if satellite } s \text{ schedules timeslot } t \text{ to terminal } k, \\ 0, \text{ otherwise;} \end{cases}$$

$$y_{sn} = \begin{cases} 1, \text{ if satellite } s \text{ selects the } n\text{-th beam pattern,} \\ 0, \text{ otherwise;} \end{cases}$$

$$z_{sk} = \begin{cases} 1, \text{ if terminal } k \text{ is associated to satellite } s, \\ 0, \text{ otherwise;} \end{cases}$$

$$\phi_{slk}[t] = \begin{cases} 1, & \text{if terminal } l \text{ decodes } k\text{'s signal at timeslot } t \text{ when associated to satellite } s, \\ 0, & \text{if terminal } k \text{ decodes } l\text{'s signal at timeslot } t \text{ when associated to satellite } s. \end{cases}$$

Fro presentation simplicity, we apply $\mathbf{p}$, $\mathbf{x}$, $\mathbf{y}$, $\mathbf{z}$, and $\boldsymbol{\phi}$ to collect all $p_{sk}[t]$, $x_{sk}[t]$, y_{sn}, z_{sk}, and $\phi_{slk}[t]$, repsectively. The objective is to minimize the sum of capacity-demand gap, which is measured by $\mathcal{F}(\mathbf{p}, \mathbf{y}) = \sum_{k\in\mathcal{K}}(R_k - D_k)^2$. This metric is widely adopted in satellite systems, which can capture the mismatch effects between offered capacity and demand. The case of R_k equaling to D_k reflects a perfect match. The gap value increases if R_k is larger or smaller than D_k. The optimization problem is formulated as,

$$\mathcal{P}_0 : \min_{\mathbf{p},\mathbf{x},\mathbf{y},\mathbf{z},\boldsymbol{\phi}} \mathcal{F}(\mathbf{p}, \mathbf{y}) \tag{6.14a}$$

$$\text{s.t.} \sum_{k\in\mathcal{K}} p_{sk}[t] \leq \bar{P}_s, \forall s \in \mathcal{S}, \forall t \in \mathcal{T}, \tag{6.14b}$$

$$p_{sk}[t] \leq x_{sk}[t]\bar{P}_s, \forall s \in \mathcal{S}, \forall k \in \mathcal{K}, \forall t \in \mathcal{T}, \tag{6.14c}$$

$$\sum_{s\in\mathcal{S}} z_{sk} \leq 1, \forall k \in \mathcal{K}, \tag{6.14d}$$

$$\sum_{k\in\mathcal{K}} z_{sk} \leq \widetilde{K}, \forall s \in \mathcal{S}, \tag{6.14e}$$

$$\sum_{k\in\mathcal{K}} x_{sk}[t] \leq \bar{K}, \forall s \in \mathcal{S}, \forall t \in \mathcal{T}, \tag{6.14f}$$

$$x_{sk}[t] \leq z_{sk}, \forall s \in \mathcal{S}, \forall k \in \mathcal{K}, \forall t \in \mathcal{T}, \tag{6.14g}$$

$$\sum_{n\in\mathcal{N}_s} y_{sn} = 1, \forall s \in \mathcal{S}, \tag{6.14h}$$

$$R_k \geq R_k^{\min} z_{sk}, \forall k \in \mathcal{K}, \forall s \in \mathcal{S}, \tag{6.14i}$$

$$\omega_{sk}[t] - \omega_{sl}[t] \leq C\phi_{slk}[t], \forall s \in \mathcal{S}, \forall k, l \in \mathcal{K}, k \neq l, \forall t \in \mathcal{T}, \tag{6.14j}$$

$$\phi_{skl}[t] + \phi_{slk}[t] = 1, \forall s \in \mathcal{S}, \forall k, l \in \mathcal{K}, k \neq l, \forall t \in \mathcal{T}. \tag{6.14k}$$

In (6.14b), the total transmit power at each timeslot should be constrained no larger than the power budget of the satellite. Constraints (6.14c) convey the relationship between $\mathbf{p}$ and $\mathbf{x}$, where $p_{sk}[t] = 0$ if $x_{sk}[t] = 0$, otherwise $p_{sk}[t] \leq P_s$. Each terminal can be associated to at most one satellite in (6.14d). In (6.14e), each satellite can support the transmission of at most $\widetilde{K}$ terminals. In (6.14f), each satellite can serve at most $\bar{K}$ terminals at each timeslot. The connection between $\mathbf{x}$ and $\mathbf{z}$ is expressed in (6.14g). If terminal k is not associated to satellite s, i.e., $z_{sk} = 0$, $x_{sk}[t]$ is restricted to zero; otherwise, $x_{sk}[t] = \{0, 1\}$. Constraints (6.14h) limit that each satellite can only select one beam radiation pattern. In (6.14i), the allocated rate for terminal k should be larger than $R_k^{\min}$ if it is associated to satellite s. Constraints (6.14j) and (6.14k) jointly express the relationship between $\omega_{sk}[t]$ and $\phi_{slk}[t]$ depicted in (6.8). Here C is a large number satisfying $C \geq \max_{s\in\mathcal{S},k\in\mathcal{K}}\{\omega_{sk}\}$. If $\omega_{sk}[t] \geq \omega_{sl}[t]$, terminal l decodes k's signal and thus $\phi_{slk}[t] = 1$ to establish $\omega_{sk}[t] - \omega_{sl}[t] \leq C$. If $\omega_{sk}[t] < \omega_{sl}[t]$, terminal k decodes l's signal. Together with (6.14k), $\phi_{slk}[t]$ is confined as 0 so that $\omega_{sk}[t] - \omega_{sl}[t] \leq 0$.

The expressions of $R_{sk}[t]$ and $\omega_{sk}[t]$ are non-convex, resulting in the non-convexity of the objective function and constraints (6.14i) and (6.14j). With the presence of binary variables $\mathbf{x}$, $\mathbf{y}$, $\mathbf{z}$, and $\boldsymbol{\phi}$, we can observe that $\mathcal{P}_0$ is identified as a MINCP problem. Considering the combinatorial properties and non-convexity, solving $\mathcal{P}_0$ is a challenging task.

6.4 JPST: A Joint Approach for Power Allocation, Beam Pattern Selection, and Terminal Scheduling

In this section, we provide an algorithmic framework on how to tackle the nonconvexity and combinatorial properties in $\mathcal{P}_0$. We first relax binary variables and then reformulate $\mathcal{P}_0$ into a continuous nonconvex problem. Next, we decompose and convexify the problem, and design a joint optimization approach, i.e., JPST, to allocate power, select beam pattern, and schedule terminals to timeslots/satellites.

6.4.1 Problem Reformulation

Since $\phi_{slk}[t]$ depends on $\omega_{sk}[t]$, we do not directly optimize $\boldsymbol{\phi}$ but decide decoding orders according to (6.8) when $\omega_{sk}[t]$ (or $p_{sk}[t]$) is updated. We relax the residual binary variables into $\mathbf{0} \preceq \mathbf{x} \preceq \mathbf{1}$, $\mathbf{0} \preceq \mathbf{y} \preceq \mathbf{1}$, and $\mathbf{0} \preceq \mathbf{z} \preceq \mathbf{1}$. We then rewrite $\mathcal{P}_0$ as the following formulation,

$$\mathcal{P}_0' : \min_{\mathbf{p},\mathbf{x},\mathbf{y},\mathbf{z}} \mathcal{F}(\mathbf{p},\mathbf{y}) + \frac{1}{\rho}(\mathcal{X}(\mathbf{x}) + \mathcal{Y}(\mathbf{y}) + \mathcal{Z}(\mathbf{z})) \tag{6.15a}$$

$$\text{s.t.} \quad (6.14\text{b}) - (6.14\text{i}), \tag{6.15b}$$

where ρ is the penalty factor and $\mathcal{X}(\mathbf{x})$, $\mathcal{Y}(\mathbf{y})$, and $\mathcal{Z}(\mathbf{z})$ are expressed as,

$$\mathcal{X}(\mathbf{x}) = \sum_{s\in\mathcal{S}}\sum_{k\in\mathcal{K}}\sum_{t\in\mathcal{T}} x_{sk}[t](1 - x_{sk}[t]), \tag{6.16a}$$

$$\mathcal{Y}(\mathbf{y}) = \sum_{s\in\mathcal{S}}\sum_{n\in\mathcal{N}} y_{sn}(1 - y_{sn}), \tag{6.16b}$$

$$\mathcal{Z}(\mathbf{z}) = \sum_{s\in\mathcal{S}}\sum_{k\in\mathcal{K}} z_{sk}(1 - z_{sk}). \tag{6.16c}$$

In (6.16a), $x_{sk}[t](1 - x_{sk}[t]) = 0$ if $x_{sk}[t] = \{0, 1\}$, and otherwise, $x_{sk}[t](1 - x_{sk}[t]) > 0$. Besides, $x_{sk}[t](1 - x_{sk}[t])$ reaches the maximum when $x_{sk}[t] = 0.5$. Similar observations can be applied to $\mathcal{Y}(\mathbf{y})$ and $\mathcal{Z}(\mathbf{z})$. Thus, $\mathcal{P}_0'$ aims to minimize the capacity-demand gap and the penalty caused by non-binary solutions of $\mathbf{x}$, $\mathbf{y}$, and $\mathbf{z}$.

6.4.2 Algorithmic Design

Due to the coupling between $\mathbf{p}$ and $\mathbf{y}$ in the nonconvex function in (6.9), solving $\mathcal{P}_0'$ is still non-trivial. We adopt the idea of block coordinate descent (BCD) to decompose $\mathcal{P}_0'$ into two subproblems with variable blocks $\{\mathbf{p}, \mathbf{x}, \mathbf{z}\}$ and $\{\mathbf{y}\}$ and iteratively optimize the variables.

Optimize $\mathbf{p}$, $\mathbf{x}$, and $\mathbf{z}$

At the i-th iteration, given $\mathbf{y}^{(i-1)}$ (the value of $\mathbf{y}$ at the $(i-1)$-th iteration), the remaining of $\mathcal{P}_0'$ is written as,

$$\mathcal{P}_1 : \min_{\mathbf{p},\mathbf{x},\mathbf{z}} \mathcal{F}(\mathbf{p};\mathbf{y}^{(i-1)}) + \frac{1}{\rho}(\mathcal{X}(\mathbf{x}) + \mathcal{Z}(\mathbf{z})) \tag{6.17a}$$

$$\text{s.t.} \quad (6.14b) - (6.14g), (6.14i). \tag{6.17b}$$

The nonconvexity lies in the objective function and constraints (6.14i). We approximate $\mathcal{F}(\mathbf{p};\mathbf{y}^{(i-1)})$ at around $\mathbf{p} = \mathbf{p}^{(i-1)}$ to a surrogate function $\widetilde{\mathcal{F}}(\mathbf{p};\mathbf{y}^{(i-1)})$, which satisfies the following assumptions [183] (*Assumption 1*):

- $\widetilde{\mathcal{F}}(\mathbf{p};\mathbf{y}^{(i-1)})$ *is strictly convex in* $\mathbf{p}$*;*
- $\nabla\widetilde{\mathcal{F}}(\mathbf{p}^{(i-1)};\mathbf{y}^{(i-1)}) = \triangledown\mathcal{F}(\mathbf{p}^{(i-1)};\mathbf{y}^{(i-1)})$.

Here, ∇ is the gradient operator. Based on the assumption, we apply the following convex function,

$$\widetilde{\mathcal{F}}(\mathbf{p};\mathbf{y}^{(i-1)}) = \nabla\mathcal{F}(\mathbf{p}^{(i-1)};\mathbf{y}^{(i-1)})(\mathbf{p}-\mathbf{p}^{(i-1)}) + \frac{1}{2a_p}\|\mathbf{p}-\mathbf{p}^{(i-1)}\|^2, \tag{6.18}$$

where $a_p > 0$. Similarly, we approximate $\mathcal{X}(\mathbf{x})$ and $\mathcal{Z}(\mathbf{z})$ at around $\mathbf{x} = \mathbf{x}^{(i-1)}$ and $\mathbf{z} = \mathbf{z}^{(i-1)}$ to the following surrogate functions,

$$\widetilde{\mathcal{X}}(\mathbf{x}) = \nabla\mathcal{X}(\mathbf{x}^{(i-1)})(\mathbf{x}-\mathbf{x}^{(i-1)}) + \frac{1}{2a_x}\|\mathbf{x}-\mathbf{x}^{(i-1)}\|^2, \tag{6.19}$$

$$\widetilde{\mathcal{Z}}(\mathbf{z}) = \nabla\mathcal{Z}(\mathbf{z}^{(i-1)})(\mathbf{z}-\mathbf{z}^{(i-1)}) + \frac{1}{2a_z}\|\mathbf{z}-\mathbf{z}^{(i-1)}\|^2, \tag{6.20}$$

where $a_x > 0$ and $a_z > 0$.

In (6.14i), the R-function can rewritten as $R_k = f_k^+(\mathbf{p},\mathbf{y}) - f_k^-(\mathbf{p},\mathbf{y})$, where

$$f_k^+(\mathbf{p},\mathbf{y}) = \sum_{t\in\mathcal{T}}\sum_{s\in\mathcal{S}} B\log(|h_{sk}|^2 p_{sk}[t] + I_{sk}^{\text{intra}}[t] + I_{sk}^{\text{inter}}[t] + \sigma^2), \tag{6.21a}$$

$$f_k^-(\mathbf{p},\mathbf{y}) = \sum_{t\in\mathcal{T}}\sum_{s\in\mathcal{S}} B\log(I_{sk}^{\text{intra}}[t] + I_{sk}^{\text{inter}}[t] + \sigma^2). \tag{6.21b}$$

Constraints (6.14i) are equivalently converted into

$$-f_k^+(\mathbf{p},\mathbf{y}) + f_k^-(\mathbf{p},\mathbf{y}) + R_k^{\min} z_{sk} \le 0, \forall k \in \mathcal{K}, \forall s \in \mathcal{S}. \tag{6.22}$$

Given $\mathbf{y}^{(i-1)}$, (6.22) is in the format of difference of convex (DC), where the nonconvexity is reflected in the concave function $f_k^-(\mathbf{p};\mathbf{y}^{(i-1)})$. We approximate $f_k^-(\mathbf{p};\mathbf{y}^{(i-1)})$ to a convex function $\widetilde{f_k^-}(\mathbf{p};\mathbf{y}^{(i-1)})$ at around $\mathbf{p} = \mathbf{p}^{(i-1)}$, which meets the following assumptions [183] (*Assumption 2*):

- $\widetilde{f_k^-}(\mathbf{p};\mathbf{y}^{(i-1)})$ *is convex;*
- $\widetilde{f_k^-}(\mathbf{p}^{(i-1)};\mathbf{y}^{(i-1)}) = f_k^-(\mathbf{p}^{(i-1)};\mathbf{y}^{(i-1)})$*;*
- $\nabla\widetilde{f_k^-}(\mathbf{p}^{(i-1)};\mathbf{y}^{(i-1)}) = \nabla f_k^-(\mathbf{p}^{(i-1)};\mathbf{y}^{(i-1)})$*;*
- $\widetilde{f_k^-}(\mathbf{p};\mathbf{y}^{(i-1)}) \le f_k^-(\mathbf{p};\mathbf{y}^{(i-1)})$.

Then we construct the following surrogate linear function,

$$\widetilde{f_k^-}(\mathbf{p};\mathbf{y}^{(i-1)}) = f_k^-(\mathbf{p}^{(i-1)};\mathbf{y}^{(i-1)}) + \nabla f_k^-(\mathbf{p}^{(i-1)};\mathbf{y}^{(i-1)})(\mathbf{p}-\mathbf{p}^{(i-1)}). \tag{6.23}$$

Then (6.22) is transformed into,

$$-f_k^+(\mathbf{p},\mathbf{y}) + \widetilde{f_k^-}(\mathbf{p},\mathbf{y}) + R_k^{\min} z_{sk} \leq 0, \forall k \in \mathcal{K}, \forall s \in \mathcal{S}. \tag{6.24}$$

Finally, $\mathcal{P}_1$ is converted to the following strongly convex inner approximation,

$$\mathcal{P}_1' : \min_{\mathbf{p},\mathbf{x},\mathbf{z}} \widetilde{\mathcal{F}}(\mathbf{p};\mathbf{y}^{(i-1)}) + \frac{1}{\rho}(\widetilde{\mathcal{X}}(\mathbf{x}) + \widetilde{\mathcal{Z}}(\mathbf{z})) \tag{6.25a}$$

$$\text{s.t.} \quad (6.14\text{b}) - (6.14\text{g}), (6.24). \tag{6.25b}$$

The optimal solution $\mathbf{p}^*$, $\mathbf{x}^*$, and $\mathbf{z}^*$ can be solved by interior-point method [50]. We can update the variables by the following rule,

$$\mathbf{p}^{(i)} = \mathbf{p}^{(i-1)} + \delta_p^{(i)}(\mathbf{p}^* - \mathbf{p}^{(i-1)}), \tag{6.26a}$$

$$\mathbf{x}^{(i)} = \mathbf{x}^{(i-1)} + \delta_x^{(i)}(\mathbf{x}^* - \mathbf{x}^{(i-1)}), \tag{6.26b}$$

$$\mathbf{z}^{(i)} = \mathbf{z}^{(i-1)} + \delta_z^{(i)}(\mathbf{z}^* - \mathbf{z}^{(i-1)}), \tag{6.26c}$$

where $\delta_p^{(i)}$, $\delta_x^{(i)}$, and $\delta_z^{(i)}$ are the stepsizes at the i-th iteration for updating $\mathbf{p}$, $\mathbf{x}$, and $\mathbf{z}$, respectively. The stepsizes can be pre-determined (constant or diminishing) or updated by line search methods [184].

Optimize $\mathbf{y}$

With $\mathbf{p}^{(i)}$, $\mathbf{x}^{(i)}$, and $\mathbf{z}^{(i)}$, $\mathcal{P}_0'$ is reduced to,

$$\mathcal{P}_2 : \min_{\mathbf{y}} \mathcal{G}(\mathbf{y}) = \mathcal{F}(\mathbf{y};\mathbf{p}^{(i)}) + \frac{1}{\rho}\mathcal{Y}(\mathbf{y}) \quad \text{s.t. (6.14h)}, \tag{6.27}$$

where the objective is nonconvex. Similar to $\mathcal{P}_1$, we approximate the objective function locally at $\mathbf{y} = \mathbf{y}^{(i-1)}$ to the following convex surrogate function:

$$\widetilde{\mathcal{G}}(\mathbf{y}) = \nabla\mathcal{G}(\mathbf{y}^{(i-1)})(\mathbf{y}-\mathbf{y}^{(i-1)}) + \frac{1}{2a_y}\|\mathbf{y}-\mathbf{y}^{(i-1)}\|^2, \tag{6.28}$$

where $a_y > 0$ and $\nabla\mathcal{G}(\mathbf{y}) = \nabla\mathcal{F}(\mathbf{y};\mathbf{p}^{(i)}) + \frac{1}{\rho}\nabla\mathcal{Y}(\mathbf{y})$. The problem is then approximated to the following convex problem,

$$\mathcal{P}_2' : \min_{\mathbf{y}} \widetilde{\mathcal{G}}(\mathbf{y}) \quad \text{s.t. (6.14h)}. \tag{6.29}$$

The optimal solution $\mathbf{y}^*$ can be solve via interior-point method. The value of $\mathbf{y}^{(i)}$ is updated by,

$$\mathbf{y}^{(i)} = \mathbf{y}^{(i-1)} + \delta_y^{(i)}(\mathbf{y}^* - \mathbf{y}^{(i-1)}), \tag{6.30}$$

where $\delta_y^{(i)}$ is the update stepsize at iteration i.

Algorithm 7 JPST

Inputs: Initialized $\mathbf{p}$, $\mathbf{x}$, $\mathbf{y}$, $\mathbf{z}$.

1: **repeat**
2: Calculate $\omega_{sk}[t]$ and update decoding orders ϕ by (6.8).
3: Obtain $\mathbf{p}^*$, $\mathbf{x}^*$, and $\mathbf{z}^*$ by solving $\mathcal{P}_1'$.
4: Compute stepsizes and update $\mathbf{p}$, $\mathbf{x}$, and $\mathbf{z}$ by (6.26).
5: Obtain $\mathbf{y}^*$ by solving $\mathcal{P}_2'$.
6: Compute stepsize and update $\mathbf{y}$ by (6.30).
7: **until** Convergence or reaching I_1 iterations

Outputs: Optimized $\mathbf{p}$, $\mathbf{x}$, $\mathbf{y}$, $\mathbf{z}$, ϕ.

Complexity analysis

The overall procedure of JPST is illustrated in Alg. 7. At the beginning of each iteration, the decoding orders are updated based on $\omega_{sk}[t]$ in line 2. Then $\mathcal{P}_1'$ is solved and $\mathbf{p}$, $\mathbf{x}$, and $\mathbf{z}$ are updated in line 3. Analogously, we solve $\mathcal{P}_2'$ and update $\mathbf{y}$ in line 5. The stepsize parameters and variables are updated in line 4 and line 6. The algorithm terminates if it reaches I_1 iterations or it converges.

The complexity of each iteration in Alg. 7 mainly lies in the process of solving $\mathcal{P}_1'$ and $\mathcal{P}_2'$ in line 3 and line 5, respectively. Since $\mathcal{P}_1'$ contains $SK(2T+1)$ decision variables, SK convex and $2SKT+SK+ST+K$ linear constraints,vthe complexity of solving $\mathcal{P}_1'$ is $\mathcal{O}(S^3K^3(2T+1)^3(2SKT+SK+ST+K))$ [185]. Similarly, the complexity of solving $\mathcal{P}_2'$ is $\mathcal{O}((SN)^3S)$ with SN decision variables and S linear constraints. Solving $\mathcal{P}_1'$ takes the lead in complexity. Thus the complexity of Alg. 7 is $\mathcal{O}(I_1S^3K^3(2T+1)^3(2SKT+SK+ST+K))$.

6.5 LC-PST: A Low-Complexity Algorithm

The complexity of the joint approach, i.e., JPST, is large, especially when the problem scale increases. To reduce the complexity, we propose a low-complexity approach, i.e., LC-PST, to accelerate the decision-making process. Before that, we analyze the underlying synergy of NOMA and adaptive beam patterns.

6.5.1 A Special Case: A Dual-Satellite Scenario

Given integer solutions, the remaining power allocation problem is written as,

$$\mathcal{P}_3: \min_{p_{sk}[t]} \sum_{s\in\mathcal{S}} \sum_{k\in\mathcal{K}_s} (R_k - D_k)^2 + \sum_{k\in\mathcal{K}_0} D_k^2 \tag{6.31a}$$

$$\text{s.t.} \quad \sum_{k\in\mathcal{K}_s} p_{sk}[t] \le \bar{P}_s, \forall s \in \mathcal{S}, \forall t \in \mathcal{T}, \tag{6.31b}$$

$$R_k \ge R_k^{\min}, \forall k \in \mathcal{K}_s, \forall s \in \mathcal{S}, \tag{6.31c}$$

where $\mathcal{K}_s$ denotes the set of the terminals associated to satellite s and $\mathcal{K}_0$ is the set containing the non-associated terminals. We start with a special case of a dual-satellite scenario with $T=1$. The index of t is omitted for presentation simplicity. Let $\mathcal{K}_1 = \{1,\ldots,K_1\}$, $\mathcal{K}_2 = \{K_1+1,\ldots,K_1+K_2\}$, and $\mathcal{K}_0 = \{K_1+K_2+1,\ldots,K\}$. Assume that the terminals' indexes are consistent with decoding orders, i.e., terminal k decodes k''s signals if $k<k'$ in $\mathcal{K}_s$. In the best case, all the associated terminals can be satisfied with demands, i.e., $R_k = D_k$, and the objective is $\sum_{k\in\mathcal{K}_0} D_k^2$. By substituting $R_k = D_k$ into

(6.9) and (6.12), we can derive the following equations based on a widely-adopted substituting approach [101],

$$\sum_{k\in\mathcal{K}_1}(\omega_{1k}-\omega_{1(k-1)})2^{\sum_{l\geq k}\frac{D_l}{W}}-\omega_{1K_1}=P_1, \tag{6.32a}$$

$$\sum_{k\in\mathcal{K}_2}(\omega_{2k}-\omega_{2(k-1)})2^{\sum_{l\geq k}\frac{D_l}{W}}-\omega_{2(K_1+K_2)}=P_2, \tag{6.32b}$$

where and $P_1=\sum_{k\in\mathcal{K}_1}p_{1k}$ and $P_2=\sum_{k\in\mathcal{K}_2}p_{2k}$. Note that $\omega_{10}=\omega_{2K_1}=0$. The equations can be rewritten as,

$$\begin{aligned}-P_1+A_1P_2+B_1=0,\\ A_2P_1-P_2+B_2=0,\end{aligned} \tag{6.33}$$

where

$$A_1=\sum_{k\in\mathcal{K}_1}\frac{|h_{2k}|^2}{|h_{1k}|^2}2^{\sum_{l>k}\frac{D_l}{W}}(2^{\frac{D_k}{W}}-1), \tag{6.34a}$$

$$B_1=\sum_{k\in\mathcal{K}_1}\frac{\sigma^2}{|h_{1k}|^2}2^{\sum_{l>k}\frac{D_l}{W}}(2^{\frac{D_k}{W}}-1), \tag{6.34b}$$

$$A_2=\sum_{k\in\mathcal{K}_2}\frac{|h_{1k}|^2}{|h_{2k}|^2}2^{\sum_{l>k}\frac{D_l}{W}}(2^{\frac{D_k}{W}}-1), \tag{6.34c}$$

$$B_2=\sum_{k\in\mathcal{K}_2}\frac{\sigma^2}{|h_{2k}|^2}2^{\sum_{l>k}\frac{D_l}{W}}(2^{\frac{D_k}{W}}-1). \tag{6.34d}$$

Thus the solution of P_1 and P_2 is derived as,

$$P_1'=\frac{A_1B_2+B_1}{1-A_1A_2}, \tag{6.35}$$

$$P_2'=\frac{A_2B_1+B_2}{1-A_1A_2}, \tag{6.36}$$

where P_s' denotes the required transmit power of satellite s to satisfy all terminals' demands.

Proposition 1: According to (6.14b)*, the transmit power for each satellite should meet* $0\leq P_s\leq\bar{P}_s$, $\forall s\in\mathcal{S}$. *The following two cases of* P_s' *can be derived:*

- *If* $0<P_s'\leq\bar{P}_s$*, all associated terminals' demand can be satisfied with* $R_k=D_k$.
- *If* $P_s'>\bar{P}_s$ *or* $P_s'<0$*, it is impossible to satisfy the demand of all the associated terminals.*

The following remark illustrates the synergy of NOMA and beam pattern selection based on Proposition 1.

Remark 1: We discuss the integer solution based on (6.36) *from the following two aspects:*

- *Given the decision of terminal association/scheduling, the optimal power allocation is achieved in the first case of Proposition 1. In this case, the solution of* $\mathbf{y}$ *is optimal. Regarding the second case, power allocation cannot satisfy terminals' demand. One can increase* $1-A_1A_2$ *such that* P_s'*, when negative, tends to be positive or* P_s' *can be reduced when* $P_s'>\bar{P}_s$*. Thus, to increase*

$1-A_1A_2$, satellites can select beam patterns with smaller $\frac{|h_{s'k}|^2}{|h_{sk}|^2}$ for $k \in \mathcal{K}_s$, i.e., beams with more concentration on the associated terminals but less inter-satellite interference to other terminals.

- *Consider that beam pattern selection is determined. In the first case of Proposition 1, the transmit power is sufficient to satisfy all the associated terminals' demand. To decrease the objective value, i.e., $\sum_{k\in\mathcal{K}_0} D_k^2$, satellites can schedule terminals with higher demand and smaller $\frac{|h_{s'k}|^2}{|h_{sk}|^2}$. A similar strategy can be applied in the second case. Terminals with smaller $\frac{|h_{s'k}|^2}{|h_{sk}|^2}$ are desired to be scheduled to increase $1-A_1A_2$ such that the capability of offering rate to associated terminals can be improved. To reduce the objective, satellites tend to serve terminals with higher demand.* □

In short, Remark 1 conveys that satellites tend to select beam patterns with smaller but concentrated beams to cover the associated terminals and schedule terminals with higher demand and better channel conditions (large channel coefficients from their associated satellites but less inter-satellite interference).

6.5.2 Algorithmic Design

The analysis of multi-satellite scenarios is much more complicated than the above special case. But we can still apply the basic findings in dual-satellite scenarios (as discussed in Remark 1) to simplify the algorithmic design. The procedure of LC-PST is summarized in Alg. 8. The basic idea is to first select beam patterns and associate terminals to satellites and then optimize terminal-timeslot scheduling and power allocation.

At the initialization stage of LC-PST, the solutions of $\mathbf{y}$ and $\mathbf{z}$ are determined following some rules, e.g., each satellite randomly selects a beam pattern and terminals are assigned to the satellites with the largest $|h_{sk}|^2$.

In the first stage, beam pattern selection and terminal association are updated iteratively. Given beam pattern selection, terminals' ratios of $\frac{|h_{sk}|^2 2^{D_k}}{\sum_{s'\in\mathcal{S}\setminus\{s\}}|h_{s'k}|^2}$ are calculated for each satellite. Then each satellite chooses $\widetilde{K}$ largest-ratio terminals for association and update $\mathbf{z}$. Based on $\mathbf{z}$, we update $\mathcal{K}_s$, which is the set of the terminals associated to satellite s. With decided terminal-satellite association, each satellite compute the ratio of $\sum_{k\in\mathcal{K}_s}\frac{|h_{sk}|^2}{\sum_{s'\in\mathcal{S}\setminus\{s\}}|h_{s'k}|^2}$ for each beam pattern and select the pattern with the largest ratio. The process terminates if the iteration number exceeds I_2 or the solutions stay unchanged. At the end of the stage, $\mathbf{y}$ and $\mathbf{z}$ are obtained.

In the second stage, terminal-timeslot scheduling and power allocation are optimized under $\mathbf{y}$ and $\mathbf{z}$. At timeslot t, terminal k's accumulated rate from timeslot 1 to $t-1$ is derived as,

$$\bar{R}_k[t] = \begin{cases} \sum_{\tau=0}^{t-1} R_k[\tau], \text{ if } t > 1; \\ 0, \text{ if } t = 0, \end{cases} \tag{6.37}$$

where $R_k[t]$ is the allocated rate of terminal k at timeslot t. The residual demand at timeslot t is $\bar{D}_k[t] = D_k - \bar{R}_k[t]$. We sort the ratios of $\frac{|h_{sk}|^2 2^{\bar{D}_k[t]}}{\sum_{s'\in\mathcal{S}\setminus\{s\}}|h_{s'k}|^2}$ among associated terminals. Define $\hat{\mathcal{K}}_s$ as the set of terminals in $\mathcal{K}_s$ with the accumulated rate smaller than the minimum requirement in (6.14i). The satellite selects $\bar{K}$ largest-ratio terminals, first in $\hat{\mathcal{K}}_s$ and then in $\mathcal{K}_s \setminus \hat{\mathcal{K}}_s$. With the terminal-timeslot assignment, the residual power allocation problem at timeslot t is written as,

$$\mathcal{P}_4(t): \min_{p_{sk}[t]} \sum_{k\in\mathcal{K}} \left(\sum_{s\in\mathcal{S}} R_{sk}[t] - \bar{D}_k[t] \right)^2 + \frac{1}{\varrho} \sum_{k\in\mathcal{K}} [R_k^{\min} - R_k[t] - \bar{R}_k[t]]^+ \tag{6.38a}$$

$$\text{s.t. (6.14b)}, \tag{6.38b}$$

Algorithm 8 LC-PST

Inputs: Initialized $\mathbf{y}$, $\mathbf{z}$.

First stage: beam pattern selection and terminal association

1: **repeat**
2: Calculate and sort $\frac{|h_{sk}|^2 2^{D_k}}{\sum_{s' \in \mathcal{S} \setminus \{s\}} |h_{s'k}|^2}$ among terminals for each satellite.
3: Each satellite select $\widetilde{K}$ largest terminals for association.
4: Update $\mathbf{z}$ and $\mathcal{K}_s$, $\forall s \in \mathcal{S}$.
5: Each satellite computes $\sum_{k \in \mathcal{K}_s} \frac{|h_{sk}|^2}{\sum_{s' \in \mathcal{S} \setminus \{s\}} |h_{s'k}|^2}$ for each beam pattern and select the one with the largest value.
6: Update $\mathbf{y}$.
7: **until** $\mathbf{y}$ and $\mathbf{z}$ stay constant or reaching I_2 iterations

Second stage: terminal-timeslot scheduling and power allocation

8: **for** $t = 1, \ldots, T$ **do**
9: Update $\bar{R}_k[t]$ and $\bar{D}_k[t]$.
10: Remove terminal k from $\mathcal{K}_s$ if $\bar{D}_k[t] \leq 0$.
11: Remove terminal k from $\hat{\mathcal{K}}_s$ if $\bar{R}_k[t] \leq 0$.
12: Calculate and sort $\frac{|h_{sk}|^2 2^{\bar{D}_k[t]}}{\sum_{s' \in \mathcal{S} \setminus \{s\}} |h_{s'k}|^2}$ for each satellite.
13: Each satellite select $\bar{K}$ largest terminals first from $\hat{\mathcal{K}}_s$ and then from $\mathcal{K}_s \setminus \hat{\mathcal{K}}_s$.
14: Solve $\mathcal{P}_4(t)$ via Alg. 7 under scheduled terminals.
15: **end for**

Outputs: Optimized $\mathbf{p}$, $\mathbf{x}$, $\mathbf{y}$, $\mathbf{z}$, $\boldsymbol{\phi}$.

where $[\cdot]^+$ is the operator equivalent to $\max\{\cdot, 0\}$. ϱ is applied to penalize the objective if the allocated rate does not satisfy (6.14i). The problem is a special case of $\mathcal{P}_1$ with fixed integer variables and can be solved by Alg. 7. Then we update $\bar{R}_k[t]$ and $\bar{D}_k[t]$. At the end, with decided $\mathbf{x}$, $\mathbf{y}$, and $\mathbf{z}$, we optimize power allocation during T timeslots via Alg. 7.

The details of LC-PST are presented in Alg. 8, where line 1 to line 7 refer to the first stage and line 8 to line 13 refer to the second stage. The complexity falls in solving multiple power allocation problems at the second stage. For solving $\mathcal{P}_4(t)$ with $S\bar{K}$ variables and S linear constraints, the complexity is $\mathcal{O}(I_1 S^4 \bar{K}^3)$, where I_1 is the maximum number of iterations of power allocation. The overall complexity is $\mathcal{O}(I_1 S^4 \bar{K}^3 T)$.

6.6 Numerical Results

6.6.1 Simulation Settings

In simulation, we consider a square area with 500×500 km^2, where the generation of terminals follows two-dimension normal distribution [177]. The main parameters are summarized in Table 6.1, unless otherwise stated. We consider beam patterns which generate circular beams on the ground with 3-dB beamwidths $\{1^\circ, 1.5^\circ, 2^\circ, 4^\circ, 8^\circ\}$ [1]. Beams with 1° beamwidth have the largest directivity to the beam center and smallest inter-satellite interference whereas those with 8° beamwidth generate the widest service range but largest interference to terminals associated to adjacent satellites. For practical consideration, we assume imperfect SIC where the error ratio is set as 10^{-3}. The results are averaged over 500 instances. For comparison, we set the following strategies as benchmarks to decide the solutions of terminal scheduling and beam pattern selection:

Table 6.1: Simulation parameters

Parameter	Value
Frequency, f^{freq}	20 GHz (Ka band)
Bandwidth, W	400 MHz
Satellite height	600 km
Number of satellites, S	5
Power budget, $\bar{P}_s$	43 dBm
Number of beam patterns, N	5
Receive antenna gain, G_{sk}^{Rx}	42, 36, 32 dBi
Noise power, σ^2	-126.47 dBW
Number of terminals, K	30
Number of timeslots, T	10
Minimum association rate, $R_k^{\min}$	500 kbps
Maximum multiplexed terminals per satellite, $\bar{K}$	3
Maximum associated terminals per satellite, $\widetilde{K}$	6
Number of iterations, I_1, I_2	2000, 20

- Round-Robin strategy (RR): Each satellite selects $\widetilde{K}$-best-channel terminals for association. Then the beam pattern with the smallest beamwidth to cover all the associated terminals is chosen. At each timeslot, terminals are scheduled following the Round-Robin basis [186].
- Best-channel strategy (BC) [187]: Terminal association and beam pattern selection are similar to RR. During each timeslot, terminals are scheduled based on their channel condition unless $\bar{D}_k[t] \leq 0$.
- Swap-matching strategy (SM) [179, 188]: The terminal-satellite-timeslot problem can be divided into two many-to-many matching problems: terminal-satellite matching and terminal-timeslot matching. The solution can be obtained by performing the swap matching approach. We select the smallest beam to cover all the associated terminals.

With the decided integer solutions, the residual power allocation problem is solved by Alg. 7.

6.6.2 Performance Evaluation

Benefits of adopting NOMA

We consider two scenarios of terminals' distribution, where the distribution in Fig. 6.6(b) is more concentrated to each beam's center than that in Fig. 6.6(a). The capacity-demand gap performance of the proposed schemes concerning $\bar{K}$ is evaluated in these two scenarios. Note that the case of $\bar{K} = 1$ refers to the conventional OMA scheme. From Fig. 6.7, a smaller capacity-demand gap is observed in the "concentrated" scenario than the "scattered" scenario. As terminals are located closer to the beam center, beam patterns with a smaller beam size can be chosen such that the inter-satellite interference can be largely reduced and thus better performance. In addition, JPST has an average reduction of 8.9% and 13.9% in minimizing the capacity-demand gap over LC-PST in "concentrated" and "scattered" scenarios, respectively. Compared to the conventional OMA scheme, NOMA has an average performance gain from 32.6% ($\bar{K} = 2$) to 56.7% ($\bar{K} = 5$) in minimizing the capacity-demand gap.

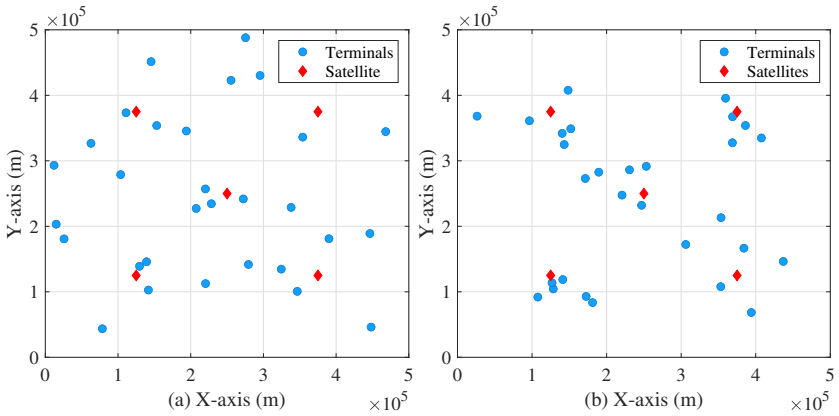

Figure 6.6: Two considered scenarios: (a) the distribution of terminals is scattered; (b) the distribution of terminals is concentrated to the centers of beams.

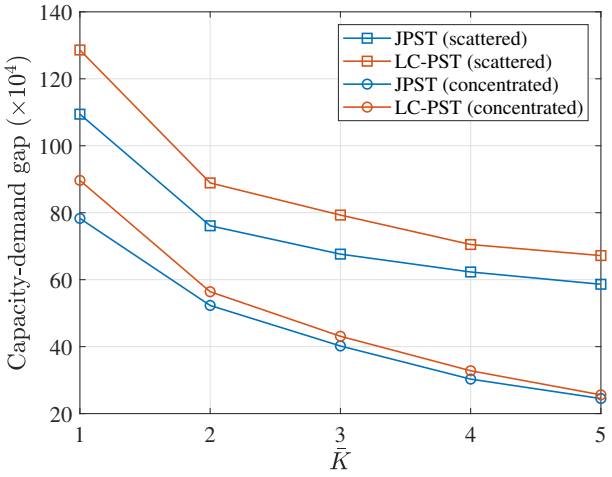

Figure 6.7: Gap performance with respect to $\bar{K}$.

Benefits of applying multiple beam patterns

In Fig. 6.8, we compare the performance of the proposed schemes between multiple beam patterns and single fixed beam pattern. Among the three fixed-pattern schemes, the one with 2° beamwidth outperforms the other two, demonstrating the necessity for an appropriate selection of beam patterns. The performance is largely improved by introducing spatial-domain flexibility compared to conventional single beam pattern schemes. Compared to the schemes with single beam pattern, the schemes with 3 beam patterns (with beamwidth 1°, 2°, and 8°) and 5 beam patterns result in 35.3% and 64.9% gain in reducing the capacity-demand gap.

In practice, LEO satellites functioned with adaptive beam patterns would coexist with those with conventional payloads in the system. We evaluate the scenarios with the coexistence of different types of LEO satellites in Fig. 6.9. By introducing satellites with adaptive beam patterns, the capacity-demand gap can be largely reduced, from 64.9×10^4 to 40.2×10^4 and 49.1×10^4 when introducing 5 and 3 beam patterns, respectively. The more satellites with spatial-domain flexibility, the more performance gain is obtained.

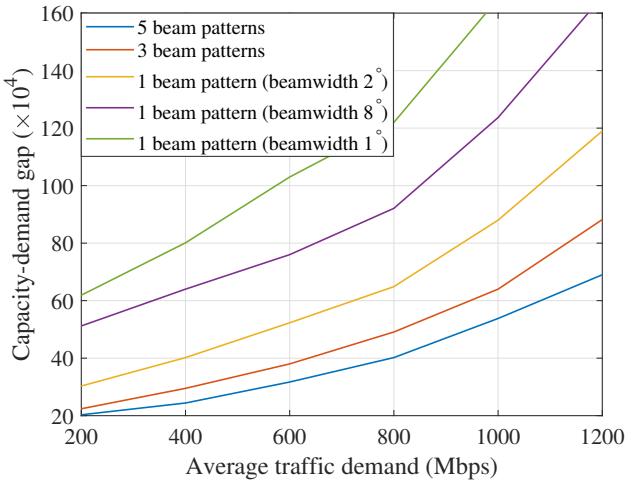

Figure 6.8: Performance evaluation in scenarios with the coexistence of satellites with single pattern and multiple patterns.

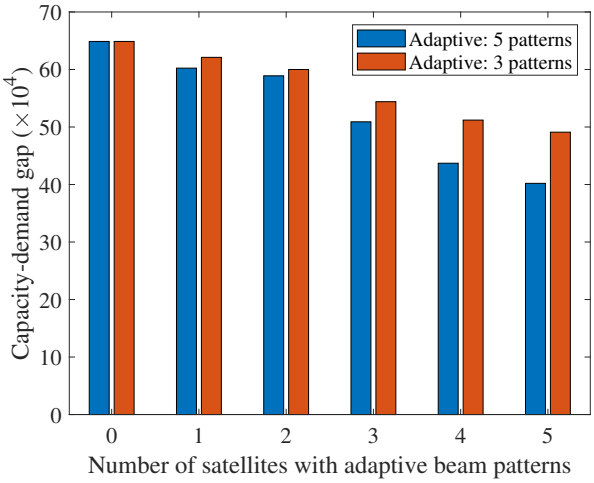

Figure 6.9: Performance evaluation in scenarios with the coexistence of satellites with single pattern and multiple patterns.

Benefits of joint optimization

In Fig. 6.10, we evaluate the performance of the proposed schemes with benchmarks, i.e., RR, BC, and SM. Compared to benchmarking schemes without joint optimization, JPSA outperforms the others. On average, JPSA has a reduction of 63.0%, 48.8%, and 37.1% in minimizing the capacity-demand gap over RR, BC, and SM, respectively, which shows the advantages of designing a joint scheme to optimize beam pattern selection and NOMA.

6.7 Conclusion

In this chapter, we have exploited multi-dimension flexibilities in power and spatial domains and investigated the synergy between NOMA and adaptive beam patterns. We have proposed a joint algorithmic framework, JPST, to optimize power allocation, beam pattern selection, and terminal scheduling. To reduce the complexity, we have analyzed the implicit synergies between adaptive beam patterns and

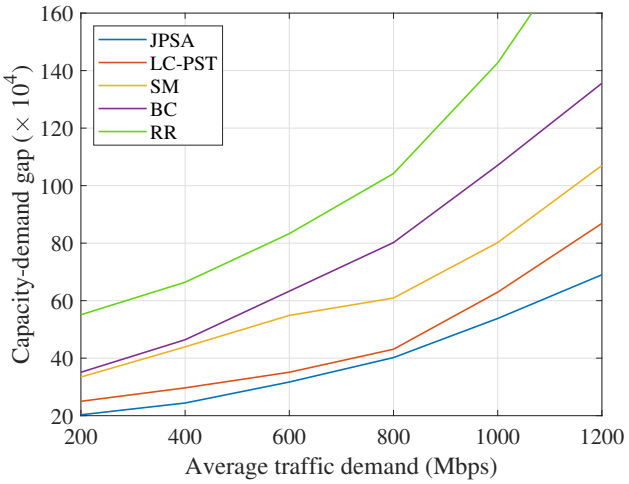

Figure 6.10: Gap performance in different schemes with respect to average traffic demand.

NOMA to simplify the problem solving. Then we have designed a low-complexity approach, LC-PST, to first decide beam patterns and terminal association and then optimize terminal scheduling and power allocation. In the end, we have evaluated the performance and demonstrated the superiority of the proposed joint schemes compared to benchmarks.

Chapter 7

Conclusions and Future Works

7.1 Conclusions

In this dissertation, we have enriched the studies on the exploitation of flexibilities and resource optimization for next-generation HTS systems, where NOMA is applied to enhance the power-domain flexibility. The dissertation has resolved the three main research questions: First, how to optimize resource allocation to minimize the mismatch effects between offered capacity and requested demand, and how much gain can be obtained when NOMA is introduced to the satellite systems? Second, how to design an efficient resource allocation scheme to achieve a good tradeoff between performance and complexity? Third, how to boost the synergies of NOMA and exploit multi-dimension flexibilities in resource optimization? The table in Fig. 7.1 illustrates the conclusion of the thesis.

Chapter 3 and Chapter 4 have investigated the resource optimization for single power-domain flexibility in NOMA-enabled satellite systems from different angles. In Chapter 3, we have designed a general resource optimization framework from the perspectives of optimization. The problems solving can be analyzed based on optimization theory, which may provide some solid theoretical guarantee of performance. By deriving mathematical closed-form expressions, some implicit relationships can be revealed to assist the problem solving. However, in order to achieve guaranteed performance, e.g., the global optimum or local optimum, the designed approaches may suffer from large computational complexity. Besides, not all the characteristics of the targeted problems can be reveal by mathematical analysis, especially problems with nonconvex and combinatorial properties.

Alternatively, we can tackle the problem with the assistance of machine learning techniques. In Chapter 4, two learning-assisted approaches have been provided to accelerate the decision-making procedure and address the feasibility issues. Compared to optimization-based approaches, learning can approximate sophisticated relationships by exploiting information from empirical data instead of deriving mathematical expressions directly. By constructing a well-trained learning model, the complexity can be largely reduced. But there are some disadvantages we need to be careful when designing learning-assisted approaches. First, when the data is hard to obtain, the training of a learning model will be extremely difficult. Second, the interpretation of learning techniques, especially deep learning, is insufficient. Third, the generalization of learning models to dynamic environment is another open challenge.

Chapter 5 and Chapter 6 have studied resource optimization for multi-dimension flexibilities. The synergies of NOMA and BH, with flexibilities of power and time domains, respectively, have been investigated in Chapter 5. We have proposed a bounding scheme to gauge the optimality and an efficient scheme to optimize power allocation, beam scheduling, and terminal-timeslot assignment. In Chapter 6, we have discussed the mutual influence between NOMA and adaptive beam patterns, in power and

<table>
<tr><td rowspan="2">Power</td><td colspan="2">Optimization:
A general resource optimization framework</td><td colspan="2">Learning:
Learning to accelerate the decision-making process and address the feasibility issue</td></tr>
<tr><td>Pros:
1. Theoretical guarantee
2. Reveal relationship with closed-form expressions</td><td>Cons:
1. Large complexity (global/local optimum)
2. Difficult analysis</td><td>Pros:
1. Approximate complex relationships
2. Low complexity</td><td>Cons:
1. Hard-to-obtain data
2. Insufficient interpretation
3. Generalization</td></tr>
<tr><td>Power & Time</td><td colspan="2">NOMA and beam hopping:
1. A bounding scheme to gauge the optimum
2. An efficient scheme to optimize power allocation, beam scheduling, and terminal-timeslot assignment</td><td colspan="2">1. Over 70% performance improvement
2. Smaller inter-beam interference by illuminating non-adjacent beams</td></tr>
<tr><td>Power & Spatial</td><td colspan="2">NOMA and adaptive beam pattern:
1. A joint scheme to optimize power allocation, beam pattern selection, and terminal scheduling
2. A low-complexity scheme</td><td colspan="2">1. Over 35% performance improvement
2. Cooperated with other interference mitigation techniques (e.g., precoding)
3. Coordination with beam hopping?</td></tr>
</table>

Figure 7.1: Conclusion of the thesis

spatial domains. A joint optimization scheme of power allocation, beam pattern selection, and terminal scheduling and a low-complexity scheme have been put forward. In numerical results, NOMA with BH has a gain of over 70% whereas NOMA with adaptive beam pattern improves the performance by over 35% compared to conventional schemes. NOMA with BH seems has more enhancement over NOMA with adaptive beam pattern. The reason behind this may be the large reduction of inter-beam interference by illuminating non-adjacent beams in BH. When confronting a choice between NOMA with BH and NOMA with adaptive beam pattern in network achitecture design, the former might be superior. For further performance improvement in the latter, more interference mitigation techniques could be introduced, e.g., precoding. Another alternative method could be the coordination of NOMA, BH, and adaptive beam pattern to facilitate more flexibilities.

7.2 Future Works

In the end, we provide the following potential directions for future extension.

Further exploitation of flexible resource allocation

The pursuit of more flexibilities of resource allocation in SatCom never stops [90, 91]. In Chapter 5 and Chapter 6, we have studied the joint optimization of NOMA + BH and NOMA + adaptive beam patterns, respectively. To achieve more performance gain, it is natural to investigate resource optimization in the context of considering the flexibilities in power, time, and spatial domains. In the targeted systems, the coordination of NOMA, BH, and adaptive beam patterns is considered, where NOMA is applied within each beam to reduce intra-beam interference while BH and adaptive beam patterns are adopted to mitigate inter-beam interference. The three techniques can also cooperate to adapt to heterogeneous traffic distribution and boost capacity-demand match. One may concern about the difficulty in dealing with the corresponding optimization problem due to the presence of multi-dimension variables, e.g., power allocation, terminal-timeslot assignment, beam scheduling, beam pattern selection, etc. To this end, we are motivated to study the implicit synergies among NOMA, BH, and adaptive beam patterns

and design an efficient scheme for the problem solving. To further embrace the trend of flexible satellite payload, full flexibilities in power, frequency, time, and spatial domains would be realized [93]. The difficulty lies in the high complexity of solving a large-scale problem with all related variables. The design of efficient schemes and the underlying relationships among different-domain flexibilities could be investigated.

Facilitating NOMA by leveraging adaptive beam patterns

In the dissertation, as well as most of the recent works, NOMA is employed within each beam to enable multi-terminal accommodation in an overloaded system, where more than one terminal is served in each beam. One open challenge lies in how to adopt NOMA to alleviate inter-beam interference in multi-beam satellite systems. Indeed, NOMA application is demonstrated as an inefficient strategy in spatial-dimension exploitation compared to MISO techniques [189], which is one of the reasons why the discussion of NOMA has been excluded from 3GPP study items. With the development of dynamic BFN/active antennas [93], the receive power imbalance could be facilitated spontaneously by leveraging adaptive beam patterns. In a large area with heterogeneous traffic distribution, for example, a narrow but concentrated beam can be used to cover the traffic-burst region whereas the wide beam serves the whole area [94]. In this context, NOMA can be applied to mitigate inter-beam interference. The power imbalance can be enlarged by employing different beam patterns to the same area, which could be advantageous to NOMA applications in exploiting performance gain in the spatial dimension. This motivates us to study how to apply adaptive beam patterns to facilitate power imbalance and design a beam-level NOMA transmission framework.

Resource optimization for multiple numerologies

In SatCom, the channel gain imbalance among terminals in the same beam (within the 3-dB or 4.3dB contour) is not large. Conventional power-driven NOMA may confront some practical issues, e.g., limited performance gain over OMA and difficulty in detecting/demodulating different signals to perform SIC. In this case, we can apply NOMA from another angle. To accommodate the properties and QoS requirements of different services, radio access network (RAN) slicing is introduced, where radio resources are reconfigured with flexible frequency spacings and time intervals. This new radio technique is also essential for the integration of satellite and terrestrial networks since the waveform parameters of both networks are different [190]. This is a new dimension of flexibility in resource optimization. However, as different frequency spacings are applied, the orthogonality among resource blocks is broken, and thus inter-numerology interference is introduced. The research question lies in how to optimize resource allocation for satellite systems with multiple numerologies. Besides, NOMA, with the properties of non-orthogonality, may multiplex various numerologies at the same frequency/time, which is advantageous to inter-numerology interference mitigation [191]. NOMA application in this context would be different from general power-domain NOMA, which calls for a novel design of superposition coding and SIC process to accommodate different numerologies.

Distributed optimization for multi-layer satellite systems

As launched satellites in the space become crowded, flexible resource allocation for multi-layer satellite systems will be challenging [94], where the properties of satellites in various orbits are different in multiple aspects, e.g., exclusive objectives, limitations of payload capability, propagation delay, channel conditions, etc. A harmonious orchestration for resource allocation in a multi-layer satellite system is necessary. However, such orchestration will be challenging in practice, e.g., the issues of synchronization

among different satellites, severe computational complexity, etc [2, 93]. Centralized methods, gathering all the information in the system and allocating resources for all the components, may not be suitable. The idea of distributed optimization is a choice for practical implementation. In distributed optimization, resource optimization is decentralized to multiple agents and the algorithmic process is executed locally at each agent side [192]. In this case, the synchronization and complexity issues could be eased to some extent. However, the design of a distributed approach may not be easy for multi-layer satellite systems. The cooperation among satellites is necessary to manage interference mitigation for better performance, but meanwhile, the competition for more resources to achieve their own goals is fierce. The challenge lies in: How to coordinate resource optimization among multiple agents to satisfy their users' demands and achieve their exclusive targets, cooperatively, competitively, or both?

Bibliography

[1] Gérard Maral, Michel Bousquet, and Zhili Sun. *Satellite communications systems: systems, techniques and technology*. John Wiley & Sons, 2020.

[2] Oltjon Kodheli, Eva Lagunas, Nicola Maturo, Shree Krishna Sharma, Bhavani Shankar, Jesus Fabian Mendoza Montoya, Juan Carlos Merlano Duncan, Danilo Spano, Symeon Chatzinotas, Steven Kisseleff, et al. Satellite communications in the new space era: A survey and future challenges. *IEEE Communications Surveys & Tutorials*, 23(1):70–109, 2020.

[3] Federica Rinaldi, Helka-Liina Maattanen, Johan Torsner, Sara Pizzi, Sergey Andreev, Antonio Iera, Yevgeni Koucheryavy, and Giuseppe Araniti. Non-terrestrial networks in 5G & beyond: A survey. *IEEE Access*, 8:165178–165200, 2020.

[4] Cisco. Cisco annual Internet report (2018-2023), March 2020.

[5] Peng Wang, Jiaxin Zhang, Xing Zhang, Zhi Yan, Barry G Evans, and Wenbo Wang. Convergence of satellite and terrestrial networks: A comprehensive survey. *IEEE access*, 8:5550–5588, 2019.

[6] Jiajia Liu, Yongpeng Shi, Zubair Md Fadlullah, and Nei Kato. Space-air-ground integrated network: A survey. *IEEE Communications Surveys & Tutorials*, 20(4):2714–2741, 2018.

[7] X Alberti, JM Cebrian, A Del Bianco, Z Katona, J Lei, MA Vázquez-Castro, A Zanus, L Gilbert, and N Alagha. System capacity optimization in time and frequency for multibeam multi-media satellite systems. In *2010 5th Advanced Satellite Multimedia Systems Conference and the 11th Signal Processing for Space Communications Workshop*, pages 226–233, 2010.

[8] Colin J Black, Peter Takats, Martin Cote, and Tho T Le-Ngoc. Data communication satellite system and method of carrying multi-media traffic, April 23 2002. US Patent 6,377,561.

[9] Christian Niephaus, Mathias Kretschmer, and Gheorghita Ghinea. Qos provisioning in converged satellite and terrestrial networks: A survey of the state-of-the-art. *IEEE Communications Surveys & Tutorials*, 18(4):2415–2441, 2016.

[10] Giuseppe Cocco, Tomaso De Cola, Martina Angelone, Zoltan Katona, and Stefan Erl. Radio resource management optimization of flexible satellite payloads for DVB-S2 systems. *IEEE Transactions on Broadcasting*, 64(2):266–280, 2017.

[11] Aleix Paris, Inigo Del Portillo, Bruce Cameron, and Edward Crawley. A genetic algorithm for joint power and bandwidth allocation in multibeam satellite systems. In *2019 IEEE Aerospace Conference*, pages 1–15. IEEE, 2019.

[12] Ana I Pérez-Neira, Miguel Ángel Vázquez, M. R. B. Shankar, Sina Maleki, and Symeon Chatzinotas. Signal processing for high-throughput satellites: Challenges in new interference-limited scenarios. *IEEE Signal Processing Magazine*, 36(4):112–131, 2019.

[13] Xinran Fang, Wei Feng, Te Wei, Yunfei Chen, Ning Ge, and Cheng-Xiang Wang. 5g embraces satellites for 6g ubiquitous iot: Basic models for integrated satellite terrestrial networks. *IEEE Internet of Things Journal*, 8(18):14399–14417, 2021.

[14] Eva Lagunas, Shree Krishna Sharma, Sina Maleki, Symeon Chatzinotas, and Björn Ottersten. Resource allocation for cognitive satellite communications with incumbent terrestrial networks. *IEEE Transactions on Cognitive Communications and Networking*, 1(3):305–317, 2015.

[15] Hayder Al-Hraishawi, Houcine Chougrani, Steven Kisseleff, Eva Lagunas, and Symeon Chatzinotas. A survey on non-geostationary satellite systems: The communication perspective. *arXiv preprint arXiv:2107.05312*, 2021.

[16] Christos N Efrem and Athanasios D Panagopoulos. Dynamic energy-efficient power allocation in multibeam satellite systems. *IEEE Wireless Communications Letters*, 9(2):228–231, 2019.

[17] Mirza Golam Kibria, Eva Lagunas, Nicola Maturo, Danilo Spano, and Symeon Chatzinotas. Precoded cluster hopping in multi-beam high throughput satellite systems. *arXiv preprint arXiv:1905.01162*, 2019.

[18] Florian Vidal, Hervé Legay, George Goussetis, Thomas Ströber, and Jean-Didier Gayrard. Benchmark of meo multibeam satellite adaptive antenna and payload architectures for broadband systems. In *2020 10th Advanced Satellite Multimedia Systems Conference and the 16th Signal Processing for Space Communications Workshop (ASMS/SPSC)*, pages 1–8. IEEE, 2020.

[19] Piero Angeletti and Marco Lisi. A survey of multiport power amplifiers applications for flexible satellite antennas and payloads. In *Proceedings of the 14th Ka and Broadband Communications Conference*, pages 1–8, 2008.

[20] Oleg A Iupikov, Jose-Ramon Perez-Cisneros, Petrie Meyer, Daniel Åkesson, Rob Maaskant, Koen Buisman, Robert Rehammar, Christian Fager, and Marianna V Ivashina. A cavity-backed patch antenna with distributed multi-port feeding, enabling efficient integration with doherty power amplifier and band-pass filter. *IEEE Transactions on Antennas and Propagation*, 69(8):4412–4422, 2021.

[21] Alexis I Aravanis, M. R. B. Shankar, Pantelis-Daniel Arapoglou, Grégoire Danoy, Panayotis G Cottis, and Björn Ottersten. Power allocation in multibeam satellite systems: A two-stage multi-objective optimization. *IEEE Transactions on Wireless Communications (TWC)*, 14(6):3171–3182, 2015.

[22] Shilong Pan, Dan Zhu, Shifeng Liu, Kun Xu, Yitang Dai, Tianliang Wang, Jianguo Liu, Ninghua Zhu, Yong Xue, and Naijin Liu. Satellite payloads pay off. *IEEE Microwave Magazine*, 16(8): 61–73, 2015.

[23] Sastri L Kota. Broadband satellite networks: trends and challenges. In *IEEE Wireless Communications and Networking Conference, 2005*, volume 3, pages 1472–1478. IEEE, 2005.

[24] Piero Angeletti, David Fernandez Prim, and Rita Rinaldo. Beam hopping in multi-beam broadband satellite systems: System performance and payload architecture analysis. In *24th AIAA International Communications Satellite Systems Conference*, page 5376, 2006.

[25] Sunil Panthi, Dirk Breynaert, Christopher McLain, and Janet King. Beam hopping: A flexible satellite communication system for mobility. In *35th AIAA International Communications Satellite Systems Conference*, page 5413, 2017.

[26] Puneeth Jubba Honnaiah, Nicola Maturo, Symeon Chatzinotas, Steven Kisseleff, and Jens Krause. Demand-based adaptive multi-beam pattern and footprint planning for high throughput GEO satellite systems. *IEEE Open Journal of the Communications Society*, 2:1526–1540, 2021.

[27] Shigenori Tani, Katsuyuki Motoyoshi, Hiroyasu Sano, Atsushi Okamura, Hiroki Nishiyama, and Nei Kato. An adaptive beam control technique for Q band satellite to maximize diversity gain and mitigate interference to terrestrial networks. *IEEE Transactions on Emerging Topics in Computing*, 7(1):115–122, 2016.

[28] Alessandro Guidotti. Beam size design for new radio satellite communications systems. *IEEE Transactions on Vehicular Technology*, 68(11):11379–11383, 2019.

[29] Behrooz Makki, Krishna Chitti, Ali Behravan, and Mohamed-Slim Alouini. A survey of noma: Current status and open research challenges. *IEEE Open Journal of the Communications Society*, 1:179–189, 2020.

[30] Aamina Akbar, Sobia Jangsher, and Farrukh A Bhatti. Noma and 5g emerging technologies: A survey on issues and solution techniques. *Computer Networks*, 190:107950, 2021.

[31] SM Riazul Islam, Nurilla Avazov, Octavia A Dobre, and Kyung-Sup Kwak. Power-domain non-orthogonal multiple access (NOMA) in 5G systems: Potentials and challenges. *IEEE Communications Surveys & Tutorials*, 19(2):721–742, 2017.

[32] Linglong Dai, Bichai Wang, Zhiguo Ding, Zhaocheng Wang, Sheng Chen, and Lajos Hanzo. A survey of non-orthogonal multiple access for 5G. *IEEE communications surveys & tutorials*, 20 (3):2294–2323, 2018.

[33] Xiaojuan Yan, Kang An, Tao Liang, Gan Zheng, Zhiguo Ding, Symeon Chatzinotas, and Yan Liu. The application of power-domain non-orthogonal multiple access in satellite communication networks. *IEEE Access*, 7:63531–63539, 2019.

[34] Ana I Pérez-Neira, Marius Caus, and Miguel Ángel Vázquez. Non-orthogonal transmission techniques for multibeam satellite systems. *IEEE Communications Magazine*, 57(12):58–63, 2019.

[35] Sunil Chinnadurai, Poongundran Selvaprabhu, and Moon Ho Lee. A novel joint user pairing and dynamic power allocation scheme in MIMO-NOMA system. In *2017 International Conference on Information and Communication Technology Convergence*, pages 951–953, 2017.

[36] Jiefei Ding, Jun Cai, and Changyan Yi. An improved coalition game approach for MIMO-NOMA clustering integrating beamforming and power allocation. *IEEE Transactions on Vehicular Technology*, 68(2):1672–1687, 2018.

[37] Beomju Kimy, Sungmook Lim, Hyungjong Kim, Sangwook Suh, Jonghyung Kwun, Sooyong Choi, Chungyong Lee, Sanghoon Lee, and Daesik Hong. Non-orthogonal multiple access in a downlink multiuser beamforming system. In *MILCOM 2013-2013 IEEE Military Communications Conference*, pages 1278–1283, 2013.

[38] Zhengxuan Liu, Lei Lei, Ningbo Zhang, Guixia Kang, and Symeon Chatzinotas. Joint beamforming and power optimization with iterative user clustering for MISO-NOMA systems. *IEEE Access*, 5:6872–6884, 2017.

[39] Junyeong Seo and Youngchul Sung. Beam design and user scheduling for nonorthogonal multiple access with multiple antennas based on pareto optimality. *IEEE Transactions on Signal Processing*, 66(11):2876–2891, 2018.

[40] Shipon Ali, Ekram Hossain, and Dong In Kim. Non-orthogonal multiple access (NOMA) for downlink multiuser MIMO systems: User clustering, beamforming, and power allocation. *IEEE Access*, 5:565–577, 2016.

[41] Marius Caus, Miguel Ángel Vázquez, and Ana I Pérez-Neira. NOMA and interference limited satellite scenarios. In *2016 50th Asilomar Conference on Signals, Systems and Computers*, pages 497–501, 2016.

[42] Lei Lei, Di Yuan, Chin Keong Ho, and Sumei Sun. Power and channel allocation for non-orthogonal multiple access in 5G systems: Tractability and computation. *IEEE Transactions on Wireless Communications (TWC)*, 15(12):8580–8594, 2016.

[43] Boya Di, Lingyang Song, and Yonghui Li. Sub-channel assignment, power allocation, and user scheduling for non-orthogonal multiple access networks. *IEEE Transactions on Wireless Communications*, 15(11):7686–7698, 2016.

[44] Jihwan P Choi and Vincent WS Chan. Optimum power and beam allocation based on traffic demands and channel conditions over satellite downlinks. *IEEE Transactions on Wireless Communications (TWC)*, 4(6):2983–2993, 2005.

[45] Zhixiang Gao, Aijun Liu, Chen Han, and Xiaohu Liang. Sum rate maximization of massive mimo noma in leo satellite communication system. *IEEE Wireless Communications Letters*, 10 (8):1667–1671, 2021.

[46] Xiaojuan Yan, Hailin Xiao, Cheng-Xiang Wang, and Kang An. Outage performance of NOMA-based hybrid satellite-terrestrial relay networks. *IEEE Wireless Communications Letters*, 7(4): 538–541, 2018.

[47] Ruisong Wang, Wenjing Kang, Gongliang Liu, Ruofei Ma, and Bo Li. Admission control and power allocation for noma-based satellite multi-beam network. *IEEE Access*, 8:33631–33643, 2020.

[48] Zining Wang, Min Lin, Shiyong Sun, Ming Cheng, and Wei-Ping Zhu. Robust beamforming for enhancing user fairness in multibeam satellite systems with noma. *IEEE Transactions on Vehicular Technology*, 2021.

[49] Zhisheng Yin, Min Jia, Wei Wang, Nan Cheng, Feng Lyu, Qing Guo, and Xuemin Shen. Secrecy rate analysis of satellite communications with frequency domain noma. *IEEE Transactions on Vehicular Technology*, 68(12):11847–11858, 2019.

[50] Stephen Boyd and Lieven Vandenberghe. *Convex optimization*. Cambridge university press, 2004.

[51] Sven Wiese. The mixed-integer conic optimizer in Mosek. `https://docs.mosek.com/slides/2018/ismp2018/ismp-wiese.pdf`. July 2, 2018.

[52] Lou Salaün, Marceau Coupechoux, and Chung Shue Chen. Joint subcarrier and power allocation in noma: Optimal and approximate algorithms. *IEEE Transactions on Signal Processing*, 68: 2215–2230, 2020.

[53] Jon Lee and Sven Leyffer. *Mixed integer nonlinear programming*, volume 154. Springer Science & Business Media, 2011.

[54] Simon P Schurr, Dianne P O'Leary, and André L Tits. A polynomial-time interior-point method for conic optimization, with inexact barrier evaluations. *SIAM Journal on Optimization*, 20(1): 548–571, 2009.

[55] Chee Wei Tan et al. Wireless network optimization by Perron-Frobenius theory. *Foundations and Trends® in Networking*, 9(2-3):107–218, 2015.

[56] Kaiming Shen and Wei Yu. Fractional programming for communication systems—Part I: Power control and beamforming. *IEEE Transactions on Signal Processing*, 66(10):2616–2630, 2018.

[57] Meisam Razaviyayn, Mingyi Hong, Zhi-Quan Luo, and Jong-Shi Pang. Parallel successive convex approximation for nonsmooth nonconvex optimization. *Advances in neural information processing systems*, 27, 2014.

[58] Meisam Razaviyayn, Mingyi Hong, and Zhi-Quan Luo. A unified convergence analysis of block successive minimization methods for nonsmooth optimization. *SIAM Journal on Optimization*, 23(2):1126–1153, 2013.

[59] Matthias Köppe. On the complexity of nonlinear mixed-integer optimization. In *Mixed Integer Nonlinear Programming*, pages 533–557. Springer, 2012.

[60] Lingying Huang, Xiaomeng Chen, Wei Huo, Jiazheng Wang, Fan Zhang, Bo Bai, and Ling Shi. Branch and bound in mixed integer linear programming problems: A survey of techniques and trends. *arXiv preprint arXiv:2111.06257*, 2021.

[61] Bob Bixby. The gurobi optimizer. *Transp. Re-search Part B*, 41(2):159–178, 2007.

[62] László Lovász and Michael D Plummer. *Matching theory*, volume 367. American Mathematical Soc., 2009.

[63] Yunan Gu, Walid Saad, Mehdi Bennis, Merouane Debbah, and Zhu Han. Matching theory for future wireless networks: Fundamentals and applications. *IEEE Communications Magazine*, 53 (5):52–59, 2015.

[64] Matteo Fischetti and Andrea Lodi. Heuristics in mixed integer programming. *Wiley Encyclopedia of Operations Research and Management Science*, 2010.

[65] Stefano Lucidi and Francesco Rinaldi. Exact penalty functions for nonlinear integer programming problems. *Journal of optimization theory and applications*, 145(3):479–488, 2010.

[66] Alessio Zappone, Marco Di Renzo, and Mérouane Debbah. Wireless networks design in the era of deep learning: Model-based, ai-based, or both? *IEEE Transactions on Communications*, 67 (10):7331–7376, 2019.

[67] Pádraig Cunningham, Matthieu Cord, and Sarah Jane Delany. Supervised learning. In *Machine learning techniques for multimedia*, pages 21–49. Springer, 2008.

[68] Ian Goodfellow, Yoshua Bengio, and Aaron Courville. *Deep learning*. MIT press, 2016.

[69] Haoran Sun, Xiangyi Chen, Qingjiang Shi, Mingyi Hong, Xiao Fu, and Nicholas D Sidiropoulos. Learning to optimize: Training deep neural networks for interference management. *IEEE Transactions on Signal Processing*, 66(20):5438–5453, 2018.

[70] Anyue Wang, Lei Lei, Eva Lagunas, Symeon Chatzinotas, and Björn Ottersten. Dual-dnn assisted optimization for efficient resource scheduling in noma-enabled satellite systems. In *2021 IEEE Global Communications Conference (GLOBECOM)*, pages 1–6. IEEE, 2021.

[71] Aldo Paraboni, Mauro Buti, Carlo Capsoni, Davide Ferraro, Carlo Riva, Antonio Martellucci, and Piero Gabellini. Meteorology-driven optimum control of a multibeam antenna in satellite telecommunications. *IEEE Transactions on Antennas and Propagation*, 57(2):508–519, 2009.

[72] Apostolos Destounis and Athanasios D Panagopoulos. Dynamic power allocation for broadband multi-beam satellite communication networks. *IEEE Communications letters*, 15(4):380–382, 2011.

[73] Feng Li, Kwok-Yan Lam, Xin Liu, Jian Wang, Kanglian Zhao, and Li Wang. Joint pricing and power allocation for multibeam satellite systems with dynamic game model. *IEEE Transactions on Vehicular Technology*, 67(3):2398–2408, 2017.

[74] Juan Jose Garau Luis, Markus Guerster, Inigo del Portillo, Edward Crawley, and Bruce Cameron. Deep reinforcement learning architecture for continuous power allocation in high throughput satellites. *arXiv preprint arXiv:1906.00571*, 2019.

[75] Juan Jose Garau Luis, Nils Pachler, Markus Guerster, Inigo del Portillo, Edward Crawley, and Bruce Cameron. Artificial intelligence algorithms for power allocation in high throughput satellites: A comparison. In *2020 IEEE Aerospace Conference*, pages 1–15. IEEE, 2020.

[76] Unhee Park, Hee Wook Kim, Dae Sub Oh, and Bon Jun Ku. Flexible bandwidth allocation scheme based on traffic demands and channel conditions for multi-beam satellite systems. In *2012 IEEE Vehicular Technology Conference (Fall)*, pages 1–5, 2012.

[77] Igor Bisio and Mario Marchese. The concept of fairness: definitions and use in bandwidth allocation applied to satellite environment. *IEEE Aerospace and Electronic Systems Magazine*, 29(3): 8–14, 2014.

[78] Igor Bisio and Mario Marchese. Power saving bandwidth allocation over geo satellite networks. *IEEE Communications Letters*, 16(5):596–599, 2012.

[79] Yuichi Kawamoto, Taiki Kamei, Masaki Takahashi, Nei Kato, Amane Miura, and Morio Toyoshima. Flexible resource allocation with inter-beam interference in satellite communication systems with a digital channelizer. *IEEE Transactions on Wireless Communications*, 19(5): 2934–2945, 2020.

[80] Unhee Park, Hee Wook Kim, Dae Sub Oh, and Bon Ju Ku. Approach to adaptive resource management based on system environments for multi-beam satellite networks. In *2013 Seventh International Conference on Next Generation Mobile Apps, Services and Technologies*, pages 165–169. IEEE, 2013.

[81] Min Jia, Ximu Zhang, Xuemai Gu, Qing Guo, Yaqiu Li, and Ping Lin. Interbeam interference constrained resource allocation for shared spectrum multibeam satellite communication systems. *IEEE Internet of Things Journal*, 6(4):6052–6059, 2018.

[82] Zhe Ji, Youzheng Wang, Wei Feng, and Jianhua Lu. Delay-aware power and bandwidth allocation for multiuser satellite downlinks. *IEEE Communications Letters*, 18(11):1951–1954, 2014.

[83] Tedros Salih Abdu, Steven Kisseleff, Eva Lagunas, and Symeon Chatzinotas. Flexible resource optimization for GEO multibeam satellite communication system. *IEEE Transactions on Wireless Communications*, 20(12):7888–7902, 2021.

[84] Ricard Alegre-Godoy, Nader Alagha, and Maria Angeles Vázquez-Castro. Offered capacity optimization mechanisms for multi-beam satellite systems. In *2012 IEEE International Conference on Communications (ICC)*, pages 3180–3184. IEEE, 2012.

[85] L. Lei, E. Lagunas, Y. Yuan, M. G. Kibria, S. Chatzinotas, and B. Ottersten. Beam illumination pattern design in satellite networks: Learning and optimization for efficient beam hopping. *IEEE Access*, 8:136655–136667, 2020.

[86] Xin Hu, Yuchen Zhang, Xianglai Liao, Zhijun Liu, Weidong Wang, and Fadhel M Ghannouchi. Dynamic beam hopping method based on multi-objective deep reinforcement learning for next generation satellite broadband systems. *IEEE Transactions on Broadcasting*, 66(3):630–646, 2020.

[87] Flor G Ortiz-Gomez, Miguel A Salas-Natera, Ramón Martínez, and Salvador Landeros-Ayala. Optimization in VHTS satellite system design with irregular beam coverage for non-uniform traffic distribution. *Remote Sensing*, 13(13):2642, 2021.

[88] Jiang Lei and María Ángeles Vázquez-Castro. Multibeam satellite frequency/time duality study and capacity optimization. *Journal of Communications and Networks*, 13(5):472–480, 2011.

[89] Masaki Takahashi, Yuichi Kawamoto, Nei Kato, Amane Miura, and Morio Toyoshima. Adaptive power resource allocation with multi-beam directivity control in high-throughput satellite communication systems. *IEEE Wireless Communications Letters*, 8(4):1248–1251, 2019.

[90] Zhiyuan Lin, Zuyao Ni, Linling Kuang, Chunxiao Jiang, and Zhen Huang. Dynamic beam pattern and bandwidth allocation based on multi-agent deep reinforcement learning for beam hopping satellite systems. *IEEE Transactions on Vehicular Technology*, 2022.

[91] Flor G Ortiz-Gomez, Daniele Tarchi, Ramón Martínez, Alessandro Vanelli-Coralli, Miguel A Salas-Natera, and Salvador Landeros-Ayala. Cooperative multi-agent deep reinforcement learning for resource management in full flexible vhts systems. *IEEE Transactions on Cognitive Communications and Networking*, pages 1–1, 2021.

[92] J Anzalchi et al. Beam hopping in multi-beam broadband satellite systems: System simulation and performance comparison with non-hopped systems. In *2010 5th Advanced Satellite Multimedia Systems Conference and the 11th Signal Processing for Space Communications Workshop (ASMS/SPC)*, pages 248–255. IEEE, 2010.

[93] Steven Kisseleff, Eva Lagunas, Tedros Salih Abdu, Symeon Chatzinotas, and Björn Ottersten. Radio resource management techniques for multibeam satellite systems. *IEEE Communications Letters*, pages 1–1, 2020. doi: 10.1109/LCOMM.2020.3033357.

[94] Yongtao Su, Yaoqi Liu, Yiqing Zhou, Jinhong Yuan, Huan Cao, and Jinglin Shi. Broadband leo satellite communications: Architectures and key technologies. *IEEE Wireless Communications*, 26(2):55–61, 2019.

[95] NTT Docomo. Evaluation methodologies for downlink multiuser superposition transmissions. In *3GPP TSG RAN WG1 Meeting*, volume 81, pages R1–153332, 2015.

[96] Yuya Saito, Anass Benjebbour, Yoshihisa Kishiyama, and Takehiro Nakamura. System-level performance evaluation of downlink non-orthogonal multiple access (NOMA). In *2013 IEEE 24th Annual International Symposium on Personal, Indoor, and Mobile Radio Communications (PIMRC)*, pages 611–615. IEEE, 2013.

[97] Zhiguo Ding, Pingzhi Fan, and H Vincent Poor. Impact of user pairing on 5G nonorthogonal multiple-access downlink transmissions. *IEEE Transactions on Vehicular Technology*, 65(8): 6010–6023, 2015.

[98] Md Shipon Ali, Hina Tabassum, and Ekram Hossain. Dynamic user clustering and power allocation for uplink and downlink non-orthogonal multiple access (NOMA) systems. *IEEE Access*, 4: 6325–6343, 2016.

[99] David Tse and Pramod Viswanath. *Fundamentals of wireless communication*. Cambridge university press, 2005.

[100] Lou Salaün, Chung Shue Chen, and Marceau Coupechoux. Optimal joint subcarrier and power allocation in noma is strongly np-hard. In *2018 IEEE International Conference on Communications (ICC)*, pages 1–7. IEEE, 2018.

[101] Lei Lei, Di Yuan, and Peter Värbrand. On power minimization for non-orthogonal multiple access (NOMA). *IEEE Communications Letters*, 20(12):2458–2461, 2016.

[102] Yan Sun, Derrick Wing Kwan Ng, and Robert Schober. Optimal resource allocation for multicarrier MISO-NOMA systems. In *2017 IEEE International Conference on Communications (ICC)*, pages 1–7, 2017.

[103] Mojtaba Vaezi, Gayan Amarasuriya, Yuanwei Liu, Ahmed Arafa, Fang Fang, and Zhiguo Ding. Interplay between NOMA and other emerging technologies: A survey. *arXiv preprint arXiv:1903.10489*, 2019.

[104] Zhiyong Chen, Zhiguo Ding, Xuchu Dai, and George K Karagiannidis. On the application of quasi-degradation to miso-noma downlink. *IEEE Transactions on Signal Processing*, 64(23): 6174–6189, 2016.

[105] Haitham Moffaqq Al-Obiedollah, Kanapathippillai Cumanan, Jeyarajan Thiyagalingam, Alister G Burr, Zhiguo Ding, and Octavia A Dobre. Energy efficient beamforming design for miso non-orthogonal multiple access systems. *IEEE Transactions on Communications*, 67(6):4117–4131, 2019.

[106] Fusheng Zhu, Zhaohua Lu, Jianyue Zhu, Jiaheng Wang, and Yongming Huang. Beamforming design for downlink non-orthogonal multiple access systems. *IEEE Access*, 6:10956–10965, 2018.

[107] Xiangming Zhu, Chunxiao Jiang, Linling Kuang, Ning Ge, and Jianhua Lu. Non-orthogonal multiple access based integrated terrestrial-satellite networks. *IEEE Journal on Selected Areas in Communications (JSAC)*, 35(10):2253–2267, 2017.

[108] Xiaojuan Yan, Hailin Xiao, Cheng-Xiang Wang, Kang An, Anthony Theodore Chronopoulos, and Gan Zheng. Performance analysis of NOMA-based land mobile satellite networks. *IEEE Access*, 2018.

[109] Tomás Ramírez, Carlos Mosquera, Nele Noels, Marius Caus, Joan Bas, Luis Blanco, and Nader Alagha. Study on the application of NOMA techniques for heterogeneous satellite terminals. In *2020 10th Advanced Satellite Multimedia Systems Conference and the 16th Signal Processing for Space Communications Workshop (ASMS/SPSC)*, pages 1–8. IEEE, 2020.

[110] Eiji Okamoto and Hiroyuki Tsuji. Application of non-orthogonal multiple access scheme for satellite downlink in satellite/terrestrial integrated mobile communication system with dual satellites. *IEICE Transactions on Communications*, 99(10):2146–2155, 2016.

[111] Antonio Arcidiacono, Daniele Finocchiaro, Riccardo De Gaudenzi, Oscar del Rio-Herrero, Stefano Cioni, Marco Andrenacci, and Riccardo Andreotti. Is satellite ahead of terrestrial in deploying NOMA for massive machine-type communications? *Sensors*, 21(13):4290, 2021.

[112] Xin Liu, Xiangping Zhai, Weidang Lu, and Celimuge Wu. QoS-guarantee resource allocation for multibeam satellite industrial internet of things with NOMA. *IEEE Transactions on Industrial Informatics*, 2019.

[113] Jian Jiao, Yunyu Sun, Shaohua Wu, Ye Wang, and Qinyu Zhang. Network utility maximization resource allocation for NOMA in satellite-based internet of things. *IEEE Internet of Things Journal*, 7(4):3230–3242, 2020.

[114] Jianhang Chu, Xiaoming Chen, Caijun Zhong, and Zhaoyang Zhang. Robust design for NOMA-based multibeam LEO satellite internet of things. *IEEE Internet of Things journal*, 8(3):1959–1970, 2020.

[115] Yazhou Zhu, Christian A Hofmann, and Andreas Knopp. Distributed resource optimization for noma transmission in beamforming satcom. *IEEE Journal on Selected Areas in Communications*, 2022.

[116] Zhi Lin, Min Lin, Jun-Bo Wang, Tomaso de Cola, and Jiangzhou Wang. Joint beamforming and power allocation for satellite-terrestrial integrated networks with non-orthogonal multiple access. *IEEE Journal of Selected Topics in Signal Processing*, 13(3):657–670, 2019.

[117] Lina Wang, Yanan Wu, Haijun Zhang, Sunghyun Choi, and Victor CM Leung. Resource allocation for noma based space-terrestrial satellite networks. *IEEE Transactions on Wireless Communications*, 20(2):1065–1075, 2020.

[118] Zhixiang Gao, Aijun Liu, Chen Han, and Xiaohu Liang. Max completion time optimization for internet of things in LEO satellite-terrestrial integrated networks. *IEEE Internet of Things Journal*, 2021.

[119] Min Jia, Qiling Gao, Qing Guo, Xuemai Gu, and Xuemin Shen. Power multiplexing noma and bandwidth compression for satellite-terrestrial networks. *IEEE Transactions on Vehicular Technology*, 68(11):11107–11117, 2019.

[120] Yaomin Zhang, Haijun Zhang, Huan Zhou, Keping Long, and George K Karagiannidis. Resource allocation in terrestrial-satellite based next generation multiple access networks with interference cooperation. *IEEE Journal on Selected Areas in Communications*, 2022.

[121] Xiaokai Zhang, Bangning Zhang, Kang An, Gan Zheng, Symeon Chatzinotas, and Daoxing Guo. Stochastic geometry-based analysis of cache-enabled hybrid satellite-aerial-terrestrial networks with non-orthogonal multiple access. *IEEE Transactions on Wireless Communications*, 2021.

[122] Ningyuan Wang, Feng Li, Dong Chen, Liang Liu, and Zeyu Bao. Noma-based energy-efficiency optimization for uav enabled space-air-ground integrated relay networks. *IEEE Transactions on Vehicular Technology*, 2022.

[123] Yunyu Sun, Ye Wang, Jian Jiao, Shaohua Wu, and Qinyu Zhang. Deep learning-based long-term power allocation scheme for NOMA downlink system in S-IoT. *IEEE Access*, 7:86288–86296, 2019.

[124] Xiaojuan Yan, Kang An, Qianfeng Zhang, Gan Zheng, Symeon Chatzinotas, and Junfeng Han. Delay constrained resource allocation for noma enabled satellite internet of things with deep reinforcement learning. *IEEE Internet of Things Journal*, 2020.

[125] Xiaojuan Yan, Kang An, Cheng-Xiang Wang, Wei-Ping Zhu, Yusheng Li, and Zhiqiang Feng. Genetic algorithm optimized support vector machine in noma-based satellite networks with imperfect csi. In *ICASSP 2020-2020 IEEE International Conference on Acoustics, Speech and Signal Processing (ICASSP)*, pages 8817–8821. IEEE, 2020.

[126] Wali Ullah Khan, Furqan Jameel, Tapani Ristaniemi, Shafiullah Khan, Guftaar Ahmad Sardar Sidhu, and Ju Liu. Joint spectral and energy efficiency optimization for downlink NOMA networks. *IEEE Transactions on Cognitive Communications and Networking*, 6(2):645–656, 2019.

[127] SnT SIGCOM. Satellite traffic emulator. `https://wwwfr.uni.lu/snt/research/sigcom/sw_simulators`.

[128] Lei Lei, Lei You, Qing He, Thang Xuan Vu, Symeon Chatzinotas, Di Yuan, and Björn Ottersten. Learning-assisted optimization for energy-efficient scheduling in deadline-aware NOMA systems. *IEEE Transactions on Green Communications and Networking*, 3(3):615–627, 2019.

[129] Xinwei Yue, Yuanwei Liu, Yuanyuan Yao, Tian Li, Xuehua Li, Rongke Liu, and Arumugam Nallanathan. Outage behaviors of NOMA-based satellite network over shadowed-rician fading channels. *IEEE Transactions on Vehicular Technology (TVT)*, 69(6):6818–6821, 2020.

[130] Lei You, Di Yuan, Lei Lei, Sumei Sun, Symeon Chatzinotas, and Björn Ottersten. Resource optimization with load coupling in multi-cell NOMA. *IEEE Transactions on Wireless Communications (TWC)*, 17(7):4735–4749, 2018.

[131] Anyue Wang, Lei Lei, Eva Lagunas, Ana I Pérez-Neira, Symeon Chatzinotas, and Björn Ottersten. On fairness optimization for NOMA-enabled multi-beam satellite systems. In *2019 IEEE 30th Annual International Symposium on Personal, Indoor and Mobile Radio Communications (PIMRC)*, pages 1–6, 2019.

[132] Dimitrios Christopoulos, Symeon Chatzinotas, and Björn Ottersten. Multicast multigroup precoding and user scheduling for frame-based satellite communications. *IEEE Transactions on Wireless Communications (TWC)*, 14(9):4695–4707, 2015.

[133] M. G. Kibria, E. Lagunas, N. Maturo, D. Spano, H. Al-Hraishawi, and S. Chatzinotas. Carrier aggregation in multi-beam high throughput satellite systems. In *2019 IEEE Global Communications Conference (GLOBECOM)*, pages 1–6, 2019.

[134] Carlos Mosquera, Roberto López-Valcarce, Tomás Ramírez, and Vahid Joroughi. Distributed precoding systems in multi-gateway multibeam satellites: Regularization and coarse beamforming. *IEEE Transactions on Wireless Communications (TWC)*, 17(10):6389–6403, 2018.

[135] Piero Angeletti and Riccardo De Gaudenzi. A pragmatic approach to massive MIMO for broadband communication satellites. *IEEE Access*, 8:132212–132236, 2020.

[136] Nusrat Fatema, Guang Hua, Yong Xiang, Dezhong Peng, and Iynkaran Natgunanathan. Massive MIMO linear precoding: A survey. *IEEE Systems Journal*, 12(4):3920–3931, 2017.

[137] ETSI EN 301 307–2. Digital video broadcasting (DVB); second generation framing structure, channel coding and modu-lation systems for broadcasting, interactive services, news gathering and other broadband satellite applications, part 2: S2-extensions (DVB-S2X). 2014.

[138] Lei Lei, Lei You, Yang Yang, Di Yuan, Symeon Chatzinotas, and Björn Ottersten. Load coupling and energy optimization in multi-cell and multi-carrier NOMA networks. *IEEE Transactions on Vehicular Technology (TVT)*, 68(11):11323–11337, 2019.

[139] Abdulkadir Celik, Ming-Cheng Tsai, Redha M Radaydeh, Fawaz S Al-Qahtani, and Mohamed-Slim Alouini. Distributed cluster formation and power-bandwidth allocation for imperfect NOMA in DL-HetNets. *IEEE Transactions on Communications*, 2018.

[140] Mari Kobayashi, Joseph Boutros, and Giuseppe Caire. Successive interference cancellation with SISO decoding and EM channel estimation. *IEEE Journal on Selected Areas in Communications (JSAC)*, 19(8):1450–1460, 2001.

[141] Rui Fa and Rodrigo C De Lamare. Multi-branch successive interference cancellation for MIMO spatial multiplexing systems: design, analysis and adaptive implementation. *IET communications*, 5(4):484–494, 2011.

[142] Yichao Huang, Chee Wei Tan, and Bhaskar D Rao. Joint beamforming and power control in coordinated multicell: Max-min duality, effective network and large system transition. *IEEE Transactions on Wireless Communications (TWC)*, 12(6):2730–2742, 2013.

[143] Liang Zheng, Desmond WH Cai, and Chee Wei Tan. Max-min fairness rate control in wireless networks: Optimality and algorithms by Perron-Frobenius theory. *IEEE Transactions on Mobile Computing*, 17(1):127–140, 2017.

[144] Liang Zheng, Y-W Peter Hong, Chee Wei Tan, Cheng-Lin Hsieh, and Chia-Han Lee. Wireless max–min utility fairness with general monotonic constraints by Perron–Frobenius theory. *IEEE Transactions on Information Theory*, 62(12):7283–7298, 2016.

[145] Clifford A Shaffer. *A practical introduction to data structures and algorithm analysis*. Prentice Hall Upper Saddle River, NJ, 1997.

[146] K Sikorski. Optimal solution of nonlinear equations. *Journal of Complexity*, 1(2):197–209, 1985.

[147] Quang-Doanh Vu, Kien-Giang Nguyen, and Markku Juntti. Weighted max–min fairness for C-RAN multicasting under limited fronthaul constraints. *IEEE Transactions on Communications*, 66(4):1534–1548, 2017.

[148] ESA. SATellite Network of EXperts (SATNEX) IV. `https://satnex4.org/`.

[149] Daosen Zhai, Ruonan Zhang, Lin Cai, and F Richard Yu. Delay minimization for massive internet of things with non-orthogonal multiple access. *IEEE Journal of Selected Topics in Signal Processing*, 13(3):553–566, 2019.

[150] ITU. Time series synthesis of tropospheric impairments. *Recommendation ITU-R P.1853-2*, 2019.

[151] Xudong Zhong, Yuanzhi He, Hao Yin, Jingchao Wang, and Zhouquan Du. Joint power and timeslot allocation based on delay priority for multi-beam satellite downlinks. In *2017 International Conference on Progress in Informatics and Computing (PIC)*, pages 389–393. IEEE, 2017.

[152] Zhe Ji, Suzhi Cao, Sheng Wu, and Wenbo Wang. Delay-aware satellite-terrestrial backhauling for heterogeneous small cell networks. *IEEE Access*, 8:112190–112202, 2020.

[153] Chong Liu, Rong Chai, and Qianbin Chen. IoT gateway association and data scheduling for delay optimization in LEO satellite systems. In *2020 IEEE/CIC International Conference on Communications in China (ICCC)*, pages 993–998. IEEE, 2020.

[154] Anyue Wang, Lei Lei, Eva Lagunas, Ana I. Pérez-Neira, Symeon Chatzinotas, and Björn Ottersten. NOMA-enabled multi-beam satellite systems: Joint optimization to overcome offered-requested data mismatches. *IEEE Transactions on Vehicular Technology*, 70(1):900–913, 2021. doi: 10.1109/TVT.2020.3047453.

[155] Yongjun Xu, Rose Qingyang Hu, and Guoquan Li. Robust energy-efficient maximization for cognitive NOMA networks under channel uncertainties. *IEEE Internet of Things Journal*, 7(9): 8318–8330, 2020.

[156] Mingzhe Chen, Ursula Challita, Walid Saad, Changchuan Yin, and Mérouane Debbah. Artificial neural networks-based machine learning for wireless networks: A tutorial. *IEEE Communications Surveys & Tutorials*, 21(4):3039–3071, 2019.

[157] Yufeng Zhang, Zhugang Wang, Yonghui Huang, Jian Ren, Yingzeng Yin, Ying Liu, Gert Frølund Pedersen, and Ming Shen. Deep neural network-based receiver for next-generation LEO satellite communications. *IEEE Access*, 8:222109–222116, 2020.

[158] Anyue Wang, Lei Lei, Eva Lagunas, Symeon Chatzinotas, and Björn Ottersten. Completion time minimization in NOMA systems: Learning for combinatorial optimization. *IEEE Networking Letters*, 3(1):15–18, 2021.

[159] Alexander Vinel and Pavlo A Krokhmal. Mixed integer programming with a class of nonlinear convex constraints. *Discrete Optimization*, 24:66–86, 2017.

[160] Miles Lubin, Emre Yamangil, Russell Bent, and Juan Pablo Vielma. Extended formulations in mixed-integer convex programming. In *International Conference on Integer Programming and Combinatorial Optimization*, pages 102–113. Springer, 2016.

[161] Jingci Luo, Jie Tang, Daniel KC So, Gaojie Chen, Kanapathippillai Cumanan, and Jonathon A Chambers. A deep learning-based approach to power minimization in multi-carrier noma with swipt. *IEEE Access*, 7:17450–17460, 2019.

[162] A Freedman, D Rainish, and Y Gat. Beam hopping: how to make it possible. In *Proc. Ka and Broadband Communication Conference*, 2015.

[163] Huan Cao, Yongtao Su, Yiqing Zhou, and Jinlong Hu. QoS guaranteed load balancing in broadband multi-beam satellite networks. In *ICC 2019-2019 IEEE International Conference on Communications (ICC)*, pages 1–6. IEEE, 2019.

[164] Peiliang Zuo, Tao Peng, Wangdan Linghu, and Wenbo Wang. Resource allocation for cognitive satellite communications downlink. *IEEE Access*, 6:75192–75205, 2018.

[165] Yu Wang, Ying Chen, Yunfei Qiao, Hejia Luo, Xiaolu Wang, Rong Li, and Jun Wang. Cooperative beam hopping for accurate positioning in ultra-dense LEO satellite networks. In *2021 IEEE International Conference on Communications Workshops (ICC Workshops)*, pages 1–6, 2021. doi: 10.1109/ICCWorkshops50388.2021.9473538.

[166] Lin Chen, Eva Lagunas, Symeon Chatzinotas, and Björn Ottersten. Satellite broadband capacity-on-demand: Dynamic beam illumination with selective precoding. In *European Signal Processing Conference (EUSIPCO), Dublin, Ireland, Aug. 2021*, 2021.

[167] Jianhang Chu, Xiaoming Chen, Caijun Zhong, and Zhaoyang Zhang. Robust design for NOMA-based multibeam LEO satellite internet of things. *IEEE Internet of Things Journal*, 8(3):1959–1970, 2021. doi: 10.1109/JIOT.2020.3015995.

[168] Anyue Wang, Lei Lei, Eva Lagunas, Symeon Chatzinotas, Ana Isabel Pérez-Neira, and Björn Ottersten. Joint beam-hopping scheduling and power allocation in NOMA-assisted satellite systems. In *2021 IEEE Wireless Communications and Networking Conference (WCNC)*, pages 1–6. IEEE, 2021.

[169] Ya-Feng Liu and Yu-Hong Dai. On the complexity of joint subcarrier and power allocation for multi-user OFDMA systems. *IEEE transactions on Signal Processing*, 62(3):583–596, 2013.

[170] Juris Hartmanis. Computers and intractability: a guide to the theory of np-completeness (michael r. garey and david s. johnson). *Siam Review*, 24(1):90, 1982.

[171] Richard M Karp. Reducibility among combinatorial problems. In *Complexity of computer computations*, pages 85–103. Springer, 1972.

[172] Alessio Zappone, Emil Björnson, Luca Sanguinetti, and Eduard Jorswieck. Globally optimal energy-efficient power control and receiver design in wireless networks. *IEEE Transactions on Signal Processing*, 65(11):2844–2859, 2017.

[173] Tao Wang and Luc Vandendorpe. Successive convex approximation based methods for dynamic spectrum management. In *2012 IEEE International Conference on Communications (ICC)*, pages 4061–4065. IEEE, 2012.

[174] Carl T Kelley. *Iterative methods for linear and nonlinear equations*. SIAM, 1995.

[175] Jingjing Cui, Yuanwei Liu, Zhiguo Ding, Pingzhi Fan, and Arumugam Nallanathan. Optimal user scheduling and power allocation for millimeter wave NOMA systems. *IEEE Transactions on Wireless Communications*, 17(3):1502–1517, 2017.

[176] Alberto Ginesi, Emiliano Re, and Pantelis-Daniel Arapoglou. Joint beam hopping and precoding in hts systems. In *International Conference on Wireless and Satellite Systems*, pages 43–51. Springer, 2017.

[177] Shiyi Xia, Quanjiang Jiang, Cheng Zou, and Guotong Li. Beam coverage comparison of LEO satellite systems based on user diversification. *IEEE access*, 7:181656–181667, 2019.

[178] Mohammed Y Abdelsadek, Halim Yanikomeroglu, and Gunes Karabulut Kurt. Future ultra-dense LEO satellite networks: A cell-free massive MIMO approach. In *2021 IEEE International Conference on Communications Workshops (ICC Workshops)*, pages 1–6. IEEE, 2021.

[179] Boya Di, Hongliang Zhang, Lingyang Song, Yonghui Li, and Geoffrey Ye Li. Ultra-dense LEO: Integrating terrestrial-satellite networks into 5G and beyond for data offloading. *IEEE Transactions on Wireless Communications*, 18(1):47–62, 2018.

[180] Kai Yuan Zhong, Yu Jian Cheng, Hai Ning Yang, and Bin Zheng. Leo satellite multibeam coverage area division and beamforming method. *IEEE Antennas and Wireless Propagation Letters*, 20(11): 2115–2119, 2021.

[181] Zhixiang Gao, Aijun Liu, Chen Han, and Xiaohu Liang. Files delivery and share optimization in LEO satellite-terrestrial integrated networks: A NOMA based coalition formation game approach. *IEEE Transactions on Vehicular Technology*, 2021.

[182] 3GPP TR 38.811. Technical specification group radio access network; Study on new radio (NR) to support non-terrestrial networks (Release 15), v15.4.0. 2020.

[183] Gesualdo Scutari, Francisco Facchinei, and Lorenzo Lampariello. Parallel and distributed methods for constrained nonconvex optimization—part i: Theory. *IEEE Transactions on Signal Processing*, 65(8):1929–1944, 2016.

[184] Yang Yang, Marius Pesavento, Zhi-Quan Luo, and Björn Ottersten. Inexact block coordinate descent algorithms for nonsmooth nonconvex optimization. *IEEE Transactions on Signal Processing*, 68:947–961, 2019.

[185] Pascal Gahinet, Arkadi Nemirovski, Alan J. Laub, and Mahmoud Chilali. *LMI Control Toolbox Users Guide*. MathWorks, 1995.

[186] Li You, Ke-Xin Li, Jiaheng Wang, Xiqi Gao, Xiang-Gen Xia, and Björn Ottersten. Massive mimo transmission for leo satellite communications. *IEEE Journal on Selected Areas in Communications*, 38(8):1851–1865, 2020.

[187] Tianqing Zhou, Zunxiong Liu, Junhui Zhao, Chunguo Li, and Luxi Yang. Joint user association and power control for load balancing in downlink heterogeneous cellular networks. *IEEE Transactions on Vehicular Technology*, 67(3):2582–2593, 2017.

[188] Anyue Wang, Lei Lei, Eva Lagunas, Ana I. Pérez-Neira, Symeon Chatzinotas, and Björn Ottersten. Joint optimization of beam-hopping design and NOMA-assisted transmission for flexible satellite systems. *IEEE Transactions on Wireless Communications*, pages 1–1, 2022. doi: 10.1109/TWC.2022.3170435.

[189] Bruno Clerckx, Yijie Mao, Robert Schober, Eduard A Jorswieck, David J Love, Jinhong Yuan, Lajos Hanzo, Geoffrey Ye Li, Erik G Larsson, and Giuseppe Caire. Is noma efficient in multi-antenna networks? a critical look at next generation multiple access techniques. *IEEE Open Journal of the Communications Society*, 2:1310–1343, 2021.

[190] Arunprakash Jayaprakash, Barry G Evans, Pei Xiao, Adegbenga B Awoseyila, and Yingnan Zhang. New radio numerology and waveform evaluation for satellite integration into 5g terrestrial network. In *ICC 2020-2020 IEEE International Conference on Communications (ICC)*, pages 1–7. IEEE, 2020.

[191] Stephen McWade, Mark F Flanagan, Juquan Mao, Lei Zhang, and Arman Farhang. Resource allocation for mixed numerology noma. *IEEE Wireless Communications Letters*, 10(10):2240–2244, 2021.

[192] Tao Yang, Xinlei Yi, Junfeng Wu, Ye Yuan, Di Wu, Ziyang Meng, Yiguang Hong, Hong Wang, Zongli Lin, and Karl H Johansson. A survey of distributed optimization. *Annual Reviews in Control*, 47:278–305, 2019.